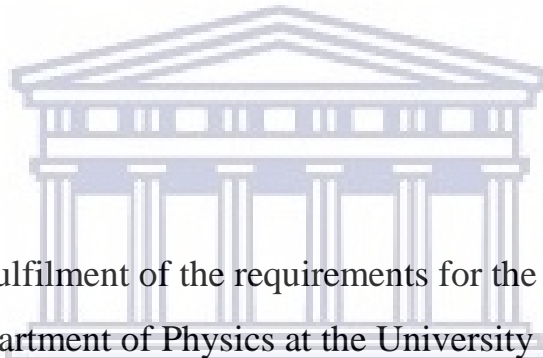


# **Development and Study of a Thoron (Rn-220) Standard Source**

Elmughera Hussein Salim Elhag



Thesis presented in fulfilment of the requirements for the degree of Doctor of Philosophy in the Department of Physics at the University of the Western Cape,

South Africa

UNIVERSITY of the  
WESTERN CAPE

Supervisor:

Prof. R. Lindsay

Department of Physics and Astronomy

University of the Western Cape

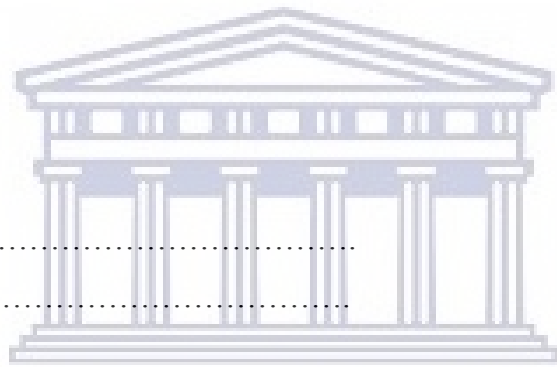
November 2019

## DECLARATION

I, the undersigned, hereby declare that the work contained in this thesis is my own original work and that I have not previously in its entirety or in part submitted it at any university for a degree.

Signature .....

Date .....



UNIVERSITY *of the*  
WESTERN CAPE

# Development and Study of a Thoron (Rn-220) Standard Source

Elmughera Hussein Salim Elhag

## KEYWORDS

Thoron standard source

Thoron measurements

Thorium Nitrate

Gamma Ray Spectroscopy

Bubbling Method

Source Activity



UNIVERSITY *of the*  
WESTERN CAPE

# Development and Study of a Thoron (Rn-220) standard Source

Elmughera Hussein Salim Elhag

Department of Physics, University of the Western Cape, Private Bag X17, Bellville, South Africa

## ABSTRACT

Thoron Rn-220 is a radioactive gas with a half-life of 55.6 s. It has been identified as a possible health concern in specific places such as monazite processing plants and (rare-earth) mines. The short half-life of Rn-220 makes Rn-220 calibration sources and chambers less common than for the isotope Rn-222. There are many Rn-220 standard sources and chambers that are widely described in the literature and used for different applications and calibration. However, some of these chambers and sources are not easy to set up in typical nuclear environmental laboratories.

In this project, we developed a Rn-220 standard source using a thorium nitrate solution ( $\text{Th}(\text{NO}_3)_4 \cdot 6\text{H}_2\text{O}$ ). The solution was split into a large volume which was used in a Marinelli beaker to characterize its strength using a Hyper Pure Germanium (HPGe) detector, and a smaller volume of around 30 ml which was poured into a small bottle. The Rn-220 is extracted by bubbling air through the solution in the small bottle using an aerator. Gamma rays from the solution were measured simultaneously using a 76.2 mm  $\times$  76.2 mm NaI(Tl) detector. The gamma rays were measured for 66 hours. The accumulated spectra were thereafter analysed using an Excel spreadsheet where the counts in the Tl-208(2614 keV) peak were extracted and used to obtain the percentage of Rn-220 pumped out of the solution in the small bottle.

A model was developed using the Bateman equations which was used to fit the experimental data. It was found that the strength of the thoron decay was reduced to about 15% of its original value which implied that about 85% of the created Rn-220 was pumped from the solution in the small

bottle. In other experiments different flow rates for pumping Rn-220 from the solution in the small bottle were utilized. It was found that the percentage of Rn-220 pumped from the solution with different flow rates did not change significantly.

The activity concentration in the exit stream could be calculated using the percentage of Rn-220 that was pumped from the solution as obtained by the fit to the NaI(Tl) detector measurements.

This value of the calculated activity concentration was compared to the measured value obtained using the Durrige RAD7. The calculated and the measured activity concentration value of Rn-220 were found to be in very good agreement.



## ACKNOWLEDGEMENTS

I would like to thank my supervisor, Prof Robbie Lindsay for his efforts and continuing guidance, advice and support throughout my PhD journey. Without your input and the feedback that I received from you, this work would not see the light of its completion. I am also grateful for his financial assistance. I thank Prof. Rob J. de Meijer, for sharing his ideas and clues when I started this project. I thank Dr Maleka from iThemba LABS for his technical assistance. Thank you Dr Joash for sharing your ideas. I thank my colleague Gharib Mohammed for the time we spent in discussion on the project and for your comments. I am grateful to the Physics Department of the University of the Western Cape (UWC) not only for providing a good environment for studies, but also for financial assistance through the work study program.

Thank you National Research Fund (NRF) for Financial Assistance through your grant.

I would not forget Ahfad University for Women; without you, I would not get this opportunity to do this project. Thank you Prof Gasim Badri and Dr Omeima Salih.

My parents, my father Hussein Salim Elhag and my mother Hameeda Mohammed Ahmed Alajab, I would never forget your prayers. Thank you for all the care that you give to me to reach this point.

I am grateful to my dearest wife for her consistent motivation and her inspiration, thank you for being there all the time to stay beside me. Although you were not physically with me, your presence all the time puts you in my thoughts. Thank you for taking all the fatherly responsibility by taking care of our son Alsajjad.

Thank you all for the encouragement.

Elmughera Hussein Salim Elhag

UWC

July 2019

# Contents

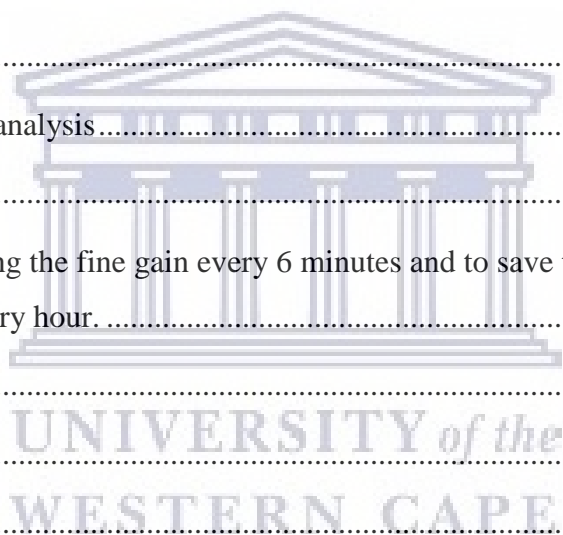
|   |     |
|---|-----|
| ABSTRACT.....   | iv  |
| ACKNOWLEDGEMENTS.....   | vi  |
| Contents .....  | vii |
| List of Figures.....  | xi  |
| List of Tables .....  | xv  |
| CHAPTER 1 .....   | 1   |
| Introduction.....   | 1   |
| 1.1 Overview of Thoron (Rn-220) .....                           | 1   |
| 1.2 Motivation and aim of the study .....                       | 4   |
| 1.3 Structure of the thesis.....                                | 6   |
| CHAPTER 2 .....   | 8   |
| Radiation detection and Bateman model.....                      | 8   |
| 2.1 Introduction.....   | 8   |
| 2.2 Simple Radioactive Decay: Half-life and Decay Constant..... | 8   |
| 2.3 Bateman equations .....                                     | 9   |
| 2.4 Types of decay Modes .....                                  | 18  |
| 2.4.1 Alpha particle decay ( $\alpha$ ).....                    | 18  |
| 2.4.1.1 RAD7 continuous monitor:.....                           | 19  |
| 2.4.2 Beta decay .....  | 21  |
| 2.4.3 Gamma emission.....                                       | 22  |
| 2.5 Interaction of gamma rays with matter .....                 | 22  |
| 2.5. 1 Gamma ray detectors used in this work.....               | 26  |
| 2.5.1.1 Sodium Iodide detector NaI(Tl).....                     | 26  |

|   |    |
|---|----|
| 2.5.1.2 The Hyper Pure Germanium Detect detector (HPGe) .....                           | 26 |
| 2.6 Summary .....   | 27 |
| CHAPTER 3 .....   | 28 |
| Literature review on Rn-220.....  | 28 |
| 3.1 Introduction.....   | 28 |
| 3.2 Review of methods for measuring Rn-220 .....  | 28 |
| 3.3 Development of Rn-220 sources.....  | 40 |
| 3.4 Summary .....   | 43 |
| CHAPTER 4 .....   | 44 |
| Novel Thoron standard source .....  | 44 |
| 4. 1 Introduction.....  | 44 |
| 4.2 The Rn-220 source preparation.....  | 44 |
| 4.2.1 Th(NO <sub>3</sub> ) <sub>4</sub> .6H <sub>2</sub> O drying.....                  | 44 |
| 4.2.2 Th(NO <sub>3</sub> ) <sub>4</sub> .6H <sub>2</sub> O solution preparation.....    | 45 |
| 4.3 Rn-220 measurements.....  | 46 |
| 4.3.1 Rn-220 source characterization using a Hyper-Pure Germanium detector (HPGe) ..... | 47 |
| 4.3.2 The bubbling method to produce an air stream of known Rn-220 concentration .....  | 49 |
| 4.3.2.1 The NaI ( Tl) detector calibration: .....                                       | 50 |
| 4.3.2.2 NaI(Tl) photo peak efficiencies .....   | 52 |
| 4.3.3 Background radiation measurements:.....   | 53 |
| 4.3.4 The bubbling method .....   | 54 |
| 4.3.5 RAD7 measurements .....   | 56 |
| 4.4 Summary .....   | 59 |
| CHAPTER 5 .....   | 60 |
| HPGe, NaI(Tl) and RAD7 Results.....   | 60 |



|  |    |
|--|----|
| 5.1 Introduction.....  | 60 |
| 5.2 HPGe detector measurements .....   | 60 |
| 5.2.1 The room background radiation.....   | 60 |
| 5.2.3 Calculated activity concentration of the $\text{Th}(\text{NO}_3)_4 \cdot 6\text{H}_2\text{O}$ solution ..... | 65 |
| 5.3 Thoron standard source Procedure using NaI(Tl) detector .....  | 66 |
| 5.3.1 Room background radiation measurements.....  | 66 |
| 5.3.2 Analysis of the Thorium nitrate solution bubbling procedure .....  | 67 |
| 5.3.4 Simulated detection photopeak efficiency of the Na(Tl) detector .....  | 72 |
| 5.3.5 The percentage of Rn-220 pumped from the $(\text{Th}(\text{NO}_3)_4 \cdot 6\text{H}_2\text{O})$ .....        | 74 |
| 5.3.6 Bubbling using different flow rates .....  | 76 |
| 5.3.7 Bubbling setup using a lead castle as shielding .....  | 79 |
| 5.3.7.1 Background measurements .....  | 79 |
| 5.4 RAD7 measurements .....  | 84 |
| 5.4.2 The Rn-220 activity concentration using a flow rate of 1 L/min.....  | 88 |
| 5.4.3 Lead Castle measurements.....  | 89 |
| 5.5 Summary .....  | 90 |
| CHAPTER 6 .....  | 92 |
| Discussions .....  | 92 |
| 6.1 Introduction.....  | 92 |
| 6.2 The HPGe measurements.....   | 92 |
| 6.3 NaI(Tl) measurements. ....   | 93 |
| 6.3.1 Why the bubbling method? .....   | 93 |
| 6.3.2 Stability of the Rn-220 source .....   | 95 |
| 6.3.3 Reproducibility of the Rn-220 source.....  | 96 |
| 6.4 Checking the effect of the height variation of the Rn-220 source .....   | 97 |

|   |     |
|---|-----|
| 6.5 RAD7 measurements .....   | 103 |
| 6.6 The disadvantages of our method .....   | 104 |
| CHAPTER 7 .....   | 106 |
| Summary, Conclusion and Future work .....   | 106 |
| 7.1 Introduction.....   | 106 |
| 7.2 Summary and Conclusion.....   | 106 |
| 7.3 Future work.....  | 109 |
| References.....   | 110 |
| Appendices.....   | 116 |
| Appendix A.....   | 116 |
| KCl solution measurement analysis.....  | 116 |
| Appendix B.....   | 118 |
| Script program for stabilizing the fine gain every 6 minutes and to save the measured spectra<br>from the Rn-220 source every hour..... | 118 |
| Appendix C.....   | 120 |
| Visual Basic program.....   | 120 |
| Appendix D.....   | 122 |
| Gamma ray spectra measured from the $\text{Th}(\text{NO}_3)_4 \cdot 6\text{H}_2\text{O}$ while bubbling.....                            | 122 |
| Appendix E.....   | 129 |
| The uncertainty calculations .....  | 129 |



## List of Figures

|  |    |
|--|----|
| Figure 1. 1: A schematic illustration of the thorium series. The cyan boxes represent $\gamma$ -ray emitting radionuclides.....                | 2  |
| Figure 2.1: The activity of Tl-208 (2614 keV) corrected for the branching as calculated using equation (2.25) with S=300 Bq.....               | 16 |
| Figure 2.2: The activity of Tl-208 (2614 keV) corrected for the branching as calculated using equation (2.25) with S=200 Bq.....               | 17 |
| Figure 2.3: The activity of Tl-208 (2614 keV) corrected for the branching as calculated using equation (2.25) with S= 100 Bq.....              | 17 |
| Figure 2.4: The activity of Tl-208 (2614 keV) corrected for the branching as calculated using equation (2.25) with S= 100, 200 and 300 Bq..... | 18 |
| Figure 2.5: RAD7 on the left and schematic diagram showing its internal parts .....  | 19 |
| Figure 2.6: Typical RAD7 spectrum.....   | 21 |
| Figure 2.7: The mechanism of Photo-electric effect absorption.....   | 22 |
| Figure 2.8: Schematic diagram that shows the Compton scattering process .....  | 23 |
| Table 3. 1 Summary of measurement system for Rn-220 .....  | 31 |
| Figure 4.2: Gamma-ray spectrum for the Th-232 reference source.....  | 50 |
| Figure 4.3: $\gamma$ – ray energy versus channel number used for the energy calibration of the NaI(Tl) .....                                   | 52 |
| Figure 4.4: The picture showing the Rn-220 standard source experiment setup (top); the schematic diagram of the setup (bottom).....            | 55 |

|  |    |
|--|----|
| Figure 4.5: Schematic diagram of Rn-220 standard source experiment setup using the lead castle.<br>.....   | 56 |
| Figure 4.6: A picture showing the RAD7 connected to the Rn-220 standard source in the<br>experiment setup (top). A schematic diagram showing the RAD7 connected to the Rn-220<br>standard source (bottom).....   | 58 |
| Figure 4.7: a) NaI(Tl) detector and the bottle containing the Rn-220 source inside the lead castle.<br>b) The lead castle set-up with the Rn-220 standard source bottle placed inside the lead castle.<br>Note that the lid of the lead castle had to be moved about 1 cm from the structure to<br>accommodate the pipes. .... | 59 |
| Figure 5.1: Gamma-ray spectrum of the room background radiation measurement. ....  | 61 |
| 5.2.2 The Rn-220 source characterization .....   | 61 |
| Figure 5.2: A typical gamma ray spectrum of the $\text{Th}(\text{NO}_3)_4 \cdot 6\text{H}_2\text{O}$ . ....  | 62 |
| Figure 5.3: The efficiency of the detector as a function of energy. ....   | 64 |
| Figure 5.4: The activity concentration (diamond), the average activity concentration (triangle)<br>and the average weighted activity concentration (square). ....  | 64 |
| Figure 5.5: Room background spectrum accumulated for one hour showing some gamma energy<br>lines of interest. ....   | 66 |
| Figure 5.6: Gamma-ray spectrum of $\text{Th}(\text{NO}_3)_4 \cdot 6\text{H}_2\text{O}$ solution for the first hour of bubbling ....  | 68 |
| Figure 5.7: Gamma-ray spectrum of $\text{Th}(\text{NO}_3)_4 \cdot 6\text{H}_2\text{O}$ solution for the 28 <sup>th</sup> hour of bubbling. ....  | 68 |
| Figure 5.8: Gamma-ray spectrum of $\text{Th}(\text{NO}_3)_4 \cdot 6\text{H}_2\text{O}$ solution for 66 <sup>th</sup> hour of bubbling. ....  | 69 |
| Figure 5.10: The net count rate of the Tl-208 (2614 keV) photopeak as a function of time. ....   | 70 |
| Figure 5.11: The net count rate of the Ac-228 (911keV) photopeak as a function of time. ....   | 71 |
| Figure 5.12: The normalized Tl-208 (2614 keV) and Ac-228 (911 keV) count rate as a function<br>of time. ....   | 72 |
| Figure 5.13: The MCNPx corrected simulated gamma-ray detection efficiencies for the NaI(Tl)<br>detector geometry and the small bottle. ....  | 73 |

|  |    |
|--|----|
| Figure 5.14: The Tl-208 activity (diamond) as calculated with the Bateman equations (Eq. 2.25 with a fitted value of the Rn-220 source of $S= 50$ Bq) and the measured, corrected activity (square) using the 2614 keV photopeak, as a function of the time.....                               | 75 |
| Figure 5.15: The measured Tl-208 (2614 keV) atoms number (square) and the calculated number of Tl-208 atoms using the Bateman equations (diamond) as a function of time. ....  | 76 |
| Figure 5.16: Gamma ray spectrum for the first hour of bubbling using flow rate 1 L/min.....  | 77 |
| Figure 5.17: Gamma ray spectrum for the 12 <sup>th</sup> hour of bubbling using a flow rate of 1 L/min. ..   | 77 |
| Figure 5.18: Combined gamma ray spectra for the first hour and 12th hour of bubbling.....  | 78 |
| Figure 5.19: The corrected activity of Tl-208 (2614 keV) as a function of time using a flow rate of 1 L/min. ....  | 79 |
| Figure 5.20: The gamma ray spectrum lines of the background when the detector was shielded by the lead castle. Comparison to Figure 5.5 shows a large reduction in background.....   | 80 |
| Figure 5.21: Gamma ray spectrum for the first hour of bubbling, with the detector shielded by the lead castle.....   | 81 |
| Figure 5.22: Gamma ray spectrum for the 72 <sup>nd</sup> hour of bubbling when the detector is shielded by the lead castle.....  | 81 |
| Figure 5.23: The gamma ray spectra of bubbling for the first hour and the 72 <sup>nd</sup> hour.....   | 82 |
| Figure 5.24: The measured activity (brown circle) using Tl-208 (2614 keV) as a function of time fitted to the new predict calculated activity (blue circle) using the Bateman equation with $S = 45$ Bq.....   | 82 |
| Figure 5.25: The measured number of Tl-208 (2614 keV) fitted to the calculated Bateman (using the new initial activity) equations (2.25) as a function of time. ....   | 83 |
| Figure 5.26: The blue circles show the Tl-208 (2614 keV) decreasing as a function of time without shielding (66 hrs measurements), with the flow rate 0.6 L/min. The brown circles show the Tl-208 (2614 keV) decreasing as a function of time with shielding and a flow rate of 1 L/min. .... | 84 |

|   |     |
|---|-----|
| Figure 5.27: The Rn-220 activity concentration at the exit stream of the pipe as obtained with the RAD7 (circle). The solid line indicates the mean calculated value. The dashed line indicates the uncertainties. ....   | 85  |
| Figure 5.28: Activity concentration as measured by the RAD7 during the initial few minutes of pumping for a cycle of 2 minutes. The pump was started at around $t = 2$ min. This figure shows that there was a clear spike in the initial measurements and then there was a steady state after about 6 minutes from the beginning. .... | 88  |
| Figure 5.29: Rn-220 activity concentration using a flow rate 1 L/min. The circles indicate the measured activity concentration. The solid line indicates the calculated activity concentration. The dashed lines indicate the standard deviation. ....  | 89  |
| Figure 5.30: The Rn-220 activity concentration in the exit stream of the pipe as obtained with the RAD7 (blue circles). The brown circles indicate the calculated activity concentration. The modified bubbler, humidified air and flow rate of 1 L/min were used. ....   | 90  |
| Figure 6.1: Experimental set up for measuring the gamma rays released from different heights of $\text{Th}(\text{NO}_3)_4 \cdot 6\text{H}_2\text{O}$ in the sample bottle. ....   | 98  |
| Figure 6.2: Gamma-ray spectrum for 15 mm height of $\text{Th}(\text{NO}_3)_4 \cdot 6\text{H}_2\text{O}$ .....   | 99  |
| Figure 6.3: Gamma-ray spectrum for the 35 mm height of $\text{Th}(\text{NO}_3)_4 \cdot 6\text{H}_2\text{O}$ .....   | 99  |
| Figure 6.4: Gamma-ray spectrum for 45 mm height of $\text{Th}(\text{NO}_3)_4 \cdot 6\text{H}_2\text{O}$ .....   | 100 |
| Figure 6.5: Gamma-ray spectrum for 60 mm height of $\text{Th}(\text{NO}_3)_4 \cdot 6\text{H}_2\text{O}$ .....   | 100 |
| Figure 6.6: Gamma-ray spectrum for 75 mm height of $\text{Th}(\text{NO}_3)_4 \cdot 6\text{H}_2\text{O}$ .....   | 101 |
| Figure 6.7: The variation of the counts of Tl-208 (2614 keV) with height. ....  | 103 |

# List of Tables

|   |    |
|---|----|
| <b>Table 1. 1:</b> Rn-220 properties.....   | 1  |
| <b>Table 2.1:</b> Data used in the Bateman equation model.....  | 15 |
| <b>Table 2.2:</b> Rn-222 and Rn-220 daughters that can be detecting by the RAD7.....  | 20 |
| <b>Table 3. 1</b> Summary of measurement system for Rn-220.....   | 31 |
| <b>Table 4.1:</b> The measured masses of some quantities used in the study. ....  | 46 |
| <b>Table 4.2:</b> Gamma-ray lines and associated branching ratios used for efficiency calibration<br>(Firestone <i>et al.</i> , 1996, <a href="http://www.nucleide.org">http://www.nucleide.org</a> ).....  | 49 |
| <b>Table 4.3:</b> The measured nuclei in the Th-232 reference source .....  | 51 |
| <b>Table 4.4 :</b> The parameters used in the MCNPX simulation .....  | 53 |
| <b>Table 5.1:</b> Gamma energy lines and their associated efficiencies .....  | 63 |
| <b>Table 5.2:</b> The efficiencies in the range of 239 keV to 2614 keV simulated using MCNPx for<br>the geometry of the NaI(Tl) detector and the partially filled small bottle with KCl solution. The<br>KCl solution in the same geometry was used to normalize the efficiency curve. .... | 73 |
| <b>Table 5.3:</b> Factors influencing the uncertainty based on equation 5.7.....  | 87 |

# CHAPTER 1

## Introduction

### 1.1 Overview of Thoron (Rn-220)

Thoron (Rn-220) is a radioactive noble gas similar to Radon (Rn-222). Both of them are isotopes of the element Radon (Rn). Radon (Rn), the element with atomic number 86 has more than thirty isotopes known but only two isotopes Thoron (Rn-220) and Radon (Rn-222), significantly contribute to the environmental radiation dose. This study will focus on Thoron (Rn-220). Rn-220 is the only gas nuclide in the thorium decay series (Th-232) which is found naturally in the environment. Rn-220 is formed directly by decay of the Radium (Ra-224) radionuclide. Rn-220 is colourless, odourless and tasteless, thus it is not possible to detect it by human sense alone. Some of the properties of Rn-220 are listed in Table 1.1 (Ramachandran, 2010; Ramachandran, S Athish, 2014).

**Table 1. 1:** Rn-220 properties

|                                       |   |
|---------------------------------------|---|
| Boiling point                         | -61.8° C  |
| Melting point                         | -71° C  |
| Partitioning Coefficient in water at: |   |
| 0° C                                  | 0.5   |
| 20° C                                 | 0.25  |
| 50° C                                 | 0.14  |
| Solubility in Acetone                 | 8.0 at 0° C   |
| Diffusion Coefficient in air          | 0.1 cm <sup>2</sup> s <sup>-1</sup> at STP                    |
| Diffusion coefficient in water        | 1.1×10 <sup>-5</sup> cm <sup>2</sup> s <sup>-1</sup> at 18 °C |



Rn-220 is a result of the decay series (Th-232) of the thorium nuclide and it has a relatively short half-life of 55.6 s. Eventually, after a series of decays, the Th-232 series ends up with a stable nuclide lead (Pb-208) as shown in Figure 1.1.

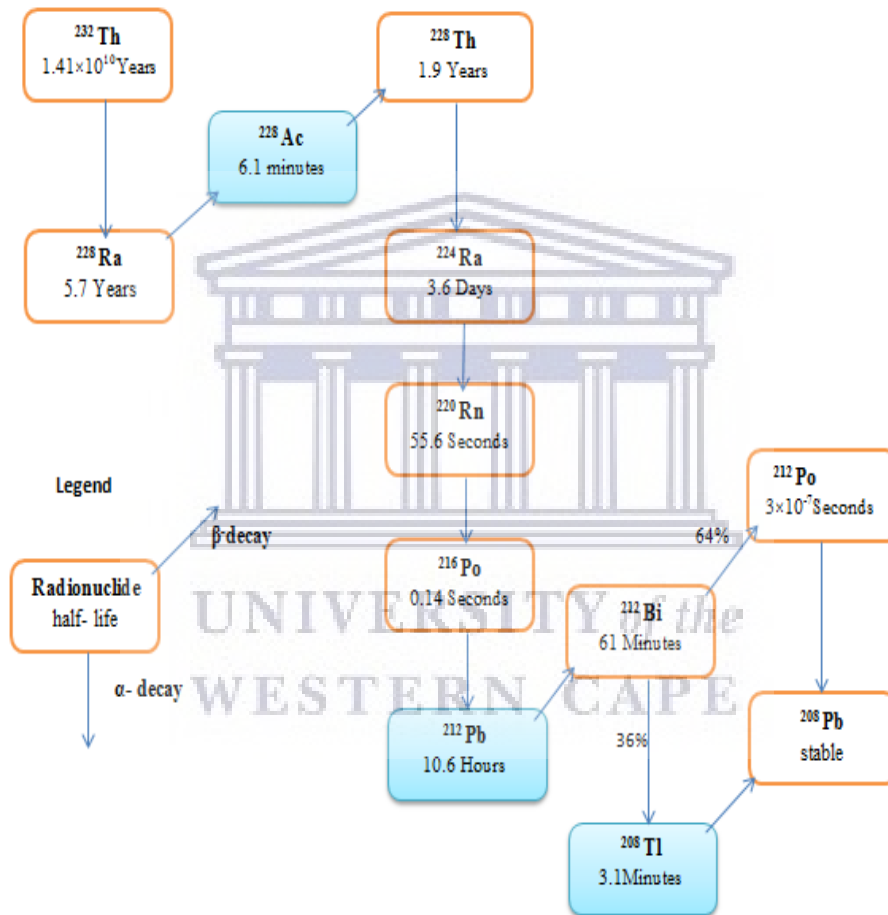


**Figure 1. 1:** A schematic illustration of the thorium series. The cyan boxes represent  $\gamma$ -ray emitting radionuclides

Rn-220 was discovered in 1899 by R.B. Owens at McGill University with some assistance from Ernest Rutherford (Schery, 1990). In that early time, the nucleus was not known, therefore, they named it thoron emanation. Rn-220 gas is created at the top layer of the earth's surface through the

diffusion from the closest source of Rn-220 which is located along the soil and rocks. Rn-220 gas can be produced in the indoor and premises mainly from the surface of walls which are rich in Th-232 (Schery, 1990).

Rn-220 and Rn-222 and their daughters contribute almost 50% of the total average annual effective dose to individuals (Dinh Chau *et al.*, 2011). This significant contribution increases the chance of getting lung cancer (BEIR 1999; Kohn, 2006). Rn-220 in the previous decades was not taken into account as a radiological hazard since it has a relatively short half-life. However, Rn-220 and its daughters have recently been recognized as a health hazard and need some attention since they can contribute to the radiation dose in some places (Akiba *et al.*, 2010). It is therefore very important to measure the Rn-220 concentration and estimate its activity concentration indoor and in workplaces as well. To estimate the dose of Rn-220, measurements of its daughters will be needed. However, it is hard to measure the Rn-220 concentration accurately due to its relatively short half-life, and the calibration of Rn-220 monitors also needs more development.

Several monitors have been developed and many methods used to measure Rn-220 (Gaware *et al.*, 2011; Kumar *et al.*, 2014; Irlinger, 2015; Pornnumpa *et al.*, 2018). Researchers kept developing the monitors and methods to estimate the radiological hazard accurately. Rn-220 monitors need to be calibrated and tested against a reference atmosphere, in other words, a standard activity concentration. Researchers in Germany (PTB) created a reference atmosphere of Rn-220 based on a certified activity standard of Th-232 (Röttger *et al.*, 2010). The National Henri Becquerel Laboratory (LNHB) in France developed a Rn-220 activity standard to be used in calibrating monitors (Sabot *et al.*, 2015)

NIRS (National Institute of Radiological Sciences, Japan, Chiba), have the facilities to calibrate Rn-220 monitors using a 150 L volume chamber. These facilities are available to calibrate Rn-222 monitors as well. However the Rn-222 chamber is bigger compared with the Rn-220 chamber and is about 24 400 L, big enough to walk inside it. These two chambers are used for conducting regular international intercomparison measurements checking and calibrating Rn-220 and Rn-222 detectors of the different laboratories from different countries (Janik *et al.*, 2014).

A Rn-220 chamber with a total volume 300 L was established at Fudan University, China. The main purpose of this chamber was the calibration and intercomparison of Rn-220 measurements. The chamber provided a Rn-220 source made from lantern mantle which was saturated with Th-232. Rn-220 sources were prepared and designed so as to be in the lattice shapes and the geometry was taken into account. The environmental parameters such as temperature and humidity are well controlled and programmed (Zhao *et al.*, 2010).

Instead of sending the Rn-220 detectors overseas in order to calibrate them, a Rn-220 source was developed in this work and used to investigate the measurements of Rn-220 detectors in our local facilities. Rn-220 can be measured by several detectors which can be associated with different methods. Examples of different Rn-220 detectors include nuclear track detectors, scintillation cell detectors (Lucas cell), solid scintillation nuclear detectors, gamma spectrometer detectors, electret ion chambers and solid-state detectors. Some of these detectors operate by passive methods and some by active methods. In our study, we investigated a solid state detector type namely the RAD7 which is available in our nuclear laboratory; more details will be provided in Chapter 2.

## 1.2 Motivation and aim of the study

Reports from detailed reliable studies such as (UNSCEAR, 2000) and BEIR(1999) show that the probability of uranium mine workers contracting lung cancer was enhanced, due to long-term exposure to Rn-222 and its daughters. Due to these studies there is great interest in Rn-222 measurements in the environment. As a result of these studies extensive data about Rn-222 is available. On the other hand, data on Rn-220 is scarce due to the general assumption that its concentration level is negligible due to its shorter half-life (55.6 s), and therefore its contribution to inhalation dose is often neglected, in the presence of the other stronger sources of natural radiation.

However, more recent research projects report that there can be a high Rn-220 concentration in the living environment (Vaupotič *et al.*, 2013; Szabó *et al.*, 2014; Chege *et al.*, 2015; Ramola *et al.*, 2016; Phon *et al.*, 2015). More studies may be required to have more data on Rn-220 concentration in the environment so as to have an idea of inhalation dose. It has been long recognized that Rn-220 can be an issue in the working environment in specific mines and in

buildings where Th-232 rich minerals, sands or products are handled in large quantities (Steinhäusler, 1996). Some studies conducted in Asia showed a high concentration level of Rn-220, which indicates a high possibility that individuals can be exposed to Rn-220 and its daughters (Doi and Kobayashi, 1994; Guo, Sun and Zhuo, 2000; Shang *et al.*, 2008).

Since Rn-220 is a decay product of Th-232 as mentioned in section one, a recent study revealed a high concentration of Th-232 in mineral sands that are mined on the west coast of South Africa (de Villiers, 2011). The estimated value of reasonably assured reserves (RAR) of Th-232 in South Africa is about 18000 tons (Ramachandran, 2010), which indicates the high probability of elevated Rn-220 in such places. In the last few years, new approaches to Rn-220 monitors were developed and used to collect several representative data for Rn-220 concentration measurements (Yamada *et al.*, 2005; Zhuo *et al.*, 2002; Guo *et al.*, 1995). "It was clear that all Rn-220 measuring instruments need a uniform standard with which they can be calibrated so that all the measurements are comparable and the uncertainty of each individual measuring instrument" explains Annette Röttger (Röttger *et al.*, 2010).

Due to an increase of Rn-220 measurements as reported in previous sections, it is clear that Rn-220 has become a radiation protection issue. To achieve accurate measurements, well calibrated Rn-220 detectors are required. In order to calibrate Rn-220 monitors regularly a well-defined chamber and standard source are needed. Solid Rn-220 sources have the same disadvantage of solid Rn-222 sources: the release of Rn-222 depends on the temperature and pressure in an undetermined and irreproducible way or may just be very low (Wang, Zhang and Guo, 2017). **For this reason, we have developed a Rn-220 source that uses a thorium nitrate solution ( $\text{Th}(\text{NO}_3)_4 \cdot 6\text{H}_2\text{O}$ ) in water as the source.**

RAD7 (www.durridge.com) is a radon detector based on a solid-state alpha detector which can measure Rn-220 and Rn-222 simultaneously and separately as well. It has been used in measuring Rn-222 and shows an accurate response to Rn-222 detection due to the several calibration methods and reliable Rn-222 chambers that are widely available (Janik, 2017). However, for measuring Rn-220 with its short half-life (55.6 s) and due to limitations in the standard chamber and lack of reliable Rn-220 sources, more development and calibration is needed to characterize its detection and response (Tan *et al.*, 2014).

The main aim of this study is to develop a simple and cheap, but reliable Rn-220 standard source, which can be used to investigate and check Rn-220 detectors. This technique will be achieved by using  $\text{Th}(\text{NO}_3)_4 \cdot 6\text{H}_2\text{O}$  crystals dissolved in distilled water; as discussed in Chapter four.

The objectives to achieve the main aim of the study are:

- Develop a theoretical model using the Bateman equations.
- Characterize the prepared Rn-220 source using a Hyper Pure Germanium detector system (HPGe).
- Use the MCNPX program to simulate the efficiency of the NaI(Tl) detector.
- Determine the strength of the source using a NaI(Tl) detector.
- Check the stability of the Rn-220 source by conducting measurements over long time.
- Check the reproducibility of the developed Rn-220 source by using different flow rates.
- Use the RAD7 detector to measure the Rn-220 concentration from the Rn-220 source, developed using thorium nitrate dissolved in water.

### 1.3 Structure of the thesis

The remaining chapters of this thesis are structured as follows in the next six chapters.

Chapter two will present the basic laws of radioactivity, types of radioactive decays, the interaction of the gamma rays with matter and the derivation of the Bateman equation which is the theoretical model for the decay products in this study. Moreover, some detectors relevant to this study will be presented.

Chapter three consists of two sections. Section one will present the review of methods and the experimental techniques developed for measuring Rn-220 in different laboratories around the world. Section two will present studies conducted to develop Rn-220 sources.

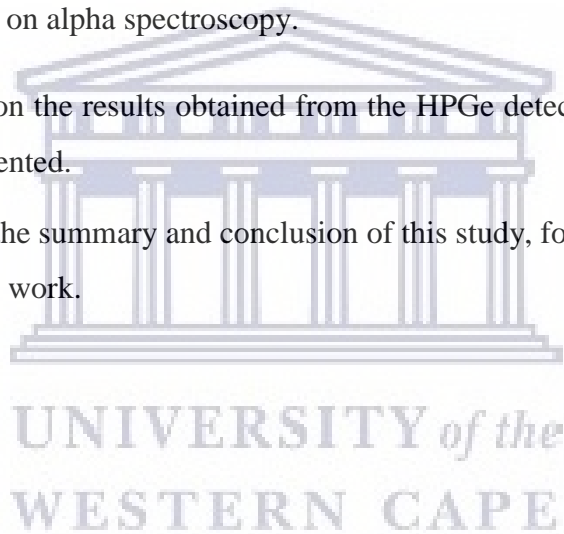
In Chapter four, the preparation of a Rn-220 source from a solution of  $\text{Th}(\text{NO}_3)_4 \cdot 6\text{H}_2\text{O}$  will be proposed, with a sodium iodide NaI(Tl) detector that simultaneously measures the gamma rays from the solution to characterize the percentage of Rn-220 that is removed from the solution by

bubbling. The RAD7 (Durridge 2015) Rn-222 / Rn-220 detector based on alpha spectroscopy of the Rn-222/Rn-220 daughters was used to measure the Rn-220 concentration. Moreover, the HPGe gamma spectrometer at (iThemba LABS) in Faure, South Africa was used in the characterization of the Rn-220 source. The setup of the novel method for developing a Rn-220 standard source to check the Rn-220 detectors (RAD7 in this study) measurements will be presented. The experiment is based on the extraction of the Rn-220 by bubbling air through the  $\text{Th}(\text{NO}_3)_4 \cdot 6\text{H}_2\text{O}$  solution using an aerator.

In Chapter five, the results of the measurements will be presented, which will include the HPGe measurements (the Rn-220 source characterisation), the NaI(Tl) detector measurements based on the gamma spectroscopy (the novel method based on the bubbling air through the source) and RAD7 measurements based on alpha spectroscopy.

In Chapter six discussions on the results obtained from the HPGe detector, NaI(Tl) detector and RAD7 detector will be presented.

Chapter seven will present the summary and conclusion of this study, followed by recommendations for future work.



# CHAPTER 2

## Radiation detection and Bateman model

### 2.1 Introduction

In this chapter we will present the concepts of radioactivity and the detection techniques of different types of radiation such as gamma radiation and alpha particles. Also we will discuss the Bateman model which describes the radioactivity in a decay chain in terms of the abundance and decay rates. The model is applied for the Pb-212 decay chain and developed by involving a source term of the Rn-220 gas. The model agreed with the experimental data performed for this project as it will be presented in details in Chapter five.

### 2.2 Simple Radioactive Decay: Half-life and Decay Constant

The usual decay law leads to the expression for the decay of a radionuclide as a function of the time(t)

$$N(t) = N^0 e^{-\lambda t} \quad (2.1)$$

where  $N(t)$  is the number of remaining nuclei after time  $t$ ,  $N^0$  is the number of nuclei at time  $t=0$  and  $\lambda$  is the decay constant. The half-life ( $t_{\frac{1}{2}}$ ) can be written in terms of the decay constant ( $\lambda$ )

$$t_{\frac{1}{2}} = \frac{\ln 2}{\lambda} \quad (2.2)$$

Another case of radioactive decay occurs when the parent nuclide decays to a daughter nuclide then the daughter decays to granddaughter and so on. To derive equations for this situation, it is assumed that the radioactive parent is  $N_p$  and its decay constant is  $\lambda_p$ ,  $N_d$  is the daughter nuclide and its decay constant is  $\lambda_d$ , then the decay equations will be:

$$\frac{dN_p}{dt} = -\lambda_p N_p \quad (2.3)$$

$$\frac{dN_d}{dt} = \lambda_p N_p - \lambda_d N_d \quad (2.4)$$

The solution of equation (2.3) above is

$N_p = N_p^0 e^{-\lambda_p t}$ . If the value of  $N_p$  is substituted in equation (2.4) and rearranged, and then integrated, the solution of the equation becomes:

$$N_d = \frac{\lambda_p}{\lambda_d - \lambda_p} N_p^0 (e^{-\lambda_p t} - e^{-\lambda_d t}) \quad (2.5)$$

We can get the ratio of the daughter nuclide ( $N_d$ ) to the parent nuclide ( $N_p$ ) at any time in the decay chain. This ratio can be represented as:

$$\frac{\lambda_d N_d}{\lambda_p N_p} = \frac{\lambda_d}{\lambda_d - \lambda_p} (1 - e^{-(\lambda_d - \lambda_p)t}) \quad (2.6)$$

We can use equation (2.6) to study two important conditions in radioactive decay of the nuclide, the secular equilibrium and transient equilibrium. In the secular equilibrium the decay constant of the daughter nuclide must be much greater than the parent nuclide, i.e.  $\lambda_d \gg \lambda_p$  and in this case the right side in equation (2.6)  $\sim 1$  and then

$$\lambda_d N_d = \lambda_p N_p \quad (2.7)$$

For the transient equilibrium state to occur, the decay constant of the daughter nuclide should be greater than the decay constant of the parent i.e.  $\lambda_d > \lambda_p$  therefore the right side of equation (2.6) is greater than unity.

In a very long radioactive nuclei chain such as for three or more successive decays, one can use the Bateman equations to calculate the number of the nuclide of interest at any time (Lilley, 2001) as discussed in the next section

### 2.3 Bateman equations

The Bateman equations are a set of differential equations derived first by Ernest Rutherford in 1905 to explain the radioactive decay chain of a long and complicated decay sequence. After 5 years, Harry Bateman developed an analytical solution for the equations. The Bateman equations depend on the initial activity of the nuclides and the time period (Magill, 2005).



Since there could be different decay modes for a nuclide, the branching ratio is included in the solution. The general solution for the nuclide involving several decays can be written as

$$N_n(t) = \sum_{i=1}^n \left[ N_i^0 \times \left( \prod_{j=1}^{n-1} \lambda_j \right) \times \left( \sum_j \left( \frac{e^{-\lambda_j t}}{\prod_{p=i, p \neq j}^n (\lambda_p - \lambda_j)} \right) \right) \right] \quad (2.8)$$

Where

$N_i^0$  = The initial number of nuclei,  $i = 1, 2, 3, \dots$

$\lambda_j$  = decay constant  $j = 1, 2, 3, \dots$

It should be noted that equation (2.8) can be modified to include source terms for which there are nuclei contributing externally at a constant rate. For this particular study, the Po-216 will be treated as the “parent” that during the bubbling which has a source term namely the Rn-220 in the solution that is not pumped out.

In the following we develop a model using the Bateman equations, which includes a source term, to express the concentration of the Rn-220 daughters as a function of the time.

In our method when the air is bubbled through the solution, not all the created Rn-220 enters the air and leaves the solution. A fraction of the Rn-220 decays in the solution so, this fraction keeps feeding the post decay nuclides in the chain and prevents the Tl-208 decay from tending to zero which leads to an equilibrium state. It is important to realize that the Tl-208 decay rate depends largely on the Pb-212 decay. Taking into account the very small half-life of Po-216 the daughter of Rn-220 (see Fig 1.1), Pb-212 effectively is the start of the decay chain.

$$\frac{dN_{Pb}}{dt} = S - \lambda_{Pb} N_{Pb} \quad (2.9)$$

$$\frac{dN_{Bi}}{dt} = \lambda_{Pb} N_{Pb} - \lambda_{Bi} N_{Bi} \quad (2.10)$$

$$\frac{dN_{Tl}}{dt} = \lambda_{Bi} N_{Bi} - \lambda_{Tl} N_{Tl} \quad (2.11)$$

Where  $N_{Pb}$ ,  $N_{Bi}$  and  $N_{Tl}$  are the number of atoms of Pb-212, Bi-212 and Tl-208 respectively.

$\lambda_{Pb}$ ,  $\lambda_{Bi}$  and  $\lambda_{Tl}$  are the decay constants of the above mentioned atoms.

S is the source term (the strength of a source feeding the Pb-212 isotope in this case.)

Solving equation (2.9) by separation of variables and integrating both sides

$$\int_{N_{Pb}^0}^{N_{Pb}} \frac{dN_{Pb}}{(S - \lambda N_{Pb})} = \int_0^t dt$$

$-\frac{1}{\lambda_{Pb}} \ln(S - \lambda_{Pb} N_{Pb})$  where the integration goes from  $N_{Pb}^0$  to  $N_{Pb}$ , and the time from 0 to t

$$\ln\left(\frac{S - \lambda_{Pb} N_{Pb}}{S - \lambda_{Pb} N_{Pb}^0}\right) = -\lambda_{Pb} t$$

Take the exponential for both side and the equation becomes

$$\frac{S - \lambda_{Pb} N_{Pb}}{S - \lambda_{Pb} N_{Pb}^0} = e^{-\lambda_{Pb} t}$$

Then,  $S - \lambda_{Pb} N_{Pb} = (S - \lambda_{Pb} N_{Pb}^0) e^{-\lambda_{Pb} t}$  and by rearrangement the equation will be

$$N_{Pb} = \frac{S}{\lambda_{Pb}} (1 - e^{-\lambda_{Pb} t}) + N_{Pb}^0 e^{-\lambda_{Pb} t} \quad (2.12)$$

To solve  $\frac{dN_{Bi}}{dt} = \lambda_{Pb} N_{Pb} - \lambda_{Bi} N_{Bi}$  (2.13)

Let  $N_{Bi}(t) = A e^{-\lambda_{Pb} t} + B e^{-\lambda_{Bi} t} + \frac{S}{\lambda_{Bi}} + N_{Bi}^0 e^{-\lambda_{Bi} t}$  (2.14)

and by differentiating:

$$\frac{dN_{Bi}}{dt} = -\lambda_{Pb} A e^{-\lambda_{Pb} t} - \lambda_{Bi} B e^{-\lambda_{Bi} t} - \lambda_{Bi} N_{Bi}^0 e^{-\lambda_{Bi} t} \quad (2.15)$$

Substituting the values of  $N_{Pb}$  and  $N_{Bi}$  in equation (2.12) we get

$$\frac{dN_{Bi}}{dt} = \lambda_{Pb} \left[ \frac{S}{\lambda_{Pb}} (1 - e^{-\lambda_{Pb}t}) + N_{Pb}^0 e^{-\lambda_{Pb}t} \right] - \lambda_{Bi} [-\lambda_{Pb} A e^{-\lambda_{Pb}t} - \lambda_{Bi} B e^{-\lambda_{Bi}t} - \lambda_{Bi} N_{Bi}^0 e^{-\lambda_{Bi}t}]$$

By re-arranging

$$\frac{dN_{Bi}}{dt} = (-S - \lambda_{Bi} A + \lambda_{Pb} N_{Pb}^0) e^{-\lambda_{Pb}t} - \lambda_{Bi} (B + N_{Bi}^0) e^{-\lambda_{Bi}t} \quad (2.16)$$

Comparing the coefficients of  $e^{-\lambda_{Pb}t}$  with equation (2.16)

Then:

$$-\lambda_{Pb} A = -S - \lambda_{Bi} A + \lambda_{Pb} N_{Pb}^0 \text{ and solving for A:}$$

$$\text{Then we get } A = \frac{-S + \lambda_{Pb} N_{Pb}^0}{-\lambda_{Pb} + \lambda_{Bi}} \quad (2.17),$$

$$\text{The initial conditions, at } t = 0, \quad N_{Bi}(t = 0) = N_{Bi}^0$$

Then apply the conditions in equation (2.15), then we get

$$0 = A + B + \frac{S}{\lambda_{Bi}} \text{ so } B = -A - \frac{S}{\lambda_{Bi}}$$

Substituting the value of A, we get

$$B = \frac{S - \lambda_{Pb} N_{Pb}^0}{-\lambda_{Pb} + \lambda_{Bi}} - \frac{S}{\lambda_{Bi}} \quad (2.18)$$

$$\text{Then we try to solve (2.13) } \frac{dN_{Tl}}{dt} = \lambda_{Bi} N_{Bi} - \lambda_{Tl} N_{Tl}$$

$$\text{Let } N_{Tl} = C e^{-\lambda_{Bi}t} + D e^{-\lambda_{Tl}t} + E e^{-\lambda_{Pb}t} + \frac{S}{\lambda_{Tl}} + N_{Tl}^0 e^{-\lambda_{Tl}t} \quad (2.19),$$

then,

$$\frac{dN_{Tl}}{dt} = -\lambda_{Bi} C e^{-\lambda_{Bi}t} - \lambda_{Tl} D e^{-\lambda_{Tl}t} - \lambda_{Pb} E e^{-\lambda_{Pb}t} - \lambda_{Tl} N_{Tl}^0 e^{-\lambda_{Tl}t} \quad (2.20)$$

Substitute the values of  $N_{Bi}$  and  $N_{Tl}$  in equation (2.11)

$$\frac{dN_{Tl}}{dt} = \lambda_{Bi} (A e^{-\lambda_{Pb}t} + B e^{-\lambda_{Bi}t} + \frac{S}{\lambda_{Bi}} + N_{Bi}^0 e^{-\lambda_{Bi}t}) - \lambda_{Tl} (C e^{-\lambda_{Bi}t} + D e^{-\lambda_{Tl}t} + E e^{-\lambda_{Pb}t} + \frac{S}{\lambda_{Tl}} + N_{Tl}^0 e^{-\lambda_{Tl}t})$$

Which leads to

$$\frac{dN_{Tl}}{dt} = (\lambda_{Bi} A - \lambda_{Tl} E) e^{-\lambda_{Pb}t} + (\lambda_{Bi} B + \lambda_{Bi} N_{Bi}^0 - \lambda_{Tl} C) e^{-\lambda_{Bi}t} - (\lambda_{Tl} D + \lambda_{Tl} N_{Tl}^0) e^{-\lambda_{Tl}t} \quad (2.21)$$

By comparing the factor of  $e^{-\lambda_{Pb}t}$  using equation (2.20) we get

$$-\lambda_{Pb} E = \lambda_{Bi} A - \lambda_{Tl} E \quad \text{Rearranging and substituting the value of A}$$

$$(-\lambda_{Pb} + \lambda_{Tl}) E = \lambda_{Bi} \left( \frac{-S + \lambda_{Pb} N_{Pb}^0}{-\lambda_{Pb} + \lambda_{Bi}} \right)$$

$$E = \frac{-\lambda_{Bi} S + \lambda_{Pb} \lambda_{Bi} N_{Pb}^0}{(-\lambda_{Pb} + \lambda_{Bi})(-\lambda_{Pb} + \lambda_{Tl})} \quad (2.22)$$

Then comparing the factors of  $e^{-\lambda_{Bi}t}$  using equation (2.20) and substituting the value of B and rearrangement we get

$$C(\lambda_{Tl} - \lambda_{Bi}) = \lambda_{Bi} \left( \frac{S - \lambda_{Pb} N_{Pb}^0}{-\lambda_{Pb} + \lambda_{Bi}} - \frac{S}{\lambda_{Bi}} \right) + \lambda_{Bi} N_{Bi}^0$$

$$C(\lambda_{Tl} - \lambda_{Bi}) = \frac{S\lambda_{Pb} - \lambda_{Pb} \lambda_{Bi} N_{Pb}^0}{-\lambda_{Pb} + \lambda_{Bi}} + \lambda_{Bi} N_{Bi}^0 \quad \text{Divide both sides by } (\lambda_{Tl} - \lambda_{Bi}):$$

$$C = \frac{S\lambda_{Pb} - \lambda_{Pb} \lambda_{Bi} N_{Pb}^0}{(-\lambda_{Pb} + \lambda_{Bi})(\lambda_{Tl} - \lambda_{Bi})} + \frac{\lambda_{Bi} N_{Bi}^0}{(\lambda_{Tl} - \lambda_{Bi})} \quad (2.23)$$

To get the value of D apply the boundary conditions in equation (2.19) at  $t=0$   $N_{Tl}^0 = N_{Tl}$

So the equation will be

$$0 = C + D + E + \frac{S}{\lambda_{Tl}}$$

$$D = -C - E - \frac{S}{\lambda_{Tl}} \text{ Substituting the values of } C \text{ and } E$$

$$D = \frac{-S\lambda_{Pb} + \lambda_{Pb} \lambda_{Bi} N_{Pb}^0}{(-\lambda_{Pb} + \lambda_{Bi})(\lambda_{Tl} - \lambda_{Bi})} - \frac{\lambda_{Bi} N_{Bi}^0}{(\lambda_{Tl} - \lambda_{Bi})} - \frac{-\lambda_{Bi} S + \lambda_{Pb} \lambda_{Bi} N_{Pb}^0}{(-\lambda_{Pb} + \lambda_{Bi})(-\lambda_{Pb} + \lambda_{Tl})} - \frac{S}{\lambda_{Tl}} \quad (2.24), \text{ then substitute}$$

the values of  $E$ ,  $C$  and  $D$  in this equation:

$$N_{Tl} = C e^{-\lambda_{Bi} t} + D e^{-\lambda_{Tl} t} + E e^{-\lambda_{Pb} t} + \frac{S}{\lambda_{Tl}} + N_{Tl}^0 e^{-\lambda_{Tl} t} \quad (2.19)$$

$$N_{Tl} = \left[ \frac{S\lambda_{Pb} - \lambda_{Pb} \lambda_{Bi} N_{Pb}^0}{(-\lambda_{Pb} + \lambda_{Bi})(\lambda_{Tl} - \lambda_{Bi})} + \frac{\lambda_{Bi} N_{Bi}^0}{(\lambda_{Tl} - \lambda_{Bi})} \right] e^{-\lambda_{Bi} t} + \left[ \frac{-S\lambda_{Pb} + \lambda_{Pb} \lambda_{Bi} N_{Pb}^0}{(-\lambda_{Pb} + \lambda_{Bi})(\lambda_{Tl} - \lambda_{Bi})} - \frac{\lambda_{Bi} N_{Bi}^0}{(\lambda_{Tl} - \lambda_{Bi})} - \right.$$

$$\left. \frac{-\lambda_{Bi} S + \lambda_{Pb} \lambda_{Bi} N_{Pb}^0}{(-\lambda_{Pb} + \lambda_{Bi})(-\lambda_{Pb} + \lambda_{Tl})} - \frac{S}{\lambda_{Tl}} \right] e^{-\lambda_{Tl} t} + \left[ \frac{-\lambda_{Bi} S + \lambda_{Pb} \lambda_{Bi} N_{Pb}^0}{(-\lambda_{Pb} + \lambda_{Bi})(-\lambda_{Pb} + \lambda_{Tl})} \right] e^{-\lambda_{Pb} t} + \frac{S}{\lambda_{Tl}} + N_{Tl}^0 e^{-\lambda_{Tl} t}$$

$$N_{Tl} = \frac{S\lambda_{Pb}}{(-\lambda_{Pb} + \lambda_{Bi})(\lambda_{Tl} - \lambda_{Bi})} e^{-\lambda_{Bi} t} - \frac{\lambda_{Pb} \lambda_{Bi} N_{Pb}^0}{(-\lambda_{Pb} + \lambda_{Bi})(\lambda_{Tl} - \lambda_{Bi})} e^{-\lambda_{Bi} t} + \frac{\lambda_{Bi} N_{Bi}^0}{(\lambda_{Tl} - \lambda_{Bi})} e^{-\lambda_{Bi} t} - \frac{S\lambda_{Pb}}{(-\lambda_{Pb} + \lambda_{Bi})(\lambda_{Tl} - \lambda_{Bi})} e^{-\lambda_{Tl} t} + \frac{\lambda_{Pb} \lambda_{Bi} N_{Pb}^0}{(-\lambda_{Pb} + \lambda_{Bi})(\lambda_{Tl} - \lambda_{Bi})} e^{-\lambda_{Tl} t} - \frac{\lambda_{Bi} N_{Bi}^0}{(\lambda_{Tl} - \lambda_{Bi})} e^{-\lambda_{Tl} t} + \frac{\lambda_{Bi} S}{(-\lambda_{Pb} + \lambda_{Bi})(-\lambda_{Pb} + \lambda_{Tl})} e^{-\lambda_{Tl} t} - \frac{\lambda_{Pb} \lambda_{Bi} N_{Pb}^0}{(-\lambda_{Pb} + \lambda_{Bi})(-\lambda_{Pb} + \lambda_{Tl})} e^{-\lambda_{Tl} t} - \frac{S}{\lambda_{Tl}} e^{-\lambda_{Tl} t} - \frac{\lambda_{Bi} S}{(-\lambda_{Pb} + \lambda_{Bi})(-\lambda_{Pb} + \lambda_{Tl})} e^{-\lambda_{Pb} t} + \frac{\lambda_{Pb} \lambda_{Bi} N_{Pb}^0}{(-\lambda_{Pb} + \lambda_{Bi})(-\lambda_{Pb} + \lambda_{Tl})} e^{-\lambda_{Pb} t} + \frac{S}{\lambda_{Tl}} + N_{Tl}^0 e^{-\lambda_{Tl} t} \quad (2.25)$$

We used equation (2.25) to fit our experimental data.

The above developed model was used to fit our experimental data (see chapter 5 section 3). After the activity of the Rn-220 source was measured using the HPGe detector, it was used to obtain the values for the model above. It should be noted that all the values in the model were known (see Table 2.1) except the source term (S) that feeds the Rn-220 daughters from the Rn-220 that decays in the solution before being pumped out. S can be found from the fit.

**Table 2.1:** Data used in the Bateman equation model.

|  |                                     |
|--|-------------------------------------|
| Activity of the source   | 331 Bq                              |
| $\lambda_{Pb}$   | $1.8 \times 10^{-5} \text{ s}^{-1}$ |
| $\lambda_{Bi}$   | $1.9 \times 10^{-4} \text{ s}^{-1}$ |
| $\lambda_{Tl}$   | $3.7 \times 10^{-3} \text{ s}^{-1}$ |
| $\lambda_{Bi,Tl}$  | $6.7 \times 10^{-5} \text{ s}^{-1}$ |
| The following values were used corresponding to the initial activity of 331 Bq for our source – see Chapter 4. |                                     |
| $N_{Pb}(0)$  | $1.831 \times 10^7$                 |
| $N_{Bi}(0)$  | $1.741 \times 10^6$                 |
| $N_{Tl}(0)$  | $3.162 \times 10^4$                 |
| S  | To be fitted                        |

The activities as a function of the time for different values of the Source term (S) are illustrated in Figures 2.1. To 2.4.

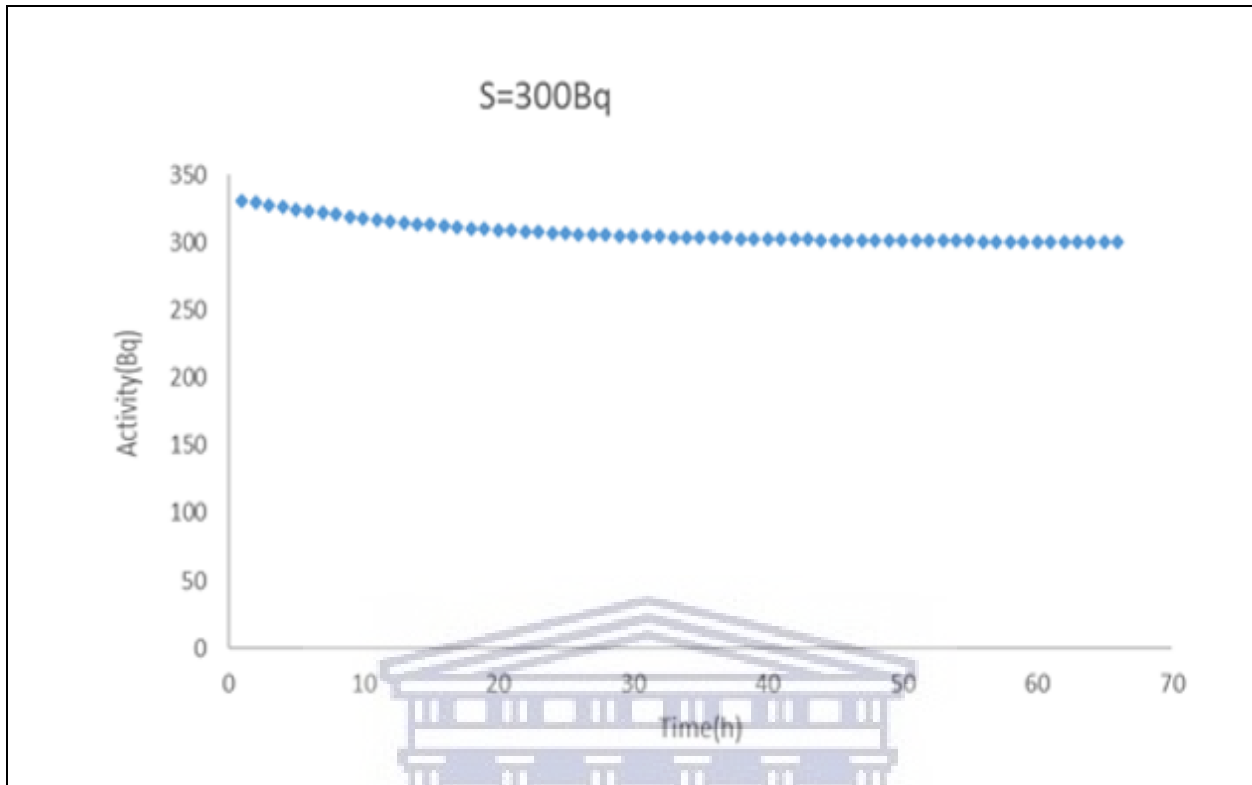


**Figure 2.1:** The activity of Tl-208 (2614 keV) corrected for the branching as calculated using equation (2.25) with  $S=300$  Bq

UNIVERSITY of the  
WESTERN CAPE

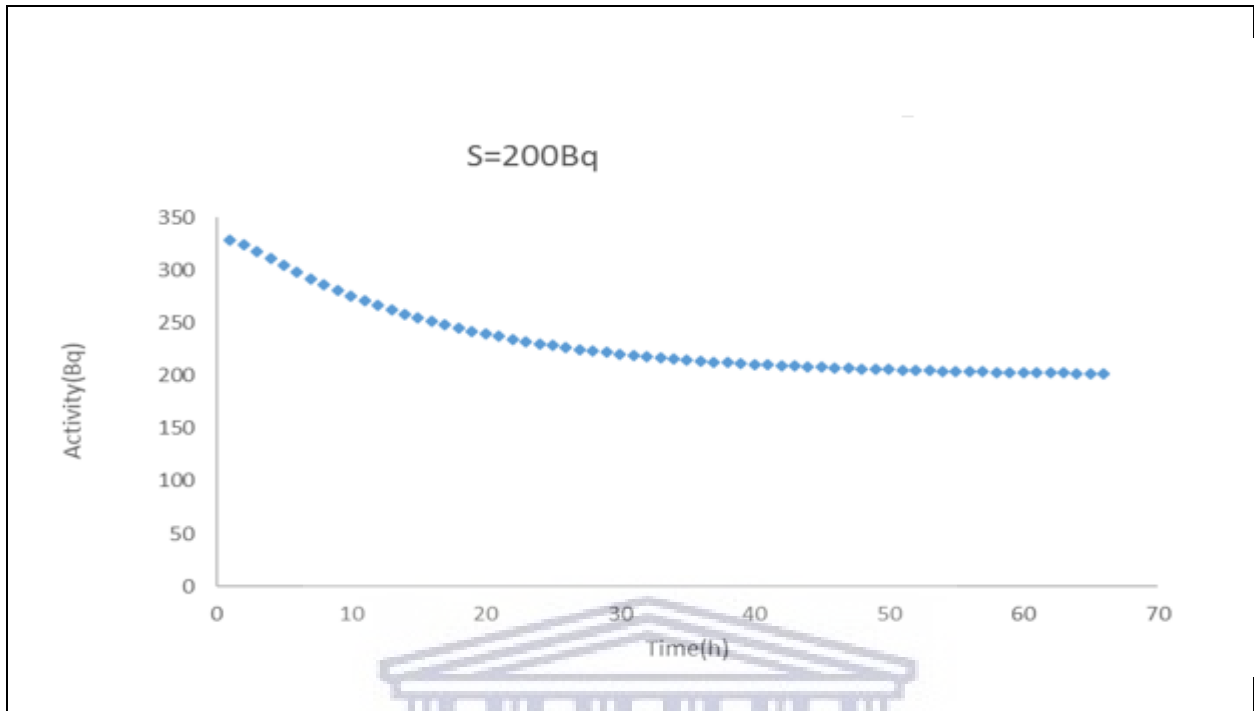


**Figure 2.2:** The activity of Tl-208 (2614 keV) corrected for the branching as calculated using equation (2.25) with  $S=200$  Bq

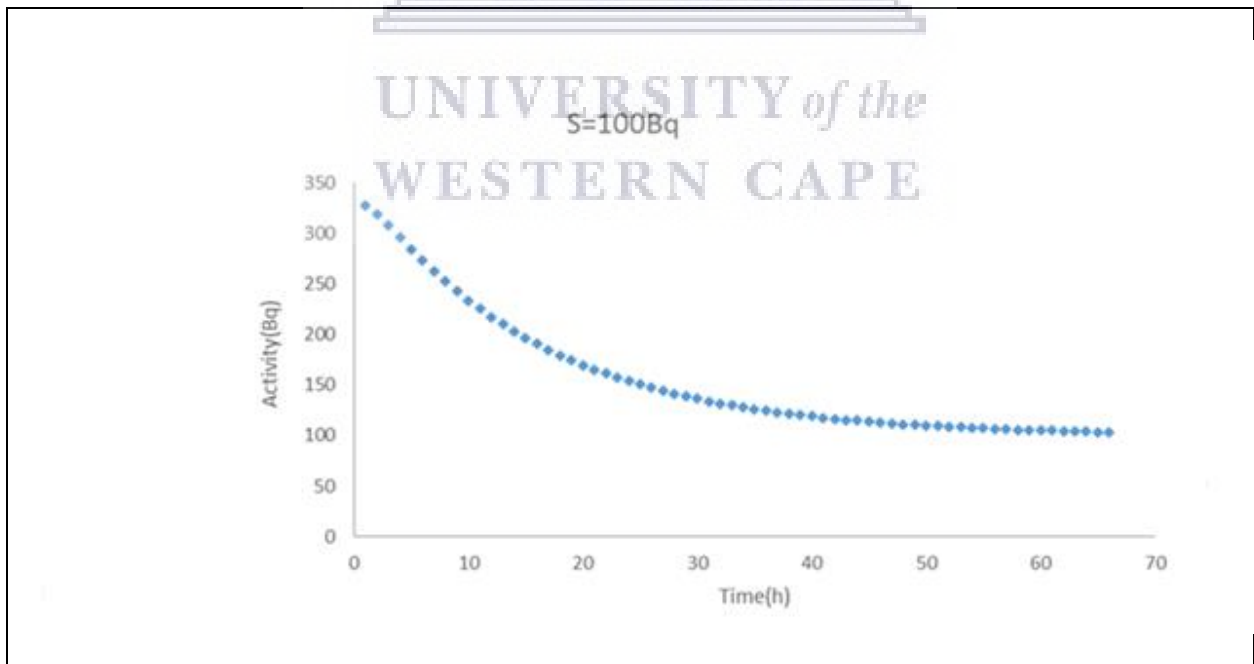


**Figure 2.3:** The activity of Tl-208 (2614 keV) corrected for the branching as calculated using equation (2.25) with  $S= 100$  Bq



Combining Figures 2.1, 2.2 and 2.3 gives Figure 2.4.

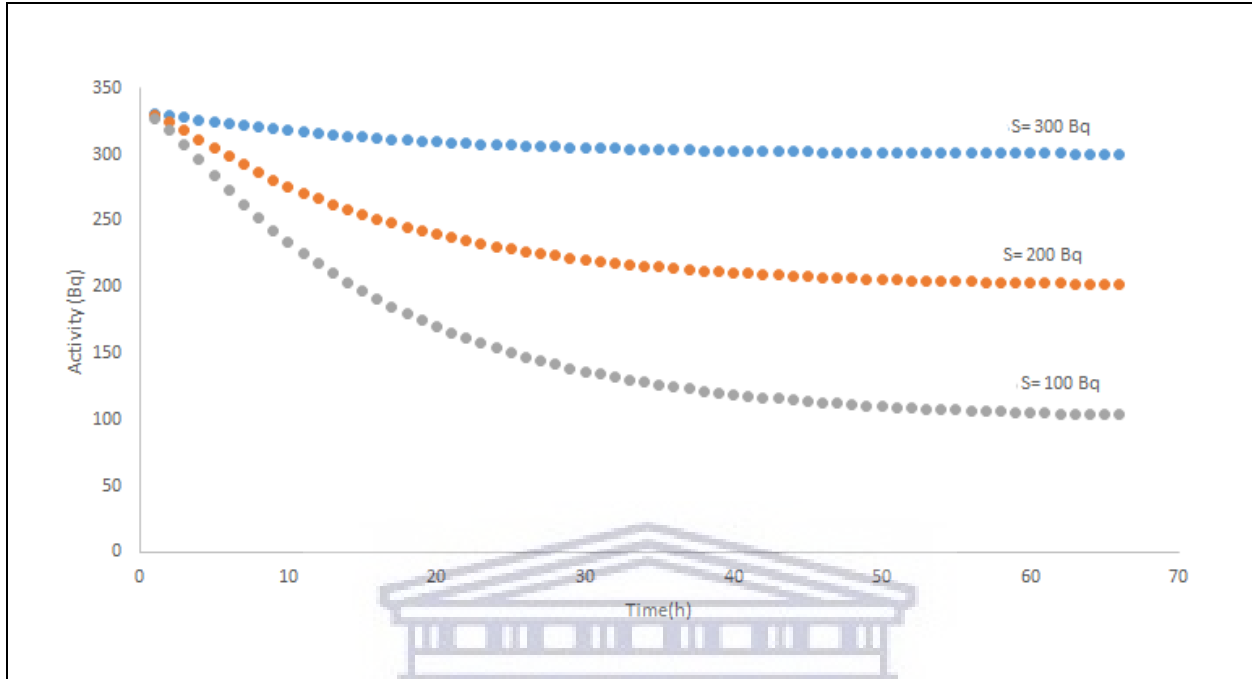


**Figure 2.4:** The activity of Tl-208 (2614 keV) corrected for the branching as calculated using equation (2.25) with S= 100, 200 and 300 Bq

## 2.4 Types of decay Modes:

The following decay modes are important in this work. The emissions of alpha ( $\alpha$ ) particles, beta ( $\beta$ ) particles and electromagnetic rays ( $\gamma$ -rays).

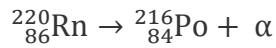
### 2.4.1 Alpha particle decay ( $\alpha$ )

In  $\alpha$  particle decay, the atomic mass of the parent nucleus decreases by two neutrons and two protons and its atomic number decreases by two. The following equation shows an example of the process and an example relevant to this work.



Where: -

P and D, are the parent and daughter nuclei respectively e.g.



There are several detectors used to detect alpha particles such as the RAD7 that is used in this work. A brief discussion on how the RAD7 detector work is presented below:

### 2.4.1.1 RAD7 continuous monitor:

A continuous radon monitor namely the DurrIDGE RAD7 (see Figure 2.5) is available for use in the Department of Physics and Astronomy at the University of the Western Cape. The RAD7 detector is designed in such a way that it can distinguish between the Rn-222 and Rn-220 daughters. Unlike other detectors, because of its ability to distinguish, it has become a detector of choice when you are investigating Rn-222 and Rn-220. Table 2.2 shows Rn-222 and Rn-220 daughters that can be detected by the RAD7.

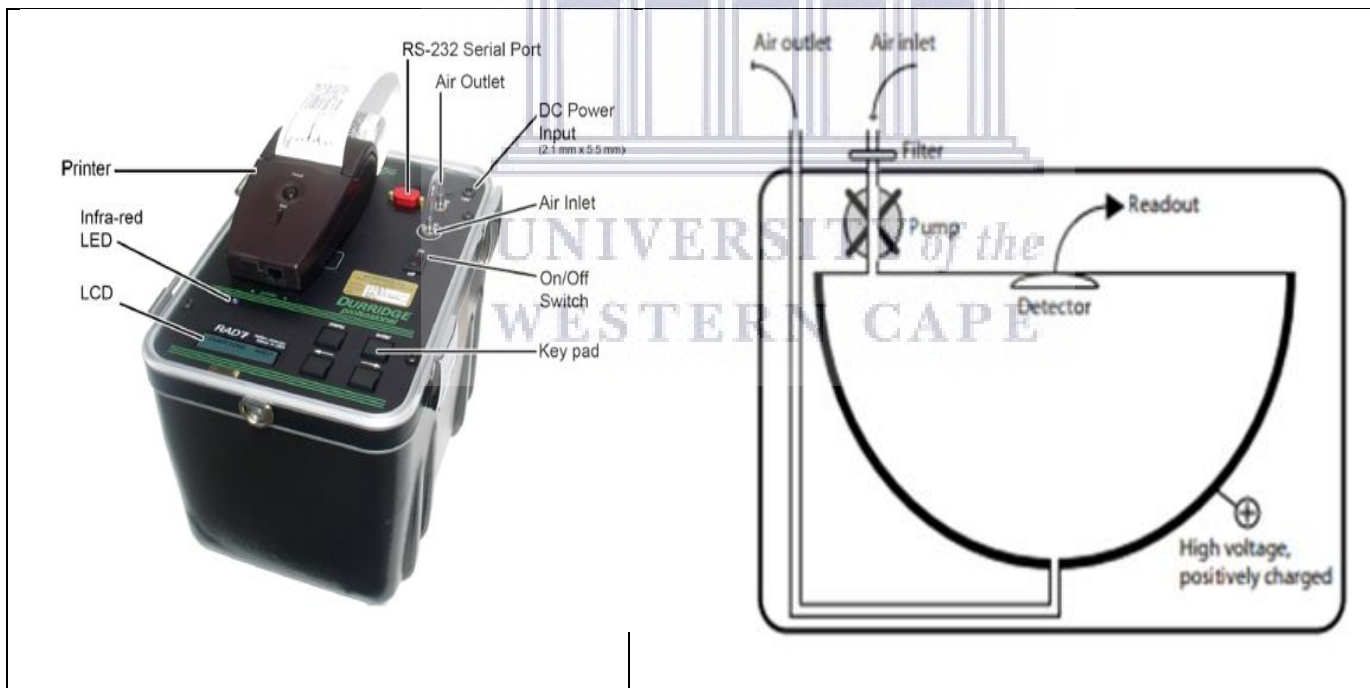


**Figure 2.5:** RAD7 on the left and schematic diagram showing its internal parts

**Table 2.2:** Rn-222 and Rn-220 daughters that can be detecting by the RAD7.

| Daughter | Energy of $\alpha$ (MeV) |
|----------|--------------------------|
| Po-218   | 6.00                     |
| Po-214   | 7.69                     |
| Po-216   | 6.78                     |
| Po-212   | 8.78                     |

The main components of the RAD7 includes (1) the solid – state detector (Knoll, 2010) that is made from a semiconductor material, namely silicon. The main function of the silicon detector is to convert the energy of the alpha released from Po-216 or Po-212 in the case of the Rn-220 and Po-218 or Po-214 in the case of Rn-222 to an electrical signal proportional to the energy. (2) A hemispherical small chamber whose volume is about 0.7 L. Note that the silicon detector is placed in the middle of this small chamber. An electrical field is created throughout the small chamber due to the electrical conductor that is charged with a potential of 2000-2500 volts. The electric field pulls the positively charged decay products Po-216 (half-life of 0.145 s; alpha energy of 6.78 MeV), and Po-212 (half-life of 299 ns; alpha energy of 8.78 MeV) to the surface of the detector to where they are deposited. The alpha particle from the subsequent decay of Po-216 (or Po-212) has a 50 % probability of striking the detector which results in an electrical signal proportional to the alpha particle energy. Due to their strength, the RAD7 amplifies filters and sort the signals. These signals are accumulated and an alpha spectrum is obtained. This spectrum is used to determine the Rn-220 and Rn-222 concentration (DurrIDGE, 2015).

The range of the RAD7 spectrum is from 0 up to 10 MeV. Our main interest is from 6 to 9 MeV because that is the energy range of the alpha particles from the decay of Rn-220 and Rn-222 daughters. For the RAD7 detector, the energy is categorized as follows: window A, B, C, D while from E to H are included in one window labelled “O” and given the name “other”. Window A (Po-

218, energy 6 MeV) and window C (Po-214, energy 7.69 MeV) correspond to new and old Rn-222 respectively. For new Rn-220 window B (Po-216, energy 6.78 MeV) is incremented and D (Po-212, energy 8.78 MeV) for older ones (see Figure 2.6).

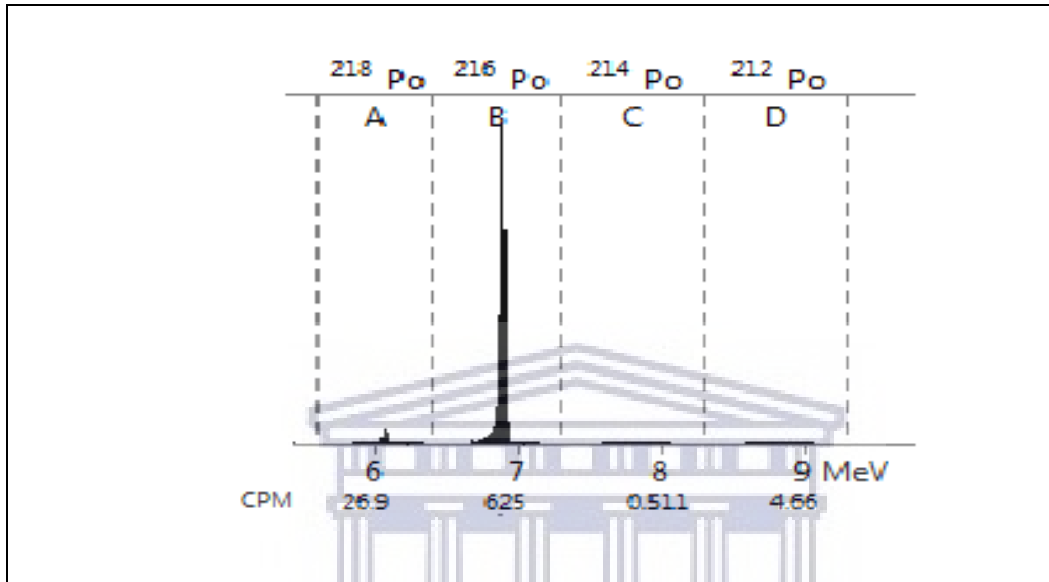
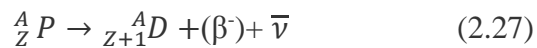


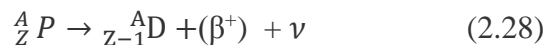
Figure 2.6: Typical RAD7 spectrum

### 2.4.2 Beta decay

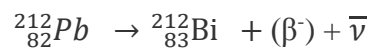
When a neutron in the nucleus decays to a proton, the nucleus emits a ( $\beta^-$ ) which is an electron, plus an anti-neutrino ( $\bar{\nu}$ ),



If the nucleus is rich in protons and one of these protons decays to a neutron, then the nucleus emits a ( $\beta^+$ ) or positron and a neutrino ( $\nu$ )



An example relevant to this work is the  $\beta^-$  decay



### 2.4.3 Gamma emission

Beta decay is often followed by Gamma emission, the third type of nuclear decay where the nucleus loses energy by emitting electro-magnetic radiation of high energy.

### 2.5 Interaction of gamma rays with matter

Gamma rays interact with matter through three processes; photo-electric effect absorption, Compton scattering and pair production which are all relevant to the gamma measurements in this work.

In the photo electric absorption, the incident photon gives all its energy to one of the electrons in the atom. The electron is ejected as a result of the absorbed energy. Figure (2.7) shows the electron with gained kinetic energy. This can be represented by

$$E_e = E_\gamma - E_b \quad (2.29)$$

Where: -

$E_e$  ≡ kinetic energy of the ejected electron

$E_\gamma$  ≡ photon energy of incident gamma ray.

$E_b$  ≡ binding energy of the electron.

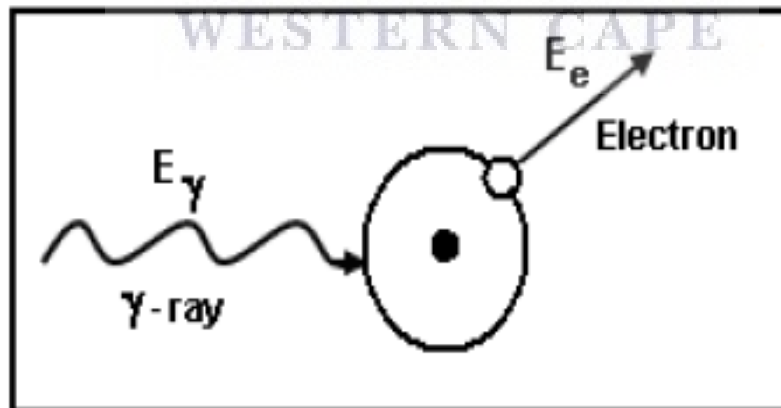


**Figure 2.7:** The mechanism of Photo-electric effect absorption

The probability of the interaction can be expressed by the cross section as follows

$$\tau = \text{constant} \times \frac{Z^{4.5}}{E_{\gamma}^3} \quad (2.30)$$

Where: -

$\tau \equiv$  The cross section

$Z \equiv$  the atomic number

From equation (2.30) it is clear that the probability of the interaction depends on  $Z$  and the energy of the photon (Debertin and Helmer, 2001). A large atomic number implies strong absorption of the photon, while low energy of the photon indicates strong probability of the absorption.

In Compton scattering a part of the incident photon energy is transferred to the ejected electron and the remaining energy is given to a secondary photon Figure (2.8).

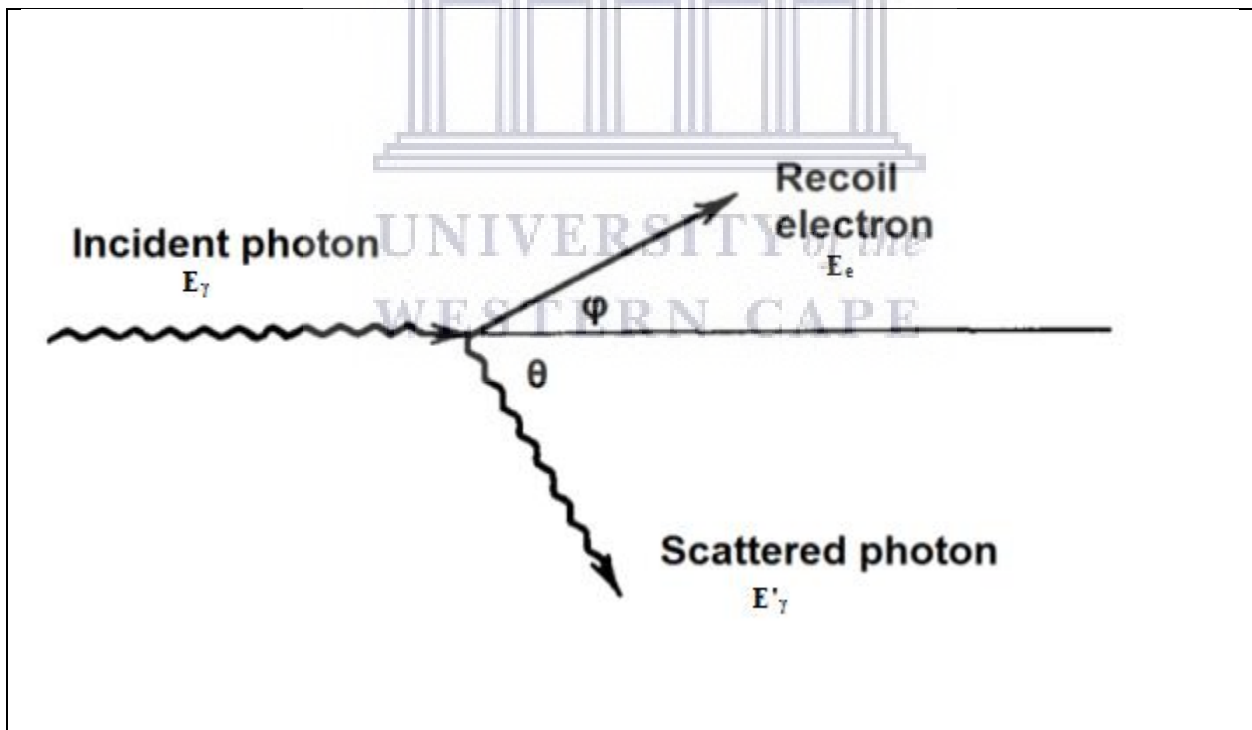


**Figure 2.8:** Schematic diagram that shows the Compton scattering process

Using the conservation of energy and momentum, the energy of the scattered photon at angle  $\theta$  can be represented by

$$E'_{\gamma} = \frac{E_{\gamma}}{1 + \frac{E_{\gamma}}{m_0 c^2} (1 - \cos \theta)} \quad (2.31)$$

Where:

$E'_{\gamma} \equiv$  the scattered photon energy

$E_{\gamma} \equiv$  the energy of the incident photon

$m_0 c^2 \equiv$  the energy corresponding to the rest mass of the electron = 511keV

$\theta \equiv$  angle of the scattered photon

Consequently, the energy of the ejected electron is

$$E_e = E_{\gamma} - \frac{E_{\gamma}}{1 + \frac{E_{\gamma}}{m_0 c^2} (1 - \cos \theta)} \quad (2.32)$$

The probability of Compton scattering depends on Z and the E (Debertin and Helmer, 2001) and is approximately given by

$$\sigma = \frac{Z}{E} \quad (2.33)$$

The process of pair production occurs when the energy of the incident photon is greater or equal to the energy of two electron rest masses (1.022 MeV). In this process the photon is converted in the Coulomb field of the nucleus and produces an electron-positron pair. The positron later interacts with an electron and annihilation resulting in two gammas of 511 keV travelling in opposite directions. The cross section of the pair production is proportional to  $Z^2$ .

The three important interactions of gamma rays with matter, namely (Photo-electric absorption, Compton scattering and pair production) are summarized and plotted in Figure (2.9). The probability of the interactions is represented by the regions where the three processes dominate as a function of energy and atomic number by showing lines where the cross sections for the processes are equal. The first region represents photoelectric absorption while the middle and the third

regions represent the Compton scattering and pair production respectively. So the line on the left shows where the photoelectric absorption and the Compton scattering are equally likely, while the line on right indicates the edge where the Compton scattering and the pair production are equally likely.

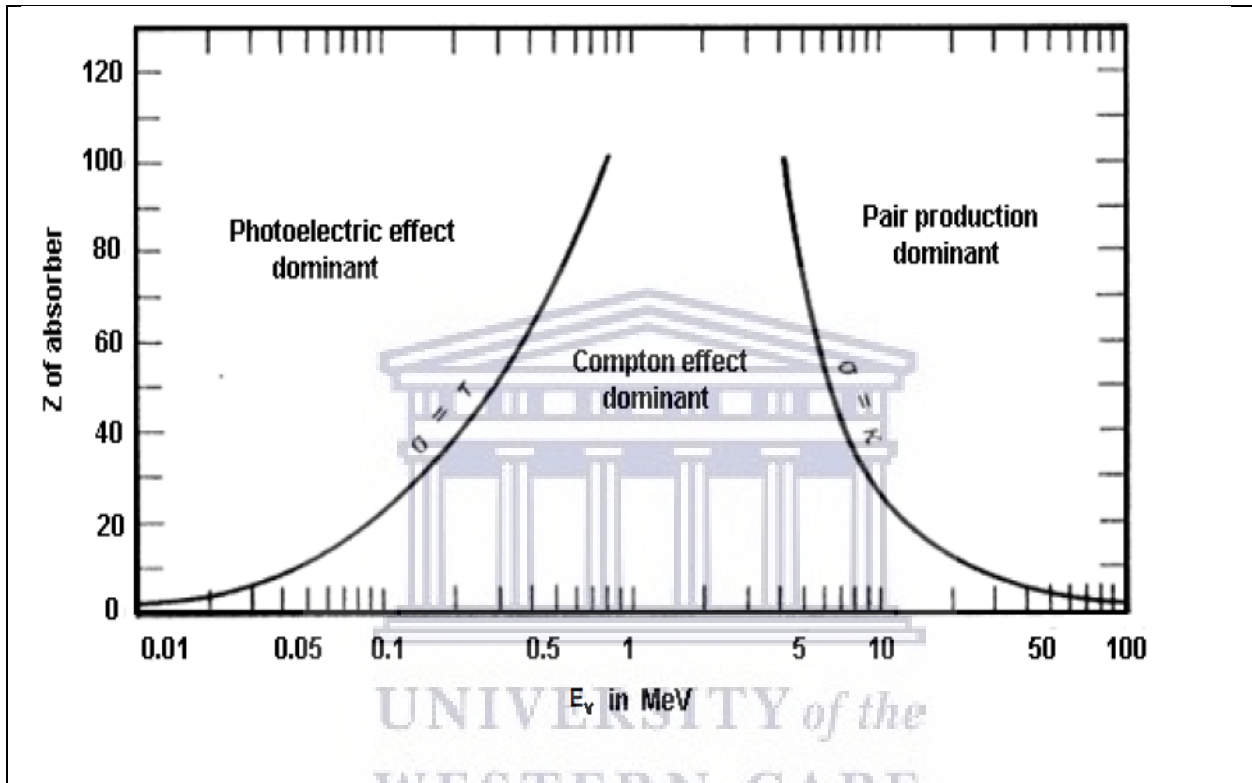


**Figure 2.9:** The regions of dominance for the three gamma interactions with matter.

In the present work, gamma rays were detected using an HPGe and (mainly) a NaI(Tl) gamma ray detector. Hereafter a brief description on the set-up of the two detectors is given while the measurements obtained using the detectors will be given in chapter 4.



## **2.5. 1 Gamma ray detectors used in this work**

### **2.5.1.1 Sodium Iodide detector NaI(Tl)**

In this study, the cubic, face-centred (FCC) NaI(Tl) detector available in the environmental nuclear physics laboratory at the University of the Western Cape was used. The detector was manufactured by REXON components, INC, USA, serial number 160229-1. It has dimensions of 76.2 mm × 76.2 mm and has a resolution of 7.6% FWHM at 662 keV for Cs-137 decay.

Briefly the detector works by the interaction of the incoming gamma radiation with the electrons in the scintillator material in the detector as described in Section 2.5 above. The electrons cause scintillation in the detector so that many photons are created that later hit the thin metal foil of the photocathode and thereby ejecting electrons. These electrons move and interact with the first dynode in the photomultiplier tube, and then release secondary electrons. The secondary electrons move from the first dynode to the second and so on. The final multiplication signal is sent to the multichannel analyser (MCA) for further processing. After that the nuclide energies of the radioactive sample are identified, and a spectrum is obtained.

For this work, the MCA used is the ScintiSPEC(FLIR electronics). The scintiSPEC is connected directly to the photomultiplier of the Na (Tl) detector via the standard 14 pins connector. The MCA has 1024 channels and it works in the range of 0 to 1200 volts. The range of the fine gain is between 0.5-2.0. The scintiSPEC has a USB cable to communicate with the winTMCA32 software installed in the computer. The software was used to analyse the accumulated spectra.

### **2.5.1.2 The Hyper Pure Germanium Detect detector (HPGe)**

A Canberra, p-type detector (model GC4520) at the Environmental Laboratory at iThemba LABS was used only for characterising the standard source. The detector has a relative efficiency of 45%. Resolution is 2 keV FWHM (full-width-at-half-maximum) at the 1.332 MeV  $\gamma$  - line of Co-60. The detector consists of a crystal with a diameter of 6.25 cm and length of 5.9 cm. To protect the detector from unwanted gamma radiation coming from the surrounding building material and cosmic rays, a 10 cm lead castle is used.

## 2.6 Summary

In this Chapter a short historical background of radioactivity was presented. Then the radioactive decay was covered. The theoretical model used in this study which is based on the Bateman equations was developed. Some important decay modes which are relevant to this study were discussed. Since gamma spectrometry was involved in this study, the interaction of gamma rays with matter was presented. Moreover the detectors used in this project were described and discussed.



# CHAPTER 3

## Literature review on Rn-220

### 3.1 Introduction

In order to conduct measurements of Rn-220 such as indoor measurements in premises or in working places, a certain protocol needs to be followed. Moreover, to check on the monitors and to test the measuring accuracy a quality assurance programme including some calibration and intercomparison with another laboratories are required. A reliable Rn-220 source is needed for such a programme. This chapter will present different methods of measuring Rn-220 in the laboratory and the development of Rn-220 sources found in the recent literature. The lack of good reliable cheap systems is a major reason for the work described in this thesis.

### 3.2 Review of methods for measuring Rn-220

In this section we describe measurement systems for Rn-220 which are also summarised in Table 3.1

Qiu (2006) developed two methods to check on the feasibility of the Rn-220 source to create a stable yield. The first method was the flow-through system with a source and where a scintillation cell was employed; the second method used active charcoal and gamma spectroscopy. The result of the two methods agreed on the stability of the source with a relative deviation of less than 3%.

Eappen, Sapra and Mayya (2007) developed a novel method for measuring Rn-220 using a scintillation cell. Different flow rates (3-10 litres/min) were set to control the flow of Rn-220 gas from Pylon model TN-1025 through the cell. To allow the registration of the counts online, the flow of the gas stopped immediately once a steady state is achieved. Due to the long half-life of the Pb-212, which results from the decay of the Rn-220, this contributed to the background via its continuous accumulation in the cell. This background was corrected by using the value of the  $y$ -

intersection of the graph which fitted the experimental data. The slope from the graph was used to calculate the real activity concentration of Rn-220. The results obtained agreed with two reference methods conducted at the same time.

Srinivasan *et al.*, (2010), used the benefit of gamma spectroscopy to develop a method based on simulating the geometry of a NaI(Tl) detector inside a 30 litres chamber using the one Curie activity of a Rn-220 source. Moreover, two other scintillation detectors were tested. The idea was to measure the gamma emitted from the Rn-220 daughters (Pb-212, Bi-212, and Tl-208) after decaying. Clear spectra have been accumulated presenting gammas emitted from Rn-220 daughters. Some corrections were made to account for the deposited Pb-212 in the chamber wall.

Kotrappa and Steck (2010), developed the Electret Ionization Chamber (EIC) to measure Rn-220 by improving its sensitivity to Rn-220 by increasing the area of the entry of the gas by making extra holes in the side of the S-chambers. The new EIC RTEIC responds to as Rn-222 and Rn-220, while the old one called REIC responds to Rn-222 only. The RTEIC has been tested for the response to Rn-220 by exposure to a stable flux of Rn-220 in a well-established chamber. Calibration factors have been obtained for different volume of RTEIC with correction factors as well.

In order to measure Rn-220 in the environment with low statistical uncertainty, Zhang *et al.*, (2010) used a locally constructed and well maintained Rn-220 chamber which is located at Peking University, China. They calibrate the Lucas Cell (LSC) detector against RAD7 as a reference device. The calibration was conducted in a pure Rn-220 atmosphere and in an atmosphere mixed with Rn-220 and Rn-222. The experimental results are supported by a mathematical formula. The results showed that whether in pure Rn-220 or in the presence of Rn-220 and Rn-222, the deviations with the RAD7 are less than 10%.

To study the influence of Rn-220 in a Rn-222 monitor, two Rn-222 monitors namely, the Alpha Guard and the Radon Scout Plus (RSP) were employed in a study conducted by C. Sumesh *et al.*, (2011). In addition, a RAD7 was simultaneously used due to its ability to measure Rn-220 and Rn-222 which is not true for Alpha Guard and RSP. The Alpha Guard measurements and the RSP were compared to RAD7 measurements and the percentage of Rn-220 interference was

determined. The percentage of Rn-220 interference for Alpha Guard and RSP was found to be 9% and 4% respectively.

Ismail and Jaafar (2011) conducted a study of the proper size of a Rn-220 detector chamber, for a passive Nuclear Track Detector (NTD), type CR39. The proper size gave a reasonable value of the calibration factor for Rn-220 measurements and also for Rn-222. It is worth noting that the calibration factor depends on the size of the detector as well as its efficiency. The best estimated dimension for measuring Rn-220 was a height of 70 mm height and diameter of 60 mm. Moreover, the calibration factor was  $8.3 \pm 0.1$  with 80% efficiency. The results agreed well with some theoretical reference studies.

A study has been done by Sumesh *et al.*, (2012) using a Lucas Scintillation Cell (LSC) and a double filter (DF) assembly to measure Rn-220 from Thorium Oxalate powder after being separated from monazite ore. The (LSC) and (DF) assembly were connected to a gas-tight chamber with 512 litres inner volume. The first method was based on measuring Rn-220 and its daughter Po-216 only. The second method was based on measuring Rn-220 daughters Bi-212 and Pb-212 which is called the delay method. The results showed low uncertainty and a good agreement of the Rn-220 measured by both of the monitors.

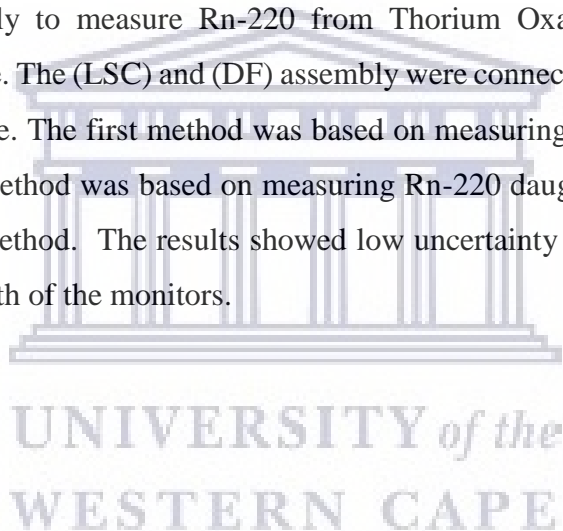


**Table 3. 1** Summary of measurement system for Rn-220

| Reference                       | Thoron measurement system                         | COMMENTS  | Source                                 |
|---------------------------------|---|---|--|
|                                 |   |   |  |
| Qiu, (2006 )                    | a) Flow through with scintillation cell           | Claim 3% accuracy. Cannot distinguish radon from thoron.                      | Aged Th(NO <sub>3</sub> ) <sub>4</sub> |
|                                 | b) Active charcoal followed by gamma spectroscopy |   |  |
| Eappen, Sapra and Mayya (2007)  | Scintillation method                              | Problem with build-up of daughters but corrected for this.                    | Pylon model TN—1025                    |
| Srinivasan <i>et al.</i> (2010) | scintillation detectors placed in chamber         | Minimum detection limited not achieved  |  |
| Kotrappa and Steck (2010)       | Electret method                                   | Not clear if the method clearly separates the radon and thoron counts         | Pylon Th-228 source                    |
| Zhang <i>et al.</i> , (2010)    | Calibration of LSC                                | The deviations of Rn-220 measurements less than 10 % when compared with RAD7. | lantern mantles                        |

|                                  |   |   |                                 |
|----------------------------------|---|---|---------------------------------|
| Csige, Szabó and Szabó (2013)    | RAD7  | Different thicknesses of building materials were measured. The generation rate of Rn-220 was found to be $142 \pm 6 \text{ Bq.m}^{-3} \text{ s}^{-1}$                                   | Building materials              |
| C. Sumesh <i>et al.</i> , (2013) | Silicon detector, RAD7 comparative Scintillation cell   | Sensitivity of RAD7 increases when the flow rate increases up to 2L/min and then decreases.   | Thorium oxalate powder (Th-232) |
| Ismail and Jaafar, (2011)        | CR-39 nuclear track detector  | The calibration factor depends of the efficiency of the detector which depends of the geometry. The optimum dimension was found for a radius of 3cm and height 7cm, with efficiency 80% | Thorium dioxide                 |
| Sumesh <i>et al.</i> , (2012)    | LSC connected to chamber, two techniques used to measure Rn-220 immediately after sampling and delay method | The method can be used to calibrate the Rn-220 gas chamber. Also it can be used in monazite processing plants where there is no Rn-222.   | Thorium oxalate powder (Th-232) |
| Kavasi <i>et al.</i> , (2012)    | Thoron experimental Room(TER)   | The humidity affected the Rn-220 measurements   | lantern mantles                 |
| Chen and Moir, (2012)            | Canadian home owners Alpha Track detectors  | Test the sensitivity of the Alpha Track detectors to Rn-220. The sensitivity factors  |                                 |

|                                   |  |  |                                   |
|-----------------------------------|--|--|-----------------------------------|
|                                   |  | relative to Rn-222 was estimated to be in the range of 0.012- 0.74   |                                   |
| Sorimachi <i>et al.</i> , (2012)  | Raduet and Radpot passive detectors  | Both detectors calibrated for the effect of the wind, humidity, and the aerosol in the air of their measurements.                  |                                   |
| Sathyabama <i>et al.</i> , (2014) | Flow through LSC   | Disequilibrium between Rn-220 and Po-216 experimentally approved. Correction needed to the flow rate above 5 L min <sup>-1</sup> . | Pylon Th-228 source model 1025(S) |
| Tan and Xiao, (2013)              | RAD 7  | RAD 7 recalibrated for measuring Rn-220 in field based on Rn-222 calibrated factor.  | solid self-source                 |
| Tan <i>et al.</i> , (2014)        | RAD7   | External pump used. The sensitivity of the Rn-220 is 30 % less than the Rn-222 sensitivity   |                                   |
| Amanat <i>et al.</i> , (2014)     | Develop Passive diffusion chamber using Solid State Nuclear detector (SSND), Lexan film. | Lexan films are cheap and can be used in a very high concentration area of Rn-222 and Rn-220                                       | Pylon source model TH-1025        |



|                                      |  |   |   |
|--------------------------------------|--|---|---|
| Agarwal <i>et al.</i> , (2014)       | Delay chamber used with computation Fluid Dynamic Techniques(CFD)    | Deviation of 22% in the experimental to simulated transfer Rn-220 factor  | Dry thorium oxalate powder              |
| Röttger, Honig and Linzmaier, (2014) | Stable reference atmosphere used for calibration Rn-220/Rn-222       | Six monitors were calibrated, one of the monitors with calibration factor estimated as 1.34.                                  | Solid source Th-228 (electrodeposition) |
| Kumar <i>et al.</i> , (2014)         | Silicon Pin diode detector   | The average sensitivity of the detector for thoron 0.169 CPH/Bq/m <sup>3</sup> and for Radon 0.408 (CPH)/(Bq/m <sup>3</sup> ) | Thorium oxalate powder (Th-232)         |
| Sabot <i>et al.</i> , (2015)         | Silicon Alpha detector included in defined volume                    | Rn-220 activity concentration developed   | Th-228 source from Pylon                |
| Kumar <i>et al.</i> , (2015)         | Small plastic bottle connected to Scintillation Rn-220 Monitor (STM) | Rn-220 exhalation rate of building material varied from 7.3 to 238 mBq.m <sup>-2</sup> h <sup>-1</sup>                        | Building material                       |
| Sorimachi <i>et al.</i> , (2016)     | calibrate silicon detectors use NIRS chamber, eleven detectors used  | Deviation of result 30% relative to standard detector, big dryers decay correction  |   |

|                                  |  |  |  |
|----------------------------------|--|--|--|
| Janik, (2017)                    | Inter-comparison of Rn-220 and Rn-222 detectors measurements | NIRS and SURO laboratories inter-compare Rn-220 measurements. NIRS uncertainties for low activity concentration 16% and 6% for high activity concentration. 10 % over all uncertainty for SURO |  |
| Pornnumpa <i>et al.</i> , (2018) | Exposure chamber used for calibration Rn-220                 | Stable Rn-220 activity concentration ranged 3500 Bq.m <sup>-3</sup> up to 29000 Bq.m <sup>-3</sup>   | Commercial Lantern mantles(M-7910, Captain Stag, Japan |
| Magnoni <i>et al.</i> , (2018)   | Thoron -scout monitor used as Rn-222 and Rn-222 detector     | Evaluate the Rn-220 exhalation rate using only Rn-222 exhalation rate and the activity concentration of Ra-224 and Ra-226  | stonny material  |
| Sumesh <i>et al.</i> (2011)      | Study Alpha Guard and RSP for thoron studies.                | Rn-220 interference in Rn-222 concentration by 9% and 4% for Alpha Guard and RSP respectively  | Thorium oxalate powder(Th-232)                         |

In 2011, a room for experimental studies related to Rn-220 and its progenies was constructed at the National Institute of Radiological Sciences (NIRS), Chiba, Japan. Based on this facility Kavasi *et al.*, (2012) conducted a study to test the stability of the Rn-220 activity concentration as well as the measurements of Rn-220 progenies. To achieve this goal, 90 commercial lantern mantles were used as Rn-220 sources, a RAD7 and a Ludlum scale ratemeter model 2200 were used as Rn-220 and Rn-220 progeny monitors respectively. The measurements were taken from three different geometries; low, middle and high with reference to the floor. The estimated activities for low, middle and high were  $1094 \pm 89$ ,  $1130 \pm 96$  and  $112 \pm 96$  Bq.m<sup>-3</sup> respectively. For the Rn-220 progenies when the air was mixed the estimated activity was  $18.6 \pm 4.1$  Bq.m<sup>-3</sup> and when the air was not mixed the activity concentration was  $225 \pm 21$  Bq.m<sup>-3</sup>. The estimated equilibrium factors in the two cases were 0.02 and 0.20. The measured results in the Rn-220 experimental room (TER) showed stability in Rn-220 concentration and its progeny-.

Chen and Moir (2012) performed a study on the sensitivity of Rn-222 detectors to Rn-220. The Rn-222 detectors were based on the Alpha Track Detector (ATD) employed to check some studies conducted for estimation of indoor Rn-222 in Canadian homes. The study was supported by Health Canadians and NIRS laboratory. The detectors were classified as A, B, C, and D. A and B were similar in design and has been used by Canadians. In addition, detectors C and D were also similar but not used by Canadians. Detectors A and B have small gaps in their chamber allowing radon to diffuse in while detectors C and D have large holes which radon can diffuse through more easily. The four detectors are exposed to Rn-220 and their sensitivity is estimated to be 1.2 %, 1.8 %, 74% and 41 % for A, B, C, and D respectively. These results revealed that Rn-222 measurements were overestimated in Canadian homes.

Sorimachi *et al.*, (2012) conducted a study using the NIRS chamber to test Rn-220 passive monitors and to check the effect of the wind, humidity and the aerosol in the air on their measurements. To do this, Raduet and Radpot, detectors that work on the alpha track principle were used (Sugino *et al.*, 2005). Each detector has two chambers; one designed to give a high exchange rate of air and the other a low exchange rate supported by CR39 films covered by sponge and a filter. The results showed that Raduet with sponges registered a lower infiltration rate of Rn-220 than Radpot with a filter. The detection response observed by the two detectors declined at high humidity in the high air-exchange rate chamber. The low wind speed affected the Radbot

detection response at high air-exchange rate while a small effect was registered for Raduet. For aerosols, a small effect was registered for both detectors.

Sathyabama *et al.*, (2014) studied the disequilibrium between Rn-220 and Po-216 for Rn-220 measurements using a flow-through LSC supported by a mathematical model in an attempt to obtain a correction factor (CF) for the Rn-220 measurements. The measurements have been done using a 125 cm<sup>3</sup> cell and a Rn-220 source based on two methods namely; monitoring counting rate and decay methods. The cell was tested for different flow rates ranging from 4 up to 10 L.min<sup>-1</sup> and the results showed that correction factors are necessary for the measurements with flow rates above 5 L. min<sup>-1</sup>.

C. G. Sumesh *et al.*, (2013) conducted a study to test the effect of the flow rate on the sensitivity of the RAD7 detector based on Rn-220 measurements. A RAD7 was equipped with a well-calibrated chamber and Rn-220 source (Sumesh *et al.* 2012). Various flow rates were applied to test the sensitivity of the detector. A clear increase in the sensitivity was observed when the flow rate increased up to 2 litres min<sup>-1</sup> after which the sensitivity dropped. The developed theoretical sensitivity agreed with the experimental sensitivity. Moreover, the study revealed that the Rn-220 activity concentration measured by the RAD7 is underestimated by 15% when it was set at the standard flow rate of 0.65 litres min<sup>-1</sup>. When RAD7 measurements were compared with LSC and double filter assembly, a good correlation was observed.

In order to measure the Rn-220 generation rate from a building material sample, Csige, Szabó and Szabó (2013) developed a mathematical method followed by an experimental study. The RAD7 detector was used to perform the measurements based on the varying thickness of adobe building material that was placed into a holder specifically made for this purpose. The generation rate of Rn-220 was found to be  $142 \pm 6 \text{ Bq.m}^{-3} \text{ s}^{-1}$

Tan and Xiao (2013) developed a method to recalibrate the readings of a RAD7 monitor to obtain the Rn-220 exhalation rate from the soil surface. The idea was when RAD7 is used in the field its battery voltage decreases which consequently may change the flow rate. Moreover, to collect the Rn-220 in the accumulating chamber needs a long time, which is not possible with the small dryer as is recommended by RAD7 company. For this reason, the big dryer is more suitable in the RAD7 setup in the field and the RAD7 was recalibrated based on the Rn-222 calibration factor of 1.12.

Tan *et al.*, (2014) conducted a study on analysing the air flow of Rn-220 in the RAD7 cell in order to test the Rn-220 sensitivity. For this purpose, mathematical formulas were developed based on the two types of air flow, namely laminar, and turbulent flow. An extra pump was added to the RAD7 pump to dilute the Rn-220 concentration due to the limitation of RAD7 measurements ( $400 \text{ kBq.m}^{-3}$ ). The study proved that the RAD7 sensitivity to Rn-220 is less by 30% than the sensitivity of Rn-222. (Tan *et al.*, 2014) concluded that the lower sensitivity of Rn-220 is a result of the Rn-220 atoms that decay before entering the cell and may also be due to the short circuit stream.

In order to measure Rn-220 and Rn-222 in the soil, a well-calibrated detector is needed. Amanat *et al.*, (2014) calibrated and developed a method to achieve this goal. To do so, Lexan Polycarbonate films were used as a Solid State Nuclear Track Detector (SSNT). The detector consists of two chambers separated by filters and films (upper and lower). The upper film registered alpha particles from Rn-220 and Rn-222 whereas the lower one recorded Rn-222 alphas only. The film was later treated by a well-selected chemical in order to magnify the alpha tracks. Moreover, the distance between the filters and the films, were optimized to give better results. The calibration factor of the upper film was obtained as  $1.76 [\text{track.cm}^{-2}(\text{kBq.m}^{-3}\text{d})^{-1}]$ .

A study was conducted by Agarwal *et al.*, (2014) using the experimental chamber which is located at the Radon Research Laboratory, Bhabha Atomic Research Centre (BARC), Mumbai. The chamber was simulated based on its dimensions. Different flow rate values of Rn-220 with two positions of the inlet and outlet were simulated using Computational Fluid Dynamics (CFD) including a delay chamber. The main idea was to estimate the transfer factor by finding the ratio of the Rn-220 concentration at the outlet to the Rn-220 concentration at the inlet. A deviation of a maximum of 22% was observed in the experimental and CFD methods.

Six Rn-220 monitors categorized into three different groups based on their working principles were calibrated in a study carried out by Röttger, Honig and Linzmaier, (2014). The reference Rn-220 atmosphere has been used with a Th-232 solid source in the calibration method. A stable activity concentration provided by the system ranged from  $280 \text{ Bq.m}^{-3}$  to  $17000 \text{ Bq.m}^{-3}$ . The calibration factors of the monitors were estimated based on the activity and the emanation of a standard source used to calibrate the specific monitor. In one of the monitors, the calibration factor was estimated to be 1.34.

Kumar *et al.*, (2014) developed a discriminative detector for measuring Rn-220 and Rn-222. The detector is based on a pin diode centralized in a 1 litre volume chamber that was used to measure the decay of Po-216, Po-212, Po-214 and Po-218 which were directed by an electrical field. The Pin diode detector was tested by a well-calibrated chamber and Rn-220 source. To improve the sensitivity of the detector to Rn-220, several voltages were applied and different humidity values were tested. The average sensitivity of the developed detector for Rn-220 measurements was estimated at 169 CPH/Bq/m<sup>3</sup>. It should be noted that the Rn-220 measurements of the pin diode detector agreed with the RAD7 detector measurements. In this experiment, the RAD7 detector was used as a reference detector.

Sabot *et al.*, (2015) used the facility of the National Henri Becquerel Laboratory (LNHB), France to develop Rn-220 activity concentration based on a silicon alpha detector and defined volume. A Th-228 source from the company Pylon created a Rn-220 atmosphere which was controlled by an electric field. In this method, Rn-220 gas and its solid daughters were measured, as observed in the developed spectra.

Due to the short half-life of Rn-220 which affects its travel and minimizing its homogeneity inside the accumulating chamber, Kumar *et al.*, (2015) used small plastic cylinder shaped bottles as thoron accumulation chambers to different samples of building materials in order to obtain their exhalation rates. The small plastic bottles were connected to a scintillation Rn-220 monitor (STM) via its inlet and outlet by a tight tube connector with small diameter. Using this setup, about 12 different types of building materials were measured. As a result, the estimation of exhalation rates varied from 7.3 to 238 mBq.m<sup>-2</sup> h<sup>-1</sup>.

Sorimachi *et al.*, (2016) used a chamber at NIRS Japan to study intercomparison for eleven detectors. These were Si detectors based on electro-static collection. Therefore, the measurement of Rn-220 was carried out under specific conditions. The result of the study showed a significant deviation, which was lower by 30% compared to the reference detector. These results indicate that each detector needs its own calibration factor. Moreover, the findings showed that the calibration factors of these detectors were highly depended on the flow rates.

Since quality control (QC) and quality assurance are very important in order to strengthen the quality of Rn-220 and Rn-222 detector measurements, an intercomparison of Rn-220

measurements was carried out in various laboratories, namely NIRS laboratory Japan and Czech metrological Institute (SURO) in almost similar conditions with slight variation in the humidity control and the Rn-220 sources. NIRS reported two uncertainties, 6% when high activity concentration was used, and 16% for low activity concentration. Whereas SURO reported an uncertainty of 10%. (Janik, 2017).

A similar study has been done at NIRS to calibrate Rn-220 and Rn-222 monitors based on quality assurance and quality control. This study was conducted at Hirosaki University (Pornnumpa *et al.*, 2018). A Rn-220 source made of Lantern mantle as standard weighing approximately 673.6 g (including its container), and generating Rn-220 gas continuously in an exposure chamber installed for the calibration of Rn-220 monitors was used. The activity concentration in the inner volume of the chamber ranged between 3500 Bq.m<sup>-3</sup> up to 29000 Bq.m<sup>-3</sup> under certain conditions such as the types of the source, flow rates, temperature and humidity. All these parameters have been well controlled and managed with trusted values and well tested.

Magnoni *et al.*, (2018) used the benefit of the relatively long half-life of Rn-222 to develop a method to measure the exhalation rate of Rn-220. The method needs only to measure the exhalation rate of the Rn-222 and use the activity concentration of Ra-224 and Ra-226. Thus the exhalation rate of Rn-220 is obtained. A mathematical formula is supported by experimental work employing the discriminative *Thoron Scout* monitor which was developed by SARAD ([www.sarad.de](http://www.sarad.de)). It can measure Rn-220 and Rn-222 based on Po-216, Po-218 and respectively.

### **3.3 Development of Rn-220 sources**

Sorimachi, Sahoo and Tokonami, (2009) carried out a study using the NIRS chamber. The study was based on measuring the Rn-220 gas from Lantern mantle (M-7910, CAPTAIN STAG, Japan). RAD7, Lucas cell (Model 330A) and portal radiation monitor (Model AB-5, Pylon Electronics Inc, Canada) were used. The study revealed that the Rn-220 gas concentration increased when the mass of Lantern mantle material increased. The Rn-220 gas concentration depends on the absolute humidity (AH) and insignificant change was observed when the flow rate was changed.

As mentioned in Chapter one, Röttger *et al.*, (2010) developed a Rn-220 reference activity concentration atmosphere. A certified Th-228 sample was used as a Ra-228 source to provide a stable Rn-220 atmosphere. The source was placed at the top of an HPGe detector in a small volume of less than 4 ml and then connected to a big volume (29.99 litre) via pipes. Two procedures were used to monitor the Rn-220 gas flow. One is the conventional line of the traceability of gamma spectrometry with the emission probabilities of the respective isotopes. The second is the “count rate” procedure yield. In this procedure the source was measured when it was open and when it was closed and this method results in the lowest uncertainty. Two gamma lines were used to measure the emanation of the Rn-220 source, Ra-224 (240.9 keV) and Pb-212 (238.6 keV). Rn-220 emanation factor and the activity concentration were found to be  $0.4105 \pm 0.0016$  and  $7960 \pm 206 \text{ Bq/m}^3$  respectively.

A Rn-220 source was made using a thorium nitrate solution mixed with clay (Jobbágy and Bety-Denissa, 2010). The physical parameters were taken into account such as volumes and the masses of the clay. Two types of samples (sphere and stick) were prepared with varying water content. The sphere sample was prepared with a lower water content compared to the stick sample. The samples were heated by using an oven and the temperature ranged from 600°C up to 1000°C. A leak-proof chamber with an inner volume of 1.5 litres was used. The results of the study showed that two factors affected the exhalation of the Rn-220 from the source, namely the temperature and the amount of water. The best exhalation was observed in the sphere sample at a temperature of 600°C. The exhalation efficiency ranged between 0.16 % - 1.44 % (Jobbágy and Bety-Denissa, 2010)

Tang *et al.*, (2012) prepared a Rn-220 source using sodium benzenesulfonate ( $\text{C}_6\text{H}_5\text{SO}_3\text{Na}$ ) resin and thorium nitrate  $\text{Th}(\text{NO}_3)_4 \cdot 4\text{H}_2\text{O}$ . The method followed in the preparation was ion exchange, the  $\text{Th}^{+4}$  in the  $\text{Th}(\text{NO}_3)_4 \cdot 4\text{H}_2\text{O}$  successfully exchanged by  $\text{N}^+$  in sodium benzene sulphonate resin. The main idea was to study the emanation properties of the ion-exchanged solid Rn-220 source. The source was studied for different temperatures and different humidity values. A RAD7 detector was used in the exposure chamber to measure the Rn-220 concentration emanated from the source. The source stability was observed via short and long-term measurements. The emanation coefficient of the source was estimated for certain conditions at 33 %.



A method has been developed by Buompane *et al.*, (2013) to characterize a Rn-220 source for the realization of a reference atmosphere. To achieve this goal, two different types of materials were used to prepare Rn-220 sources, namely; lantern mantles, and thorium oxide powder. The sources were measured by an HPGe detector in two different ways, i.e. when the source is sealed and, when it was unsealed. A special box was designed for this purpose. The gamma line with energy 300 keV of Pb-212 was measured in the two cases to calculate the exhalation activity of the source which was used to calculate the specific activity of Rn-220 after the source was placed in a 32.7 litre chamber equipped with an electrostatic monitor.

The powder sandwich technique by Kanse *et al.*, (2013) aimed to measure the mass emanation rate and emanation coefficient of Rn-220. To do so, three Rn-220 sources were made from thorium oxide and ammonium di-urate (ADU), rich in U-232 which decays to Ra-224. From each source, eight samples with variant masses and a very thin layer (1 mm-2 mm) were formed. The thin layer of the powder samples is placed between two fibre glass filters and is stuck to a ring that has the same base as the filter. Then the powder sandwich was linked to a closed loop, including a pump and scintillation cell when a high flow rate was used. For low flow rate, only the RAD7 was included. In order to measure the emanation coefficient of the sources, the Ra-224 content was measured by gamma spectroscopy. The values of the emanation masses were found to be 0.33 g, 0.31 g, and 3.57 g, the estimation of the emanation coefficients were 0.079, 0.012 and 0.074.

Csordás *et al.*, (2015) has prepared a Rn-220 source from thorium nitrate and identified ceramics. The prepared sources were tested for a different range of temperature 200°C, 600°C, and 900°C in order to observe correlation between the emanation coefficient of the source and the temperature. Moreover, the effects of the types of the ceramics and the contents of thorium nitrate in the sources and the emanation coefficient were observed. To do so, a chamber with 0.0014 m<sup>3</sup> equipped with a SARAD RTM 2100 detector was used to measure the activity concentration which was used to obtain the emanation coefficient. A significant correlation was observed between the effect of temperature and the types of the ceramics while no significant correlation was found with the thorium nitrate and emanation coefficient of the source. The emanation coefficient obtained ranged from  $0.34 \pm 0.03\%$  to  $7.69 \pm 0.13\%$ .

A study has been done (Wang, Zhang and Guo, 2017) to measure the emanation power of a flow-through Rn-220 source. Incandescent gas mantles with a known mass were used as a Rn-220 source. Three batches were studied. The RAD7 was connected to the end of the exhalation pipe and each batch was tested for different flow rates. The emanation power was obtained from fitting a curve which was plotted using the change of the flow rates versus the measured activity concentration. The fitting curve agreed with a mathematical formula derived for this purpose. The emanation power of the three batches obtained were  $1.33\% \pm 0.17\%$ ,  $0.77\% \pm 0.1\%$  and  $0.57\% \pm 0.07\%$ . This result agreed with the emanation power measured using a LaBr<sub>3</sub> gamma detector.

### 3.4 Summary

In this Chapter a review of measurement systems for Rn-220 was given, as well as a summary of different Rn-220 sources and measurement chambers that have been developed. In most of these methods, solid sources were used where the emanation of these sources depends on environmental parameters such as temperature, pressure, etc. The Rn-220 reference activity concentration atmosphere method developed by Röttger *et al.*, (2010) is very accurate and it produces a higher percentage of Rn-220 with low uncertainty compared to the other developed sources. However it is expensive and it is not practical for small laboratories to duplicate it.

Most of the methods discussed in this chapter are expensive in terms of resources. This led to the development of an alternative method. We developed a Rn-220 source that uses a liquid solution of Th(NO<sub>3</sub>)<sub>4</sub>.6H<sub>2</sub>O which is independent of the environmental parameters and produces appreciable Rn-220 when air is bubbled through the solution. The details of the Rn-220 source will be presented in Chapter four. The new method is simple, cheap and gives reliable results.

# CHAPTER 4

## Novel Thoron standard source

### 4.1 Introduction

In this chapter, the procedure for making a novel Rn-220 standard source will be presented. The preparation of the Rn-220 standard source which is made from  $\text{Th}(\text{NO}_3)_4 \cdot 6\text{H}_2\text{O}$  will be described. Then the measurement of the of the Rn-220 concentration using the HPGe will be discussed followed by the description of the novel procedure for producing a stable stream of Rn-220 by bubbling. Finally, the procedure for the of Rn-220 measurements using the RAD7 will be presented.

### 4.2 The Rn-220 source preparation

A bottle of  $\text{Th}(\text{NO}_3)_4 \cdot 6\text{H}_2\text{O}$  has been in the physics department of the University of the Western Cape for more than 15 years. A certain amount of the  $\text{Th}(\text{NO}_3)_4 \cdot 6\text{H}_2\text{O}$  was used in this study to prepare a Rn-220 source. The details of the source preparation are discussed in the following sub-section.

#### 4.2.1 $\text{Th}(\text{NO}_3)_4 \cdot 6\text{H}_2\text{O}$ drying

A mass of 12.2 g of  $\text{Th}(\text{NO}_3)_4 \cdot 6\text{H}_2\text{O}$  was taken from the stored bottle and was put in a pre-weighed crucible and heated up to  $140^\circ\text{C}$ . The heating process was continued until all water evaporated from the sample and the mass of the sample was found every five minutes until there was no change in the mass of the sample (Figure 4.1.a.). The weight of the sample was determined using a scale (Scout-Pro, OHAUS) which is depicted in Figure 4.1.c. The weights of the sample were obtained by subtracting the mass of the empty crucible and the mass of the crucible with the sample. The final dry mass of the  $\text{Th}(\text{NO}_3)_4 \cdot 6\text{H}_2\text{O}$  was 10.2 g. This mass was used in the preparation of the thorium nitrate solution.

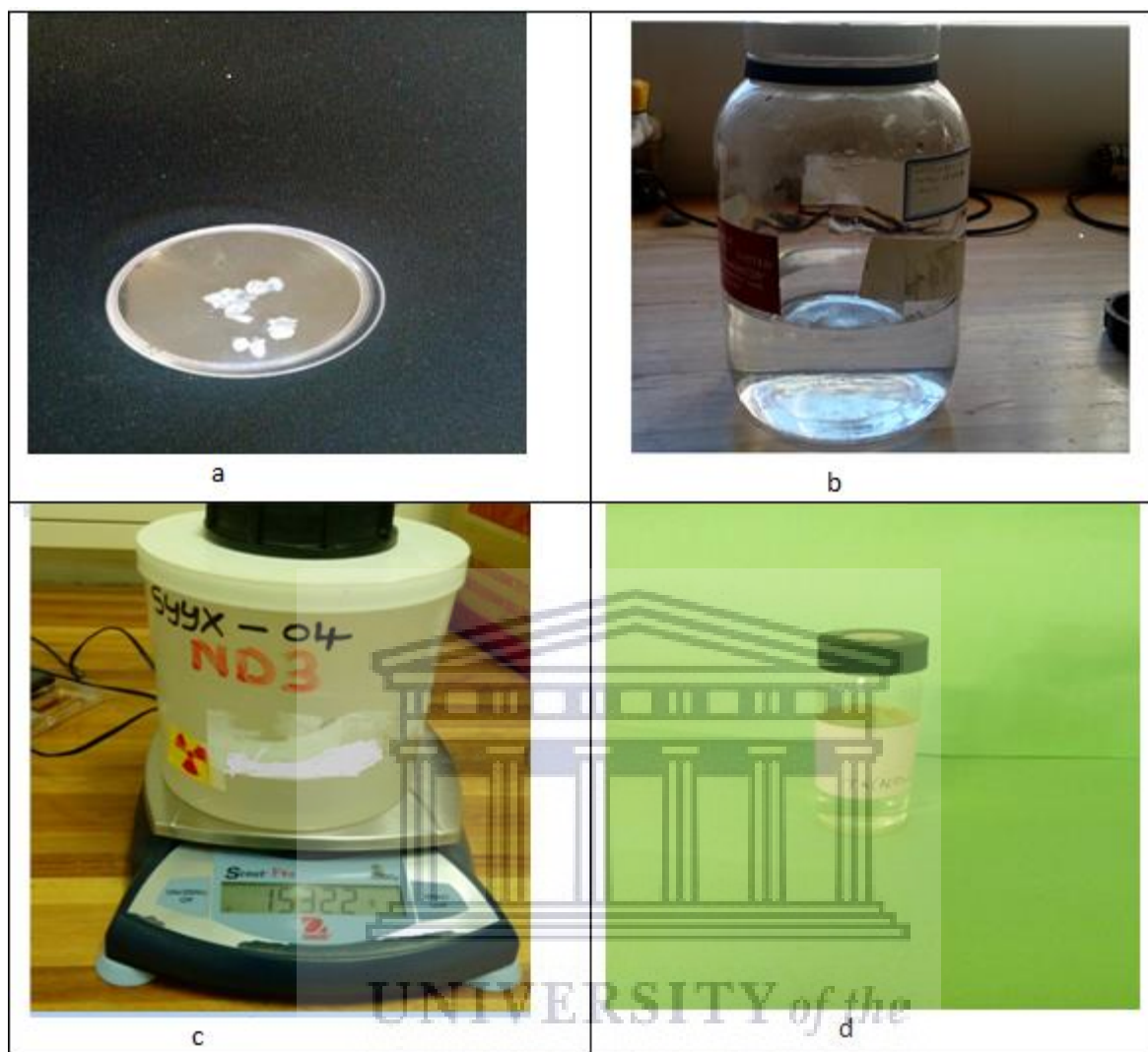


**Figure 4.1:** a) The Rn-220 source preparation by drying the  $\text{Th}(\text{NO}_3)_4 \cdot 6\text{H}_2\text{O}$ . b) The bulk of the  $\text{Th}(\text{NO}_3)_4 \cdot 6\text{H}_2\text{O}$  solution c) The scale and the  $\text{Th}(\text{NO}_3)_4 \cdot 6\text{H}_2\text{O}$  in the Marinelli beaker used for the characterization by the HPGe detector. d) The  $\text{Th}(\text{NO}_3)_4 \cdot 6\text{H}_2\text{O}$  solution in the small bottle used for bubbling.

#### 4.2.2 $\text{Th}(\text{NO}_3)_4 \cdot 6\text{H}_2\text{O}$ solution preparation

The 10.2 g sample of the dried  $\text{Th}(\text{NO}_3)_4 \cdot 6\text{H}_2\text{O}$ , the common form of thorium nitrate at room temperature (Benz *et al.*, 1987), was dissolved in distilled water of 1314.2 ml (Figure 4.1.b). Some of the solution was transferred into a small bottle (total volume around 40 ml) and the mass of  $\text{Th}(\text{NO}_3)_4 \cdot 6\text{H}_2\text{O}$  solution was obtained by subtracting the pre-weighted empty bottle from the filled

one, Figure 4.1.d. The rest of the  $\text{Th}(\text{NO}_3)_4 \cdot 6\text{H}_2\text{O}$  solution was transferred to a Marinelli beaker. The mass of the  $\text{Th}(\text{NO}_3)_4 \cdot 6\text{H}_2\text{O}$  solution in the Marinelli beaker was calculated by subtracting the mass of the pre-weighed empty Marinelli beaker from the filled Marinelli beaker as shown in Figure 4.1.c. Note that 5.7 g from the total mass of the solution was lost during the transferring process through drops stuck on the wall of the big bottle so that the concentration was not changed. Table 4.1 presents some of the masses used in this study.

**Table 4.1:** The measured masses of some quantities used in the study.

| Quantity  | Mass(g)           |
|---|-------------------|
| Small bottle  | $26.6 \pm 0.1$    |
| The total dried thorium nitrate                         | $10.20 \pm 0.14$  |
| The thorium nitrate in the small bottle                 | $0.220 \pm 0.003$ |
| The thorium nitrate in the Marinelli beaker             | $9.93 \pm 0.14$   |
| The solution of the thorium nitrate in the small bottle | $28.70 \pm 0.14$  |
| Thorium nitrate solution in the Marinelli beaker        | $1290 \pm 0.14$   |

The  $\text{Th}(\text{NO}_3)_4 \cdot 6\text{H}_2\text{O}$  solution in the small bottle was kept at the Environmental Nuclear Laboratory at the University of the Western Cape for measurements. The prepared  $\text{Th}(\text{NO}_3)_4 \cdot 6\text{H}_2\text{O}$  sample solution in the Marinelli beaker was sent to iThemba LABS for characterization.

### 4.3 Rn-220 measurements

To generate Rn-220 gas in order to investigate Rn-220 monitors such as the RAD7 to measure Rn-220 concentrations accurately, air is bubbled through the  $\text{Th}(\text{NO}_3)_4 \cdot 6\text{H}_2\text{O}$  solution. The Rn-220 activity in the solution is calculated by finding the activity of the solution in the Marinelli beaker using the HPGe detector. The percentage of the Rn-220 gas that is pumped out from the source is

obtained during the bubbling by simultaneously using a NaI(Tl) detector to measure gamma rays from the Rn-220 daughters. The latter measurement gives the percentage of the Rn-220 that is **not** pumped out which allows the calculation of the percentage that is pumped out. The RAD7 was used to measure the activity concentration of the Rn-220 in the exit stream which can be compared to the value predicted from the percentage pumped out.

### **4.3.1 Rn-220 source characterization using a Hyper-Pure Germanium detector (HPGe)**

To characterize the Rn-220 source, the filled Marinelli beaker with  $\text{Th}(\text{NO}_3)_4 \cdot 6\text{H}_2\text{O}$  (Figure 4.1c) was measured by using the HPGe detector which is located at iThemba LABS, Environmental Radiation Department. The measurements first checked that there secular equilibrium was reached between Tl-208 and Ac-228, which turned out to be true due to the age of the source despite the relatively long half-life of Th-228 (1.9 years). The detector is in a low counting set-up shielded by blocks of lead during the measurements.

The semi-conductor detector is equipped with standard electronics including a multi-channel analyser (MCA) to obtain the gamma-ray spectrum. For the calculation of the activity concentration of the source, certain lines of the nuclides were analysed and counts extracted from the photopeaks from Ac-228 and Tl-208 energy lines. The following subsection describes the efficiency calibration method.

#### **4.3.1.1 Efficiency calibration**

To determine the Rn-220 source activity concentration, the absolute efficiency of the gamma lines of interest at the same geometry as the source measurements is needed. In measuring the detection efficiency of the detector the relative efficiency of the interested gamma lines was measured and then converted to absolute efficiency. The method followed in measuring the photopeak detection efficiencies is similar to that explained in (Croft and Hutchinson, 1999, Talha *et al.*, 2008). The following procedure describes the steps:

$$\varepsilon_{rel} = \frac{N(E_i) - N(E_i)_b}{B \times t} \quad (4.1)$$

Where:

$\varepsilon_{rel}$  = The relative full energy peak efficiency

$N(E_i)$  = The counts in the peak of interest

$N(E_i)_b$  = The background counts in the peak

$B$  = The Branching ratio corresponding to the peak

$t$  = the time of measurements

The relative efficiencies of the photopeak energies were obtained by measuring with the Marinelli beaker filled to the top with the  $\text{Th}(\text{NO}_3)_4 \cdot 6\text{H}_2\text{O}$  solution. To obtain the absolute efficiencies, a KCl solution measurement was conducted with the same volume and geometry as the sample. The absolute efficiency of K-40 is obtained by using the formula

$$\varepsilon(E) = \frac{N}{(A \times B \times t)} \quad (4.2)$$

Where  $N$  is the counts in the K-40 peak corrected for the background radiation and  $A$  is the activity of the dissolved KCl as calculated in Appendix A. Then the scale factor,  $Z$ , used to convert the relative efficiencies to absolute efficiency is obtained by the formula.

$$Z = \varepsilon_{\text{K-40}(\text{abs})} / \varepsilon_{\text{K-40}(\text{rel})} \quad (4.3)$$

The energy lines used to obtain the absolute efficiencies are listed in the table 4.2. For more detail on how the absolute efficiency is obtained using the same method, see (Talha Abdalla, 2009 and Talha *et al.*, 2008).

**Table 4.2:** Gamma-ray lines and associated branching ratios used for efficiency calibration (Firestone *et al.*, 1996, <http://www.nucleide.org>)

| Radionuclide | Energy(keV) | Branching ratio |
|--------------|-------------|-----------------|
| Ac-228       | 338.32(2)   | 0.1125(3)       |
|              | 794.95(6)   | 0.0434(4)       |
|              | 911.205(4)  | 0.2660(7)       |
|              | 968.97(10)  | 0.1617(3)       |
|              | 583.19(2)   | 0.3041(17)      |
| Tl-208       | 860.56(3)   | 0.045(10)       |
|              | 2614.53(10) | 0.356(6)        |
| K-40         | 1460.83     | 0.1055(11)      |

### 4.3.2 The bubbling method to produce an air stream of known Rn-220 concentration

The equipment listed below was used in order to conduct an experiment using the bubbling method to produce a stable stream of Rn-220 gas to investigate the RAD7 detector measurements. The equipment is depicted in Figure 4.4 as well:

- NaI(Tl) detector 76.2 mm×76.2 mm manufactured by REXON components, INC, USA, serial number 160229-1.
- Multiple channel analyser (MCA) scintiSPEC.
- A pump model TD-3LS, BRAILSFORD & CO. NC. RYE, NEW YOURK. USA.
- .Flow meter - Dwyer Instruments. INC serial N (MMA-21). USA.
- Stainless steel aerator and air-tight gas pipes as a part of RAD7 accessories.
- Computer with winTMCA32™ software installed.
- The small bottle with the (Th(NO<sub>3</sub>)<sub>4</sub>.6H<sub>2</sub>O) solution that acts as the source of Rn-220.



#### 4.3.2.1 The NaI (TI) detector calibration:

The NaI(Tl) detector with the attached ScintiSpec multi-channel analyser is connected to the computer via a USB cable. A Th-232 reference source with nominal activity 110 kBq was used for the energy calibration of the NaI(Tl) detector system. A clear spectrum with well-defined energy peaks were obtained as shown in Figure 4.2. The different radionuclides with their characteristic gamma-ray energies, extending up to 2614 keV are indicated on the figure. The nuclides that were measured are listed in table 4.3

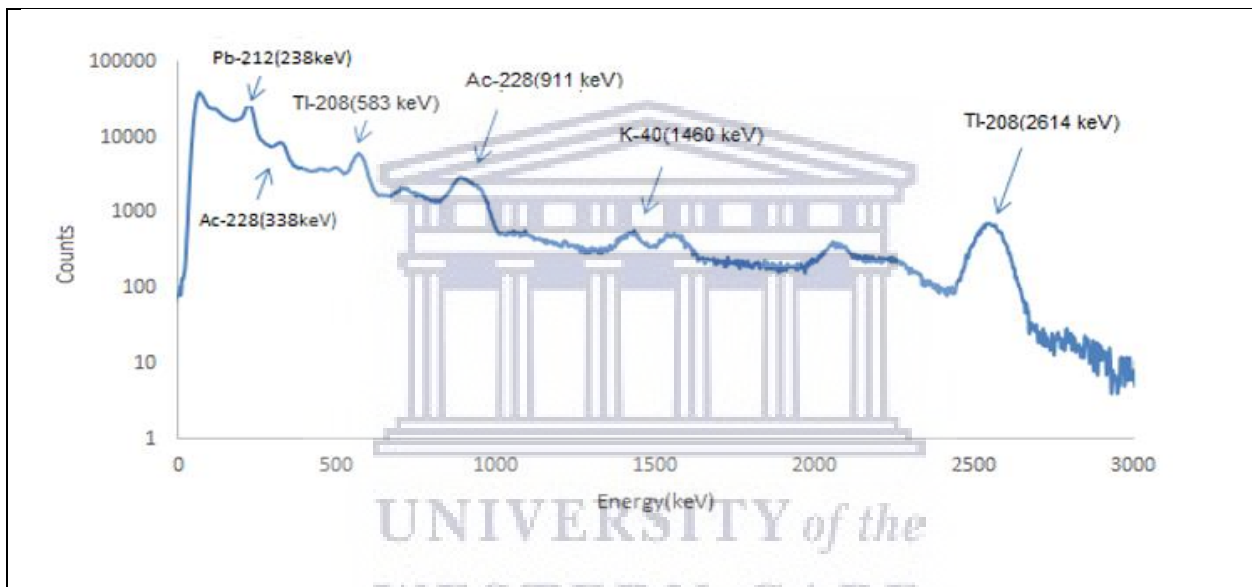


**Figure 4.2:** Gamma-ray spectrum for the Th-232 reference source

**Table 4.3:** The measured nuclei in the Th-232 reference source

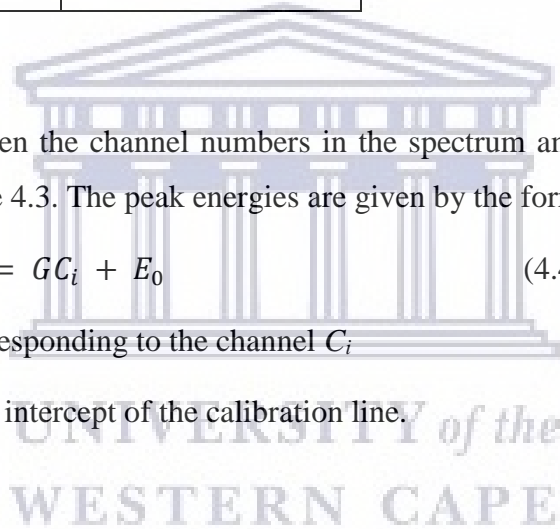
| Nuclide | Energy(keV) |
|---------|-------------|
| Tl-208  | 583         |
|         | 2614        |
| Ac-228  | 338         |
|         | 911         |
| Pb-212  | 238         |
| K-40    | 1460        |

A linear relationship between the channel numbers in the spectrum and gamma-ray energies is obtained as shown in Figure 4.3. The peak energies are given by the formula

$$E_i = GC_i + E_0 \quad (4.4)$$

Where  $E_i$  is the energy corresponding to the channel  $C_i$

$G$  is the gradient and  $E_0$  the intercept of the calibration line.



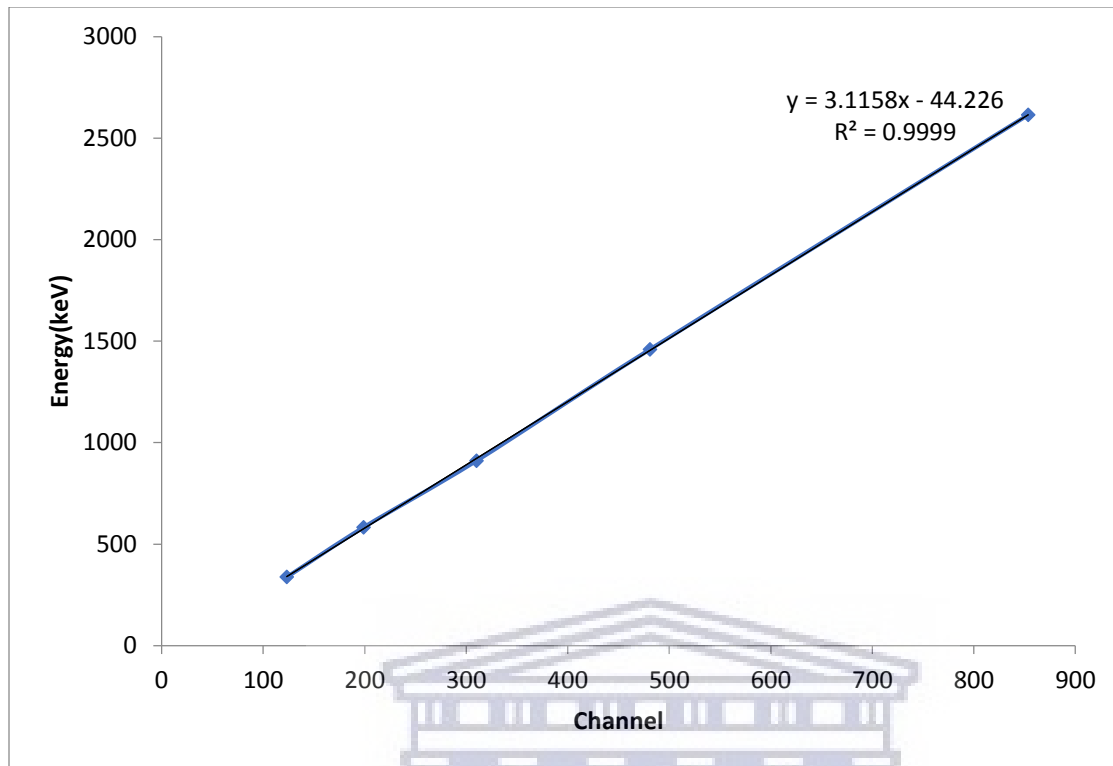


**Figure 4.3:**  $\gamma$  – ray energy versus channel number used for the energy calibration of the NaI(Tl)

### 4.3.2.2 NaI(Tl) photo peak efficiencies

#### 4.3.2.2.1 KCl solution measurements

To obtain the absolute efficiency of the NaI detector, 9.6 grams of KCl was dissolved in 29.7 grams of distilled water in a small bottle, similar to the one used for the Rn-220 source. The KCl solution was measured using the NaI(Tl) detector. The measurements were conducted for several hours with the same geometry for the KCl solution as for the Rn-220 measurements. The gamma-ray peak of the K-40 at 1460 keV was detected and the net counts were calculated by subtracting the contribution of the background radiation to this peak which was already measured before the KCl measurements were conducted. Later these net counts were used to calculate the absolute efficiency for this peak which was derived from the activity concentration of the 9.6 g of KCl from the KCl powder bought from MERCK Inc. (99.5% purity). More detail of the activity calculation of the KCl solution is presented in Appendix A.

#### 4.3.2.2 MCNPx simulation

As an extra check on the detection efficiency of the NaI(Tl) detector at the energy peaks of interest, a calculation using the MCNPx (Monte Carlo N-Particle extended) code was used to simulate the geometry of the NaI(Tl) detector and the small bottle with the solutions. The MCNPx (Monte Carlo N-Particle extended) is a multi-purpose Monte Carlo radiation transport code with 3D geometry and continuous – energy transport of several particles and light ions. (Maleka et al, 2011; Briesmeister, 2000; Waters *et al.*, 2007). Table 4.4 shows some of the parameters used in the simulation process. The simulated efficiencies were normalised by the absolute efficiency of K-40 (1460keV).

**Table 4.4 :** The parameters used in the MCNPX simulation

|  |                 |
|--|-----------------|
| Detector size                            | 76.2 mm×76.2 mm |
| Aluminium cover thickness                | 0.5 mm          |
| Diameter of the cylindrical glass bottle | 27.6 mm         |
| The thickness of the glass bottle        | 2 mm            |
| The volume of KCl solution               | 29.7 ml         |
| The height of the KCl solution           | 68.8 mm         |
| The mass of KCl powder                   | 9.6 g           |

#### 4.3.3 Background radiation measurements:

For quality assurance, the room background gamma radiation was measured before and after the Rn-220 measurements. Before the Rn-220 source measurements were conducted, the background radiation was measured during the night and during the day. The measurements taken during the night were conducted for 12 hours. The second measurement was taken for several hours. The background radiation measurements were taken before and after the Rn-220 measurements so as to be sure that the background radiation did not change. No significant change in the background

radiation measurements was found. For consistency checks, background radiation measurements for one hour were regularly taken and used for this study.

In order to try to improve our set-up, a separate measurement was done where the bottle with the solution was all enclosed in a lead shield to reduce the background radiation. The results of this experiment will also be shown in the next Chapter.

#### 4.3.4 The bubbling method

After the NaI(Tl) detector was calibrated for energy and efficiency, it was included in the bubbling set-up as shown in Figure 4.4. The small bottle with  $\text{Th}(\text{NO}_3)_4 \cdot 6\text{H}_2\text{O}$  solution (Figure 4.1d) was placed up against the NaI(Tl) detector. A pump connected to a flow meter was used to pump the air through the solution using the stainless steel aerator supplied as a part of the radon in water accessories of the RAD7 system. The choice of the flow rate was usually set at 0.6 L/min. The aerator has a glass tube that forces air through a glass frit inside the solution. While bubbling air and pumping the Rn-220 off the solution, the gamma rays released from the solution were measured simultaneously to find the activity of the thoron daughters and hence the fraction of the thoron not pumped away.

The gamma-ray spectrum was obtained using a scintiSPEC Multi-Channel Analyser system which provides a spectroscopy system via a USB interface. The winTMCA32 software, serial number 20-10047977 version 2.6.00 was used to operate the MCA. The usual problems of (Gilmore, 2008) slight gain drift can be a major problem when measuring samples over several hours as in this study. A gain stabilization method was used to keep the 1460 keV peak in more or less the same position by changing the fine gain every 6 minutes. The software allows for this to be done automatically, but we preferred to do this with a batch file which allows us to interrogate the amount of drift (see Appendix B).

The measurements were conducted over a period of more than 2 days. The spectra were automatically collected and saved after every hour.

To check the reproducibility, the bubbling method was repeated for different flow rates and with a locally developed bubbler. Moreover, in order to reduce the room background radiation, a lead castle was used in a series of separate measurements as shown schematically in Figure 4.5 and 4.7.

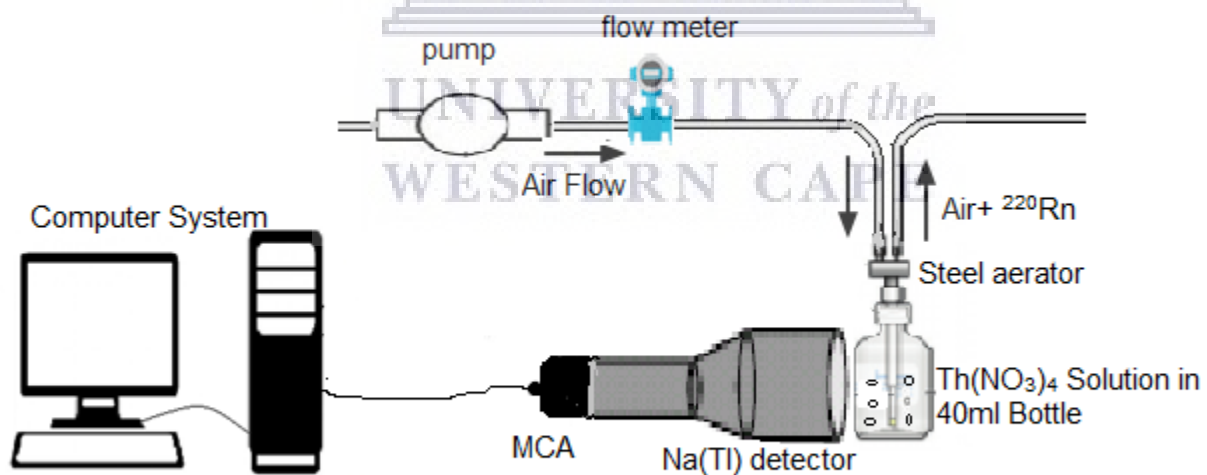
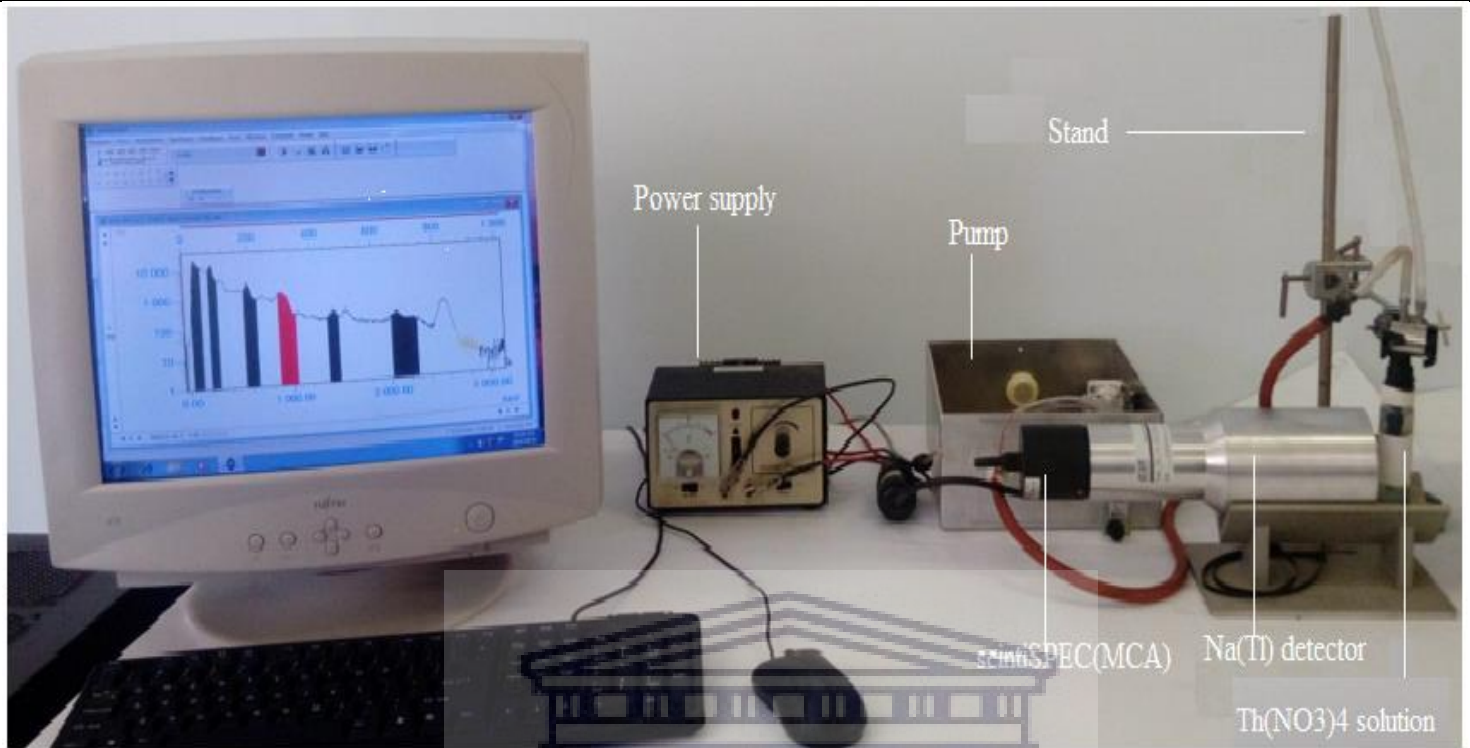


**Figure 4.4:** The picture showing the Rn-220 standard source experiment setup (top); the schematic diagram of the setup (bottom).

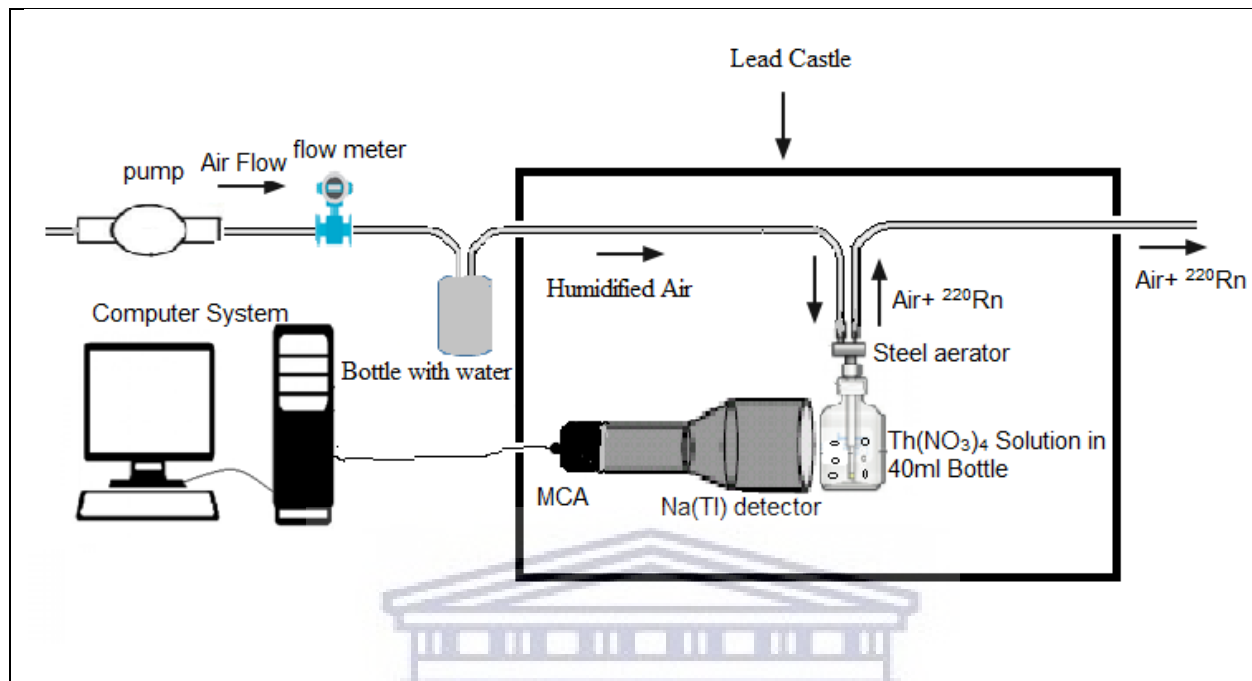


**Figure 4.5:** Schematic diagram of Rn-220 standard source experiment setup using the lead castle.

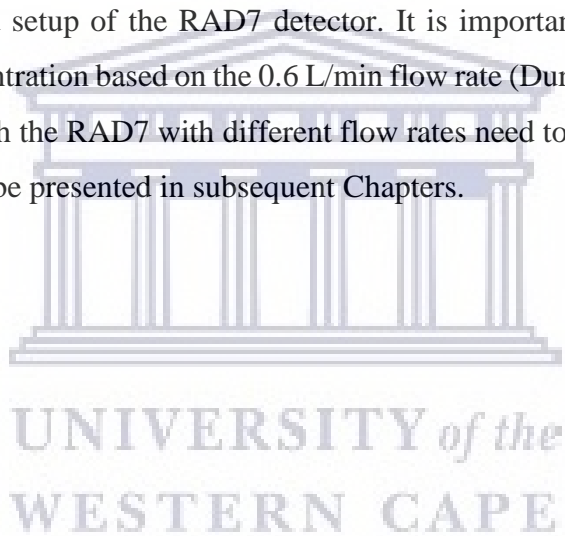
#### 4.3.5 RAD7 measurements

In order to use the RAD7 to conduct Rn-220 measurements, the setup recommended in the RAD7 manual was used. The pipe tubing used for the Rn-220 path from the sample point to the inlet filter has a length of less than one meter. It has a diameter of 0.476 cm which is reduced to 0.318 cm at the inlet filter. The relative humidity inside the RAD7 cell can reduce the sensitivity of the Rn-220 measurement. To maintain a low humidity inside the RAD7, a 15 cm drying unit tube filled with desiccant was used while the measurements were conducted. For the thoron setup the RAD7 measurements were performed using the sniff mode with 5 cycles and zero recycle. The internal RAD7 pump was switched off and the external pump was used that was set on 0.6 L/min as mentioned in section 4.3.4. Some researchers have reported that the RAD7 pump is not reliable (Sorimachi 2016). Before the measurements were conducted, the RAD7 was purged in a closed

loop using a big dryer unit filled with desiccant to reduce the relative humidity of the internal cell and to clean the cell from daughters of Rn-220 and Rn-222.

The Rn-220 activity concentration was measured by sending the exit stream from the bubbler (see Figure 4.4) to the small drying unit and from there to the inlet filter on the RAD7 detector (see Figure 4.6). The measurements of the Rn-220 activity concentration were repeated during the bubbling over more than two days in order to check the stability of the Rn-220 source. Intermittent measurements every one hour for six hour periods were conducted.

In order to test our system under different conditions for Rn-220 measurements proposed in this work, different flow rates were used. To check on the reproducibility of the source, additional measurements were conducted (see Figure 4.7). The flow rates were changed to values not recommend as the standard setup of the RAD7 detector. It is important to note that the RAD7 measures the activity concentration based on the 0.6 L/min flow rate (Durridge, 2015). The activity concentration measured with the RAD7 with different flow rates need to be corrected. The results of these different tests will be presented in subsequent Chapters.





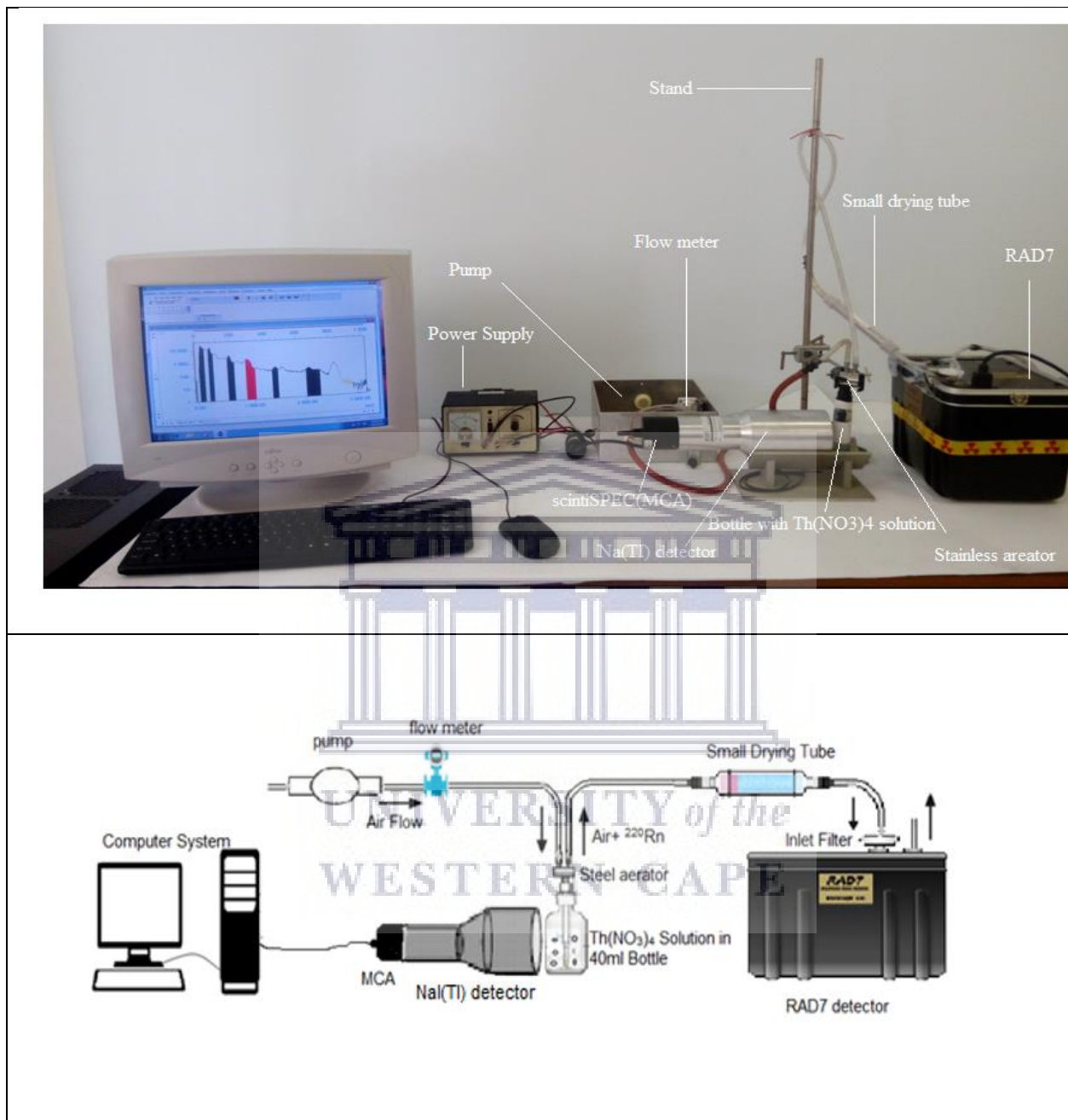


**Figure 4.6:** A picture showing the RAD7 connected to the Rn-220 standard source in the experiment setup (top). A schematic diagram showing the RAD7 connected to the Rn-220 standard source (bottom).

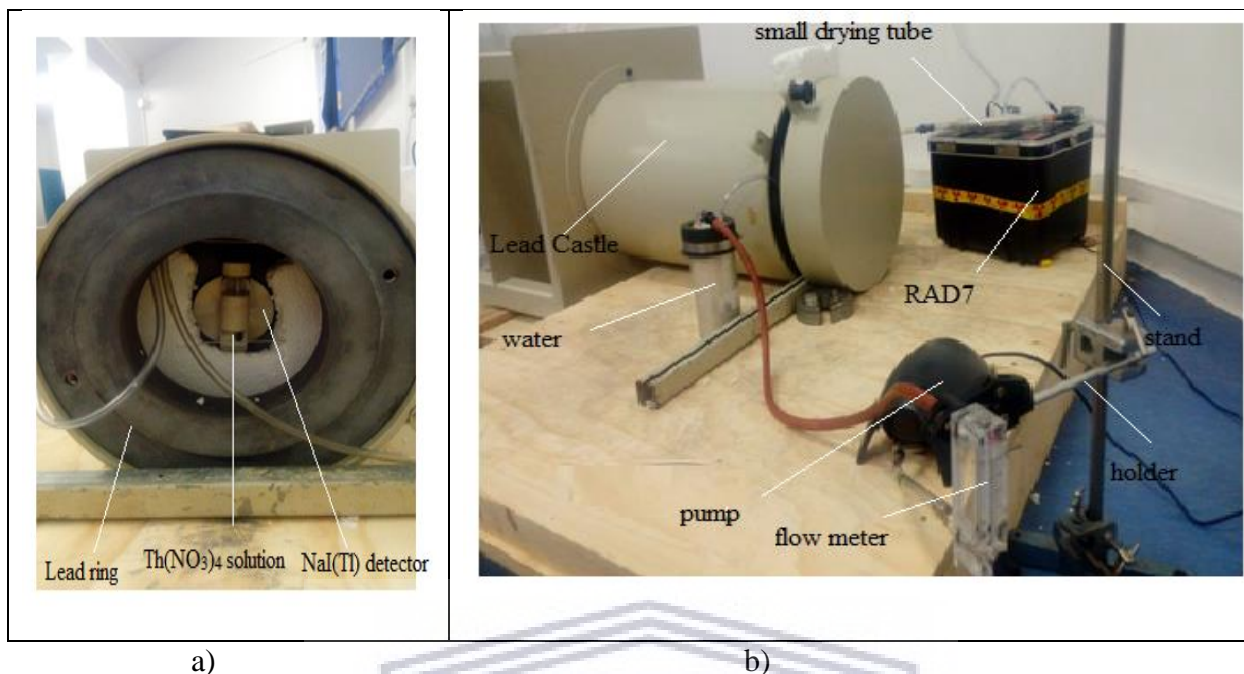
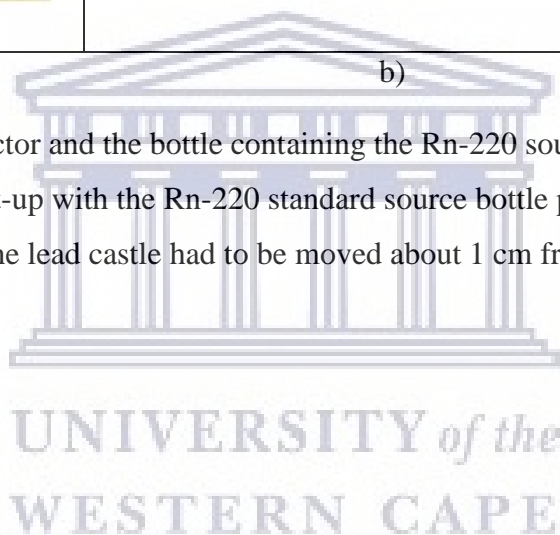


**Figure 4.7:** a) NaI(Tl) detector and the bottle containing the Rn-220 source inside the lead castle. b) The lead castle set-up with the Rn-220 standard source bottle placed inside the lead castle. Note that the lid of the lead castle had to be moved about 1 cm from the structure to accommodate the pipes.



#### 4.4 Summary

The preparation of the Th(NO<sub>3</sub>)<sub>4</sub>·6H<sub>2</sub>O solution which was used as Rn-220 source was presented in this chapter. The procedure of characterizing the Rn-220 source using the HPGe detector was explained.

The setup of the bubbling system and measurement procedure for creating a steady air stream containing the Rn-220 gas was presented. The procedure of using the RAD7 to measure the activity concentration of the Rn-220 that was pumped off the solution by the bubbling method were explained. The next chapter will present the results of the HPGe, NaI(Tl) and RAD7 detector measurements.

# CHAPTER 5

## HPGe, NaI(Tl) and RAD7 Results

### 5.1 Introduction

In the present chapter the measurements obtained using: 1. The gamma ray detectors namely NaI(Tl) and HPGe and 2. Alpha detector in the RAD7, will be presented. The details on how these detectors work were presented in chapter 2.

### 5.2 HPGe detector measurements

Before the HPGe detector is used to detect gamma rays from the actual sample, which has a relatively low activity, it is important to take background measurements.

#### 5.2.1 The room background radiation

In order to characterize the Rn-220 source, room background radiation measurements were conducted for 236024 s. To reduce the room background radiation, the HPGe detector is shielded with lead blocks and a thin layer of copper is inserted to protect the detector from the x-rays which could be produced from the lead. Figure 5.1 illustrates the spectrum collected from the room background.

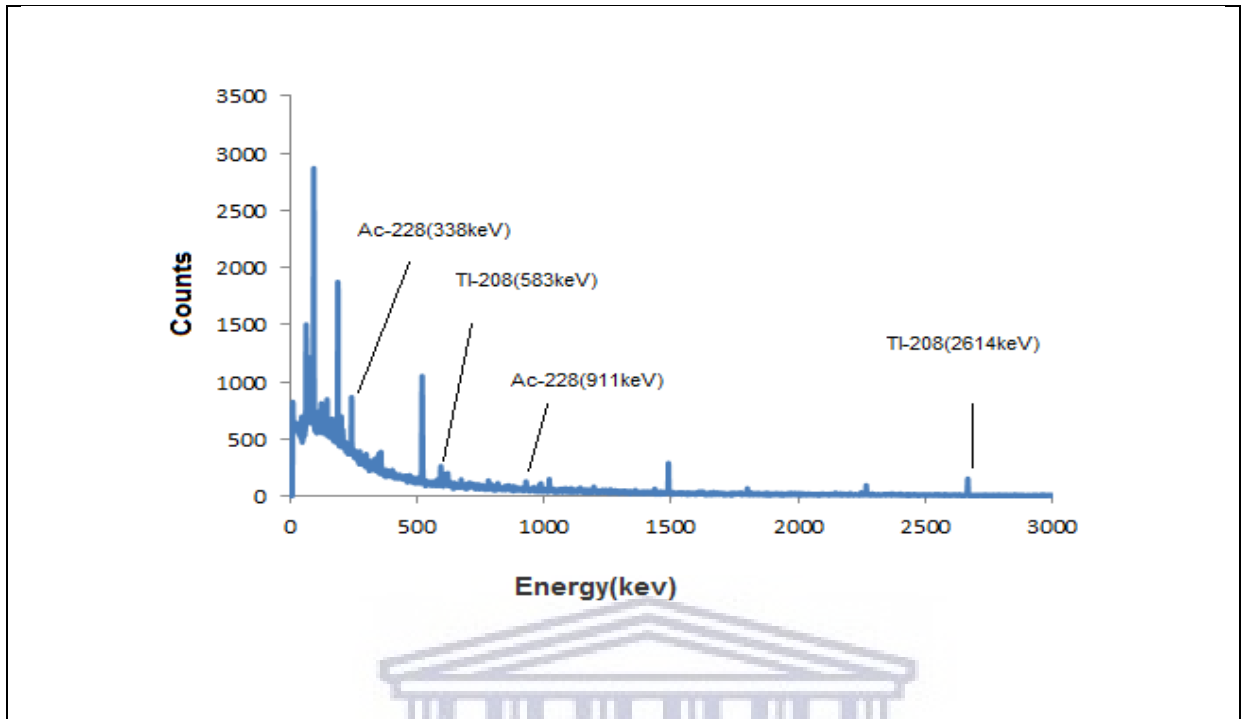


**Figure 5.1:** Gamma-ray spectrum of the room background radiation measurement.

### 5.2.2 The Rn-220 source characterization

To characterize the Rn-220 source, the 1.3 L solution of  $\text{Th}(\text{NO}_3)_4 \cdot 6\text{H}_2\text{O}$  was measured in a Marinelli beaker. The measurements were done for 3600 s. The spectrum was analysed using the Palmtop software, which entailed selecting the regions of interest for both spectra of the source and the background. A typical gamma spectrum of 3600 s live time is illustrated in Figure 5.2.

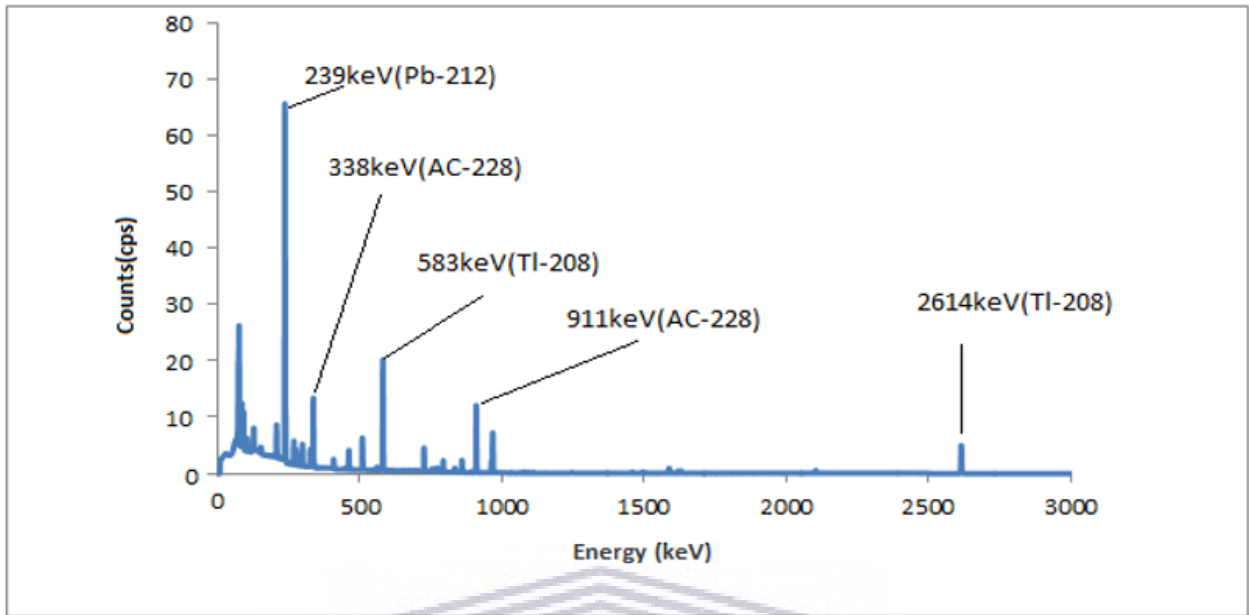


**Figure 5.2:** A typical gamma ray spectrum of the  $\text{Th}(\text{NO}_3)_4 \cdot 6\text{H}_2\text{O}$ .

The activity concentration of the source was calculated using the following expression.

$$A(\text{Bq/kg}) = \frac{N_{net}}{B \cdot \epsilon \cdot t_s \cdot m} \quad (5.1)$$

where:

$N_{net}$  is the net counts under the photopeak corrected for the background radiation

$$N_{net} = N_s - \frac{t_s}{t_b} N_b \quad (5.2)$$

$N_s$  is the total number of the counts of the photopeak in the source spectrum,  $N_b$  is the total number of the corresponding counts in the photopeak in the background spectrum,  $t_s$  is the measurement live time in seconds for the source spectrum and  $t_b$  is the live time for the background radiation spectrum.  $B$  is the branching ratio of the nuclide,  $m$  is the mass of the source measured in (kg) and  $\epsilon$  is the photopeak efficiency.

In order to calculate the activity concentration of the Rn-220 source, the detection efficiency of the nuclei of interest which were used in estimating the activity concentration of the Rn-220 source

needed to be measured. The method of obtaining the efficiencies has been explained in (Talha, 2009 and Croft, 1999). The efficiencies of the lines used in calculating the activity concentration of the Rn-220 source are presented in Table 5.1 and plotted in Figure 5.3 as well.

**Table 5.1:** Gamma energy lines and their associated efficiencies

| E(keV) | Efficiency( $\epsilon$ ) |
|--------|--------------------------|
| 338    | $0.02438 \pm 0.00057$    |
| 794    | $0.01302 \pm 0.00022$    |
| 911    | $0.01178 \pm 0.00018$    |
| 968    | $0.01126 \pm 0.00017$    |
| 583    | $0.01634 \pm 0.00031$    |
| 860    | $0.01228 \pm 0.00020$    |
| 2614   | $0.00543 \pm 0.00004$    |

UNIVERSITY of the  
WESTERN CAPE

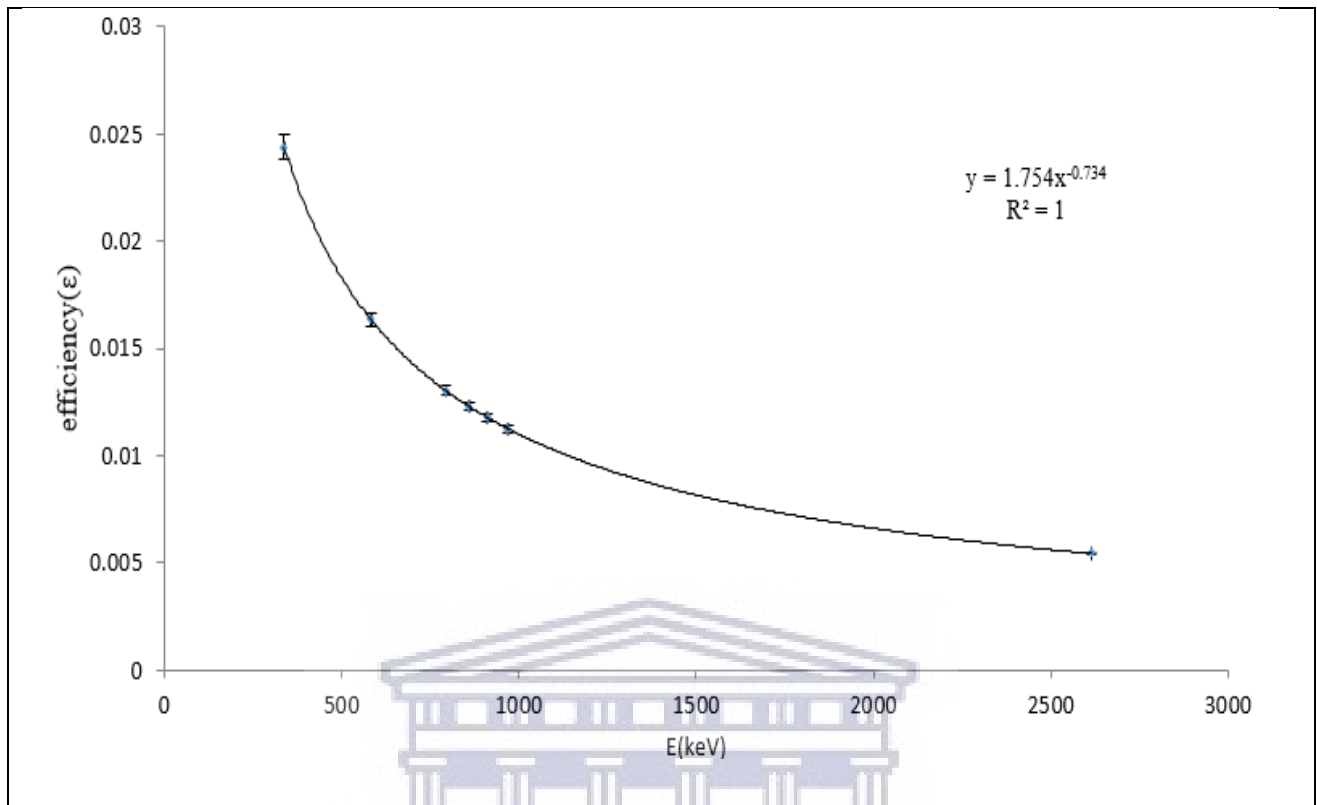


**Figure 5.3:** The efficiency of the detector as a function of energy.

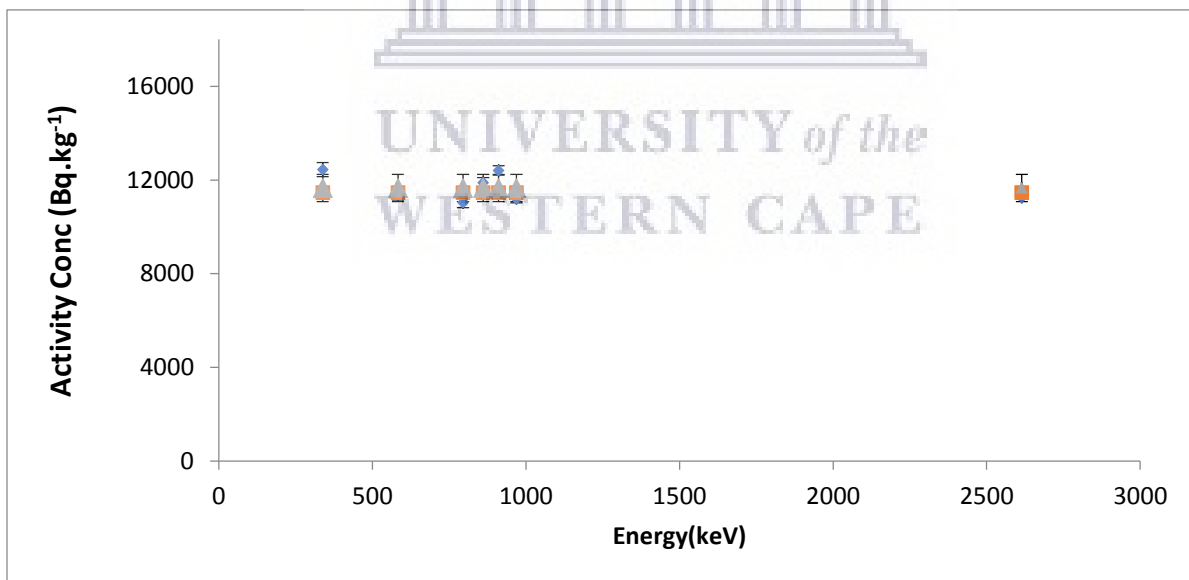


**Figure 5.4:** The activity concentration (diamond), the average activity concentration (triangle) and the average weighted activity concentration (square).

After obtaining the efficiencies, the activity concentration was determined using equation 5.1. Figure 5.4 illustrates the activity concentration obtained.

### 5.2.3 Calculated activity concentration of the $\text{Th}(\text{NO}_3)_4 \cdot 6\text{H}_2\text{O}$ solution

In order to calculate the activity of the Rn-220 source,  $\text{Th}(\text{NO}_3)_4 \cdot 6\text{H}_2\text{O}$ , a 10.2 g of the dried sample crystals was dissolved in 1314.2 g distilled water. Some amount of the solution (28.7 g) was transferred to a small bottle and the rest was transferred to a Marinelli beaker (1290 g) as discussed in section 4.2.2. To enable the use of the solution which was transferred into the Marinelli beaker, the amount of  $\text{Th}(\text{NO}_3)_4 \cdot 6\text{H}_2\text{O}$  in the Marinelli beaker was obtained by using the following formula.

$$\frac{\text{(Mass of the Th(NO}_3)_4 \cdot 6\text{H}_2\text{O solution in the Marinelli beaker)}}{\text{(total mass of the solution in large bottle)}} \times \text{(mass of the Th(NO}_3)_4 \cdot 6\text{H}_2\text{O)} \quad (5.3)$$

When the values are substituted, we get = 9.93 g.

The above-obtained value of  $\text{Th}(\text{NO}_3)_4 \cdot 6\text{H}_2\text{O}$  was used to calculate the expected activity in the Marinelli beaker using the basic equation ( $A = \frac{m \times 6.02 \times 10^{23} \times \lambda}{M}$ ), where  $m$  is the mass of  $\text{Th}(\text{NO}_3)_4 \cdot 6\text{H}_2\text{O}$ ,  $M$  the Molar mass of  $\text{Th}(\text{NO}_3)_4 \cdot 6\text{H}_2\text{O}$  and  $\lambda$  the decay constant of Th-232. The absolute activity was found to be  $15960 \pm 225$  Bq, therefore, the activity concentration in the volume of the Marinelli beaker (1.3 L) is predicted to be  $12280 \pm 140$  Bq/L

The weighted average measured activity concentration of the solution as measured with the HPGe was found to be about  $11460 \pm 180$  Bq/L. Since we are uncertain about the purity of the  $\text{Th}(\text{NO}_3)_4 \cdot 6\text{H}_2\text{O}$  crystals, we decided to use the measured activity.

The result found from the analysis of the activity concentration in the solution in the Marinelli beaker using the HPGe detector helps us in the characterization of our sample in the small bottle since it formed part of the solution. We use the ratio of the masses of the solutions to obtain the initial activity of the solution in the small bottle. The next section presents the analysis and the results of the solution in the small bottle using the bubbling method with the NaI(Tl) setup.



## 5.3 Thoron standard source Procedure using NaI(Tl) detector

### 5.3.1 Room background radiation measurements

Before the Rn-220 standard source measurements were conducted, the room background radiation was measured. The detector was placed in the same geometry as all the measurements of the Rn-220 source. All the spectra files were accumulated using the winTMCA32 software which saves the files as SPC files which were read into an Excel spreadsheet using a Visual Basic program (see Appendix C). Figure 5.5 represents the spectrum of room background radiation. The spectrum was obtained for one hour.

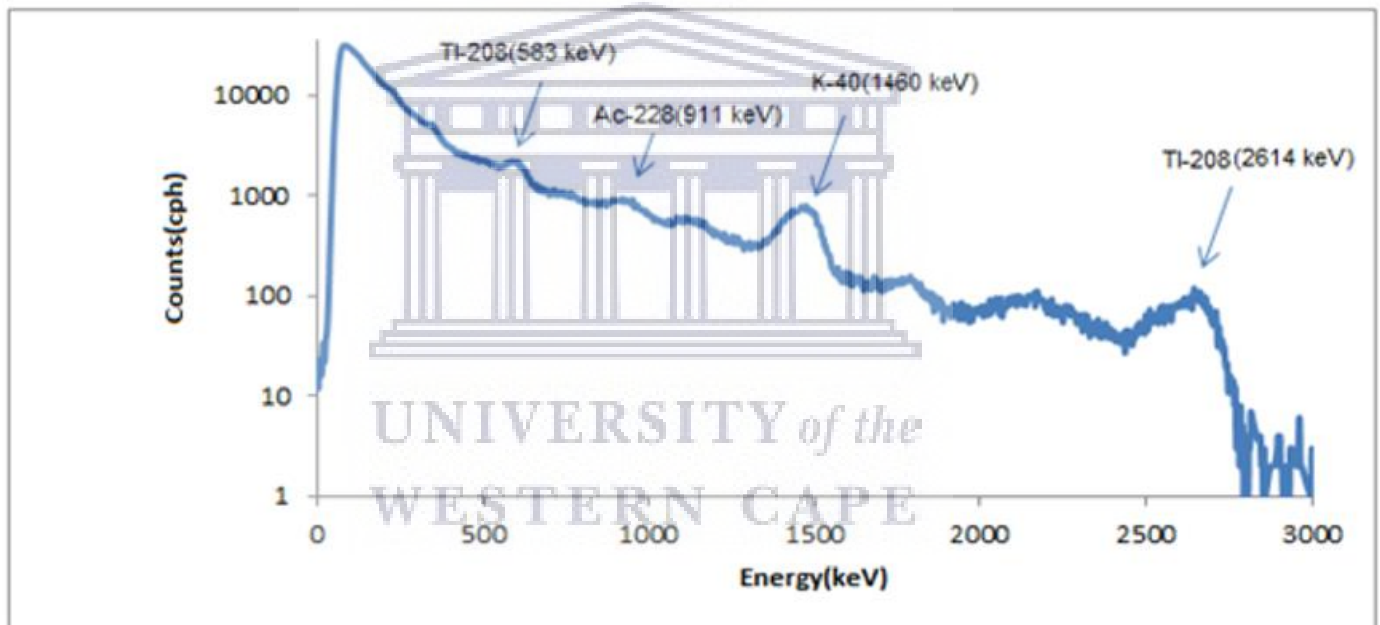


**Figure 5.5:** Room background spectrum accumulated for one hour showing some gamma energy lines of interest.

From Figure 5.5, three gamma energies have been identified which belong to the Th-232 decay series namely 583 keV, 911 keV and 2614 keV while the 1460 keV line represents the decay of K-40.

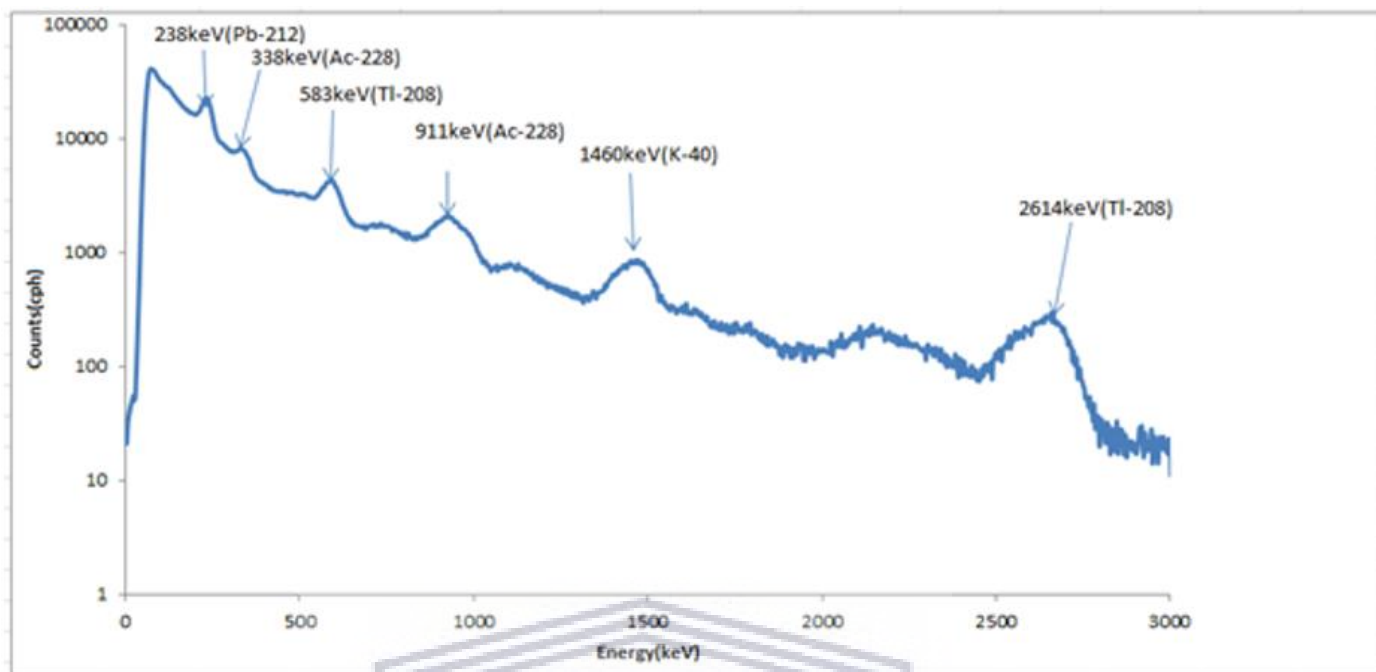
To calculate the number of counts in the photopeaks, *Regions of Interest* were set manually and then the number of counts were determined automatically. Later the background counts were subtracted from the number of counts in the photopeak of interest to obtain the net counts.

### **5.3.2 Analysis of the Thorium nitrate solution bubbling procedure**

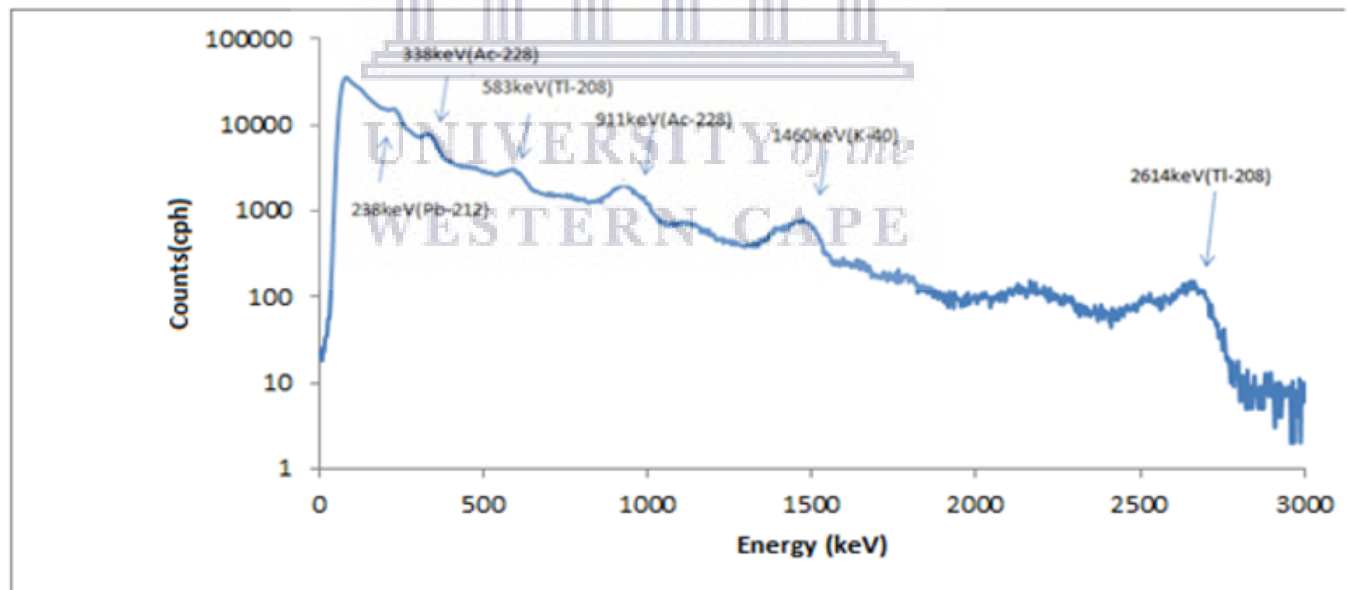
The bubbling procedure was used to pump Rn-220 out of the  $\text{Th}(\text{NO}_3)_4 \cdot 6\text{H}_2\text{O}$  solution. At the same time the gamma rays emitted from the solution were measured using the NaI(Tl) as mentioned in section (4.3.4) and the spectra were collected. Measurements were conducted for 66 hours and the accumulated spectra were collected every one hour. A computer script was written using the winTMCA software in order to collect a separate spectrum every hour- see Appendix D. Figure 5.6 shows the spectrum of the  $\text{Th}(\text{NO}_3)_4 \cdot 6\text{H}_2\text{O}$  solution after one hour of pumping Rn-220 from the solution. The spectrum regions of interest were set on the Ac-228 peaks (338 keV, 911 keV), Pb-212 (238 keV), K-40 (1460 keV), and Tl-208 (583keV, 2614keV). Figure 5.7 represents a gamma spectrum collected from the solution for the 28<sup>th</sup> hour of pumping Rn-220 from the solution, while Figure 5.8 shows the gamma ray spectrum collected from the solution for the 66<sup>th</sup> hour of pumping Rn-220. In order to study the behaviour of the nuclei while Rn-220 was pumped off the solution, the combination of the three spectra are plotted in Figure 5.9.



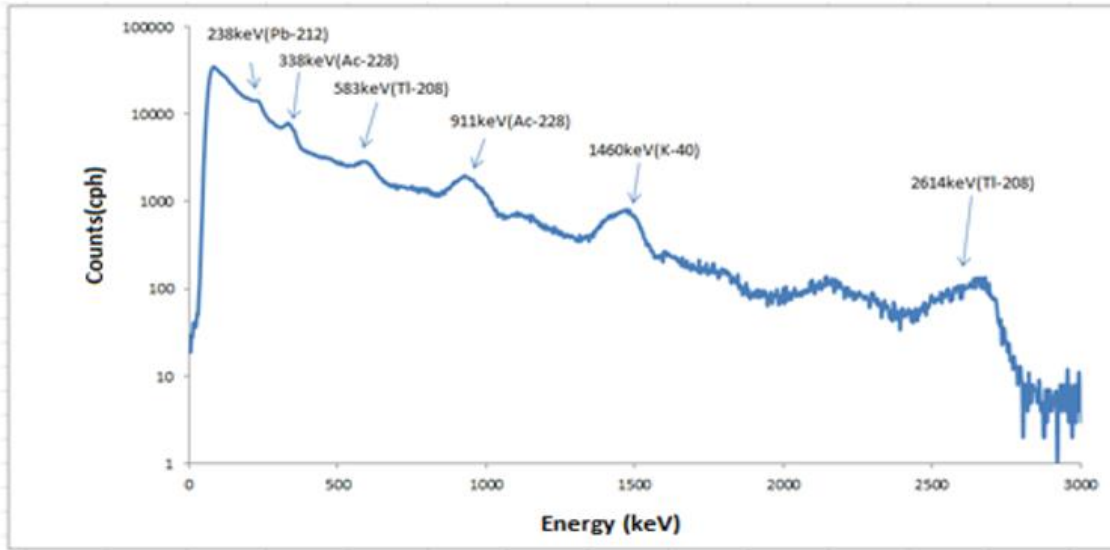
UNIVERSITY of the  
WESTERN CAPE



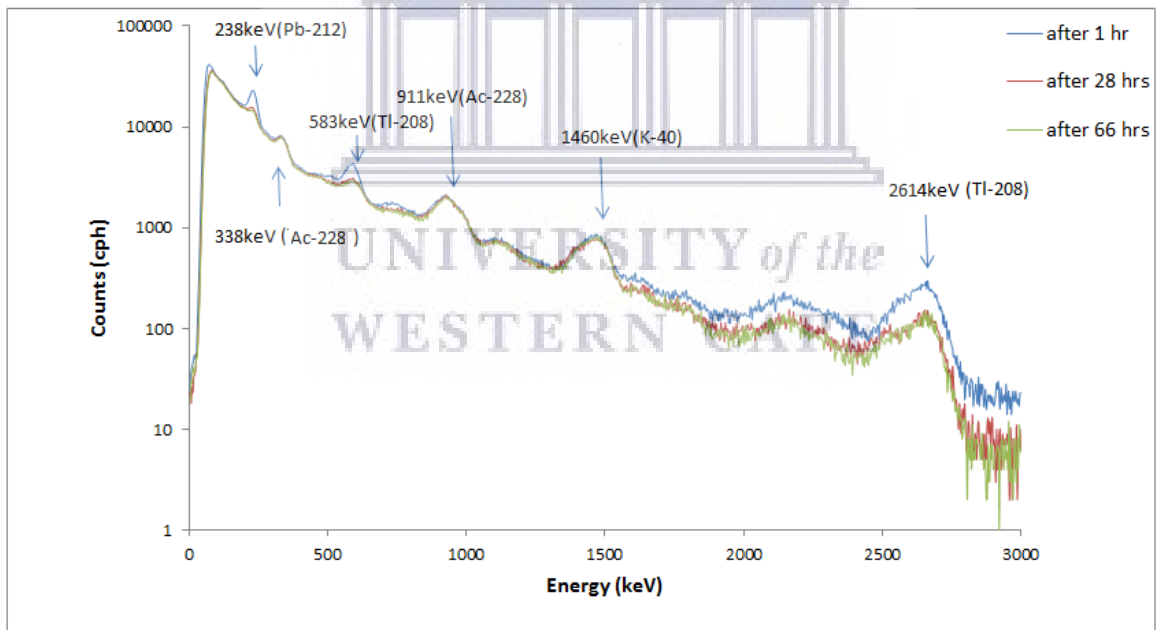
**Figure 5.6:** Gamma-ray spectrum of  $\text{Th}(\text{NO}_3)_4 \cdot 6\text{H}_2\text{O}$  solution for the first hour of bubbling



**Figure 5.7:** Gamma-ray spectrum of  $\text{Th}(\text{NO}_3)_4 \cdot 6\text{H}_2\text{O}$  solution for the 28<sup>th</sup> hour of bubbling.



**Figure 5.8:** Gamma-ray spectrum of  $\text{Th}(\text{NO}_3)_4 \cdot 6\text{H}_2\text{O}$  solution for 66<sup>th</sup> hour of bubbling.



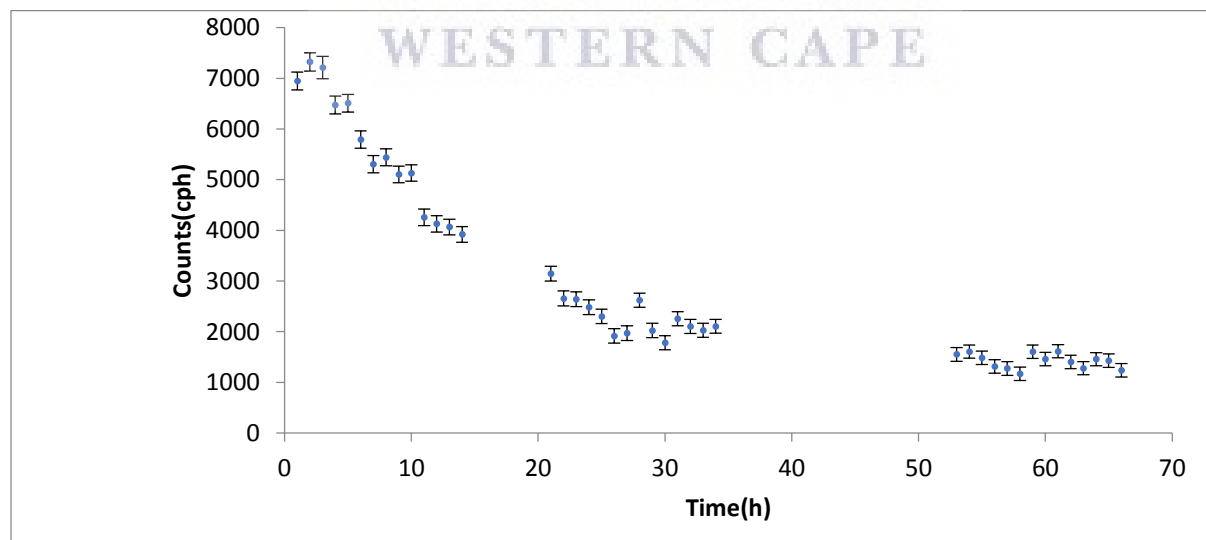
**Figure 5.9:** The gamma ray spectra of bubbling for the first hour, 28<sup>th</sup> hour and 66<sup>th</sup> hour.

Figure 5.9 shows a combination of the spectra accumulated for the first hour, 28<sup>th</sup> hour and 66<sup>th</sup> hour of bubbling respectively. From Figure 5.9 the reduction of the gamma intensity of the Rn-

220 daughters Pb-212 (238 keV), Tl-208 (583, 2614 keV), while bubbling air through the solution and the Rn-220 gas is pumped from the  $\text{Th}(\text{NO}_3)_4 \cdot 6\text{H}_2\text{O}$  solution can be clearly seen. Take note that the nuclide before Rn-220 in the decay chain (see Figure 1.1) were not affected as the  $\text{Th}(\text{NO}_3)_4 \cdot 6\text{H}_2\text{O}$  solution was bubbled with air. There was no significant change in the Ac-228 (338, 911 keV) peaks. Since a NaI(Tl) detector was used, it is difficult to distinguish between the 860 keV, 911 keV and 968 keV peaks. It must be noted that the 968 keV line is from the Ac-228 nuclide but the 860 keV line is from the decay of the Tl-208 nuclide but it has a very small branching ratio which only has a small effect on the lower energy side of the peak. The stabilized K-40 (1460 keV) peak was not affected by the bubbling process since it is not in the Th-232 series which can be seen clearly in the combination spectra.

The rest of the collected gamma spectra are presented in Appendix D. The difference in the gamma ray intensity depends on the fraction of the Rn-220 that was pumped from the solution. It is possible to estimate the Rn-220 fraction pumped from the  $\text{Th}(\text{NO}_3)_4 \cdot 6\text{H}_2\text{O}$  solution, as shown in Figures (5.10, 5.12 and 5.14).

The main focus is on the Tl-208(2614 keV) photopeak for which the total number of counts extracted for every one hour was corrected for the room and continuum background radiation. Then the net count rate of the 66 hours of bubbling is plotted.



**Figure 5.10:** The net count rate of the Tl-208 (2614 keV) photopeak as a function of time.

In addition to that, the extracted net counts under the 911 keV photopeak were corrected for the room and the continuum background radiation. After the corrections were done the count rate is as indicated in Figure 5.11

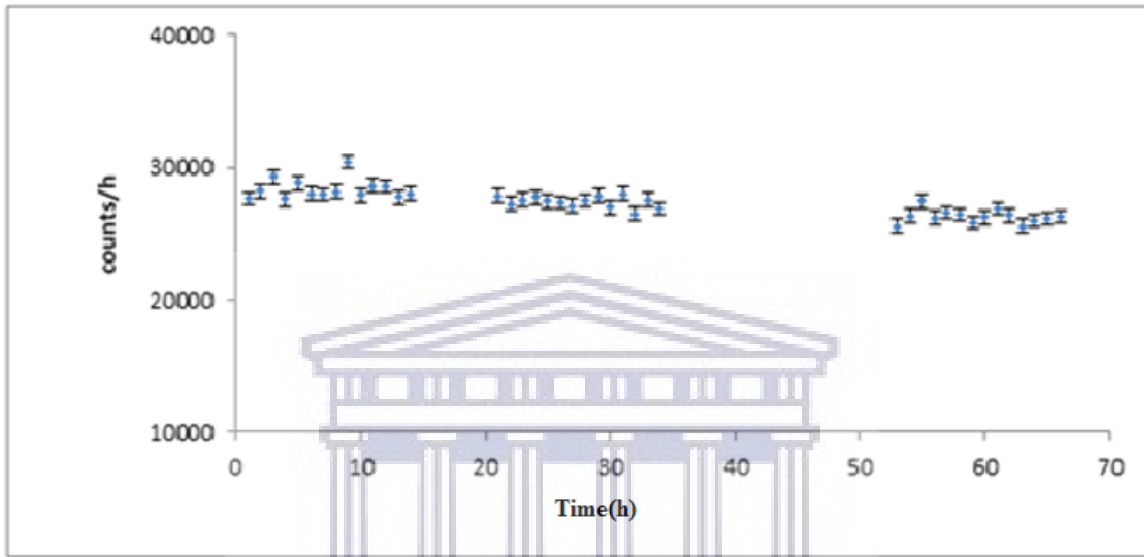


**Figure 5.11:** The net count rate of the Ac-228 (911keV) photopeak as a function of time.

For both Ac-228 (911 keV) and Tl- 208 (2614 keV) the count rates were normalized and plotted in Figure 5.12

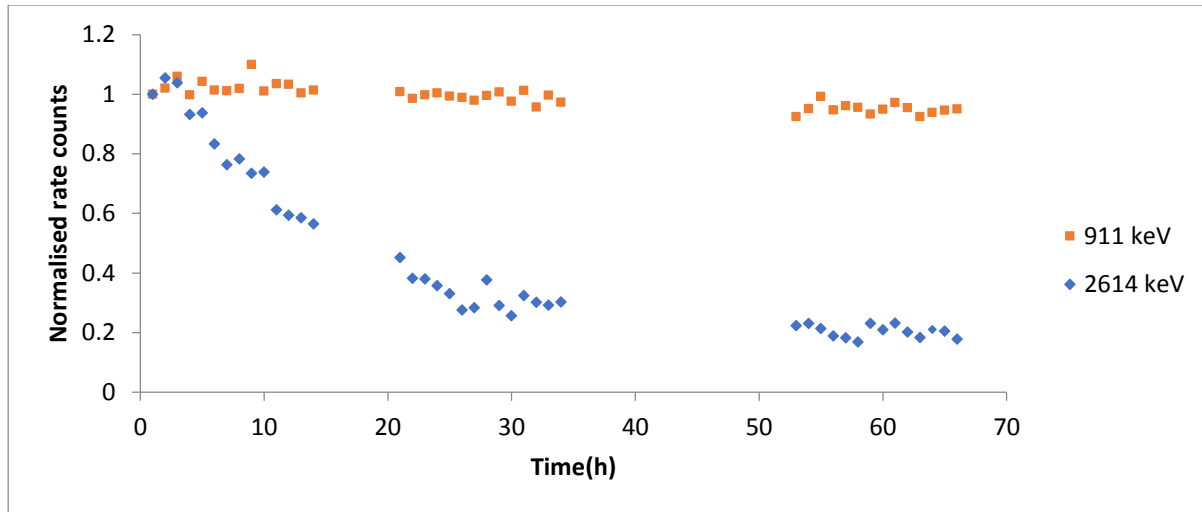


**Figure 5.12:** The normalized Tl-208 (2614 keV) and Ac-228 (911 keV) count rate as a function of time.

To obtain the activity of Tl-208 (2614 keV), the photopeak efficiency of interest need to be measured. The next section presents the simulated photopeak efficiency.

### 5.3.4 Simulated detection photopeak efficiency of the Na(Tl) detector

In order to monitor the activity of the source during the bubbling process, the detection efficiency of the detector is useful, though not essential. Therefore the efficiency for the geometry of the detector and the partially filled small bottle with KCl solution was simulated using MCNPx. The parameters used are presented in table 4.3, see chapter 4 section 4.3.2.2.2.

After obtaining the absolute efficiency of the 1460 keV photopeak (see Appendix A), this value is used to scale the simulated detection photopeak efficiencies. Table 5.2 shows the simulated efficiency found in this study.

**Table 5.2:** The efficiencies in the range of 239 keV to 2614 keV simulated using MCNPx for the geometry of the NaI(Tl) detector and the partially filled small bottle with KCl solution. The KCl solution in the same geometry was used to normalize the efficiency curve.

| E(keV) | Efficiency |
|--------|------------|
| 239    | 0.139      |
| 583    | 0.064      |
| 911    | 0.044      |
| 1460   | 0.029      |
| 2614   | 0.018      |

The simulated efficiencies were fitted according to the equation  $\epsilon = a\left(\frac{E}{E_0}\right)^{-b}$  with the parameters  $a = 15.674 \pm 2.708$ ,  $b = 0.863 \pm 0.029$  and,  $E_0=1$  keV and E the energy of interest. The simulated efficiencies are plotted in Figure (5.13) as a function of energy.

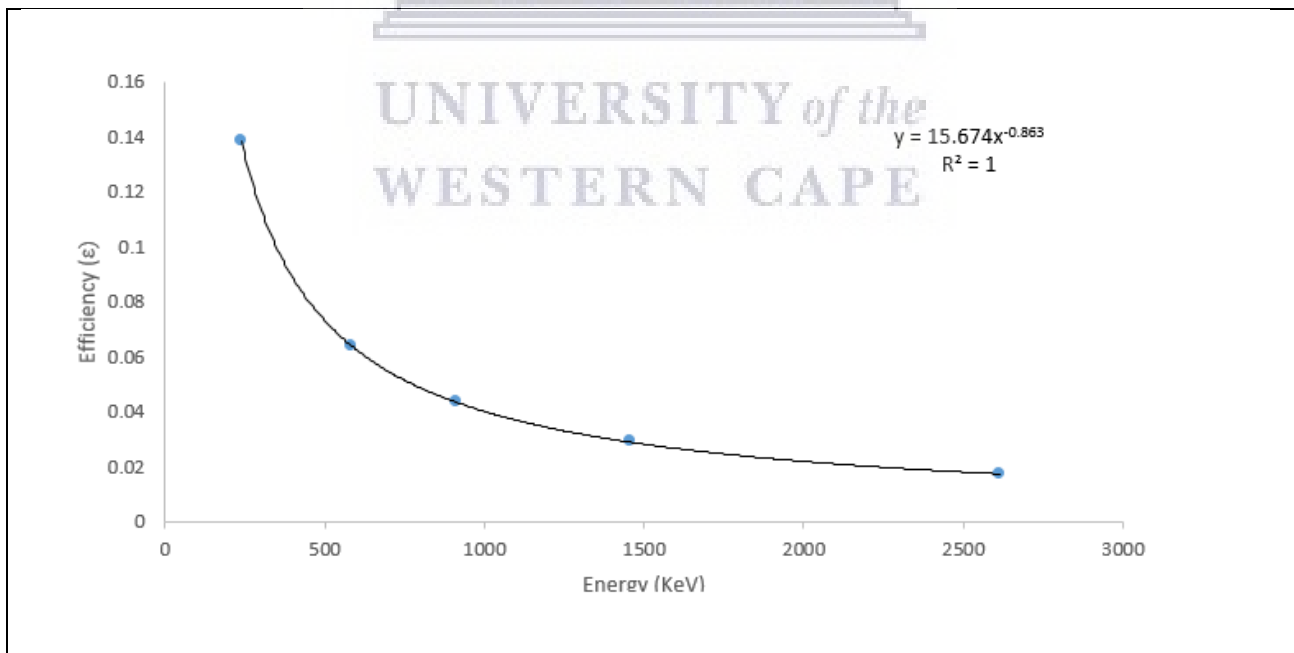


**Figure 5.13:** The MCNPx corrected simulated gamma-ray detection efficiencies for the NaI(Tl) detector geometry and the small bottle.



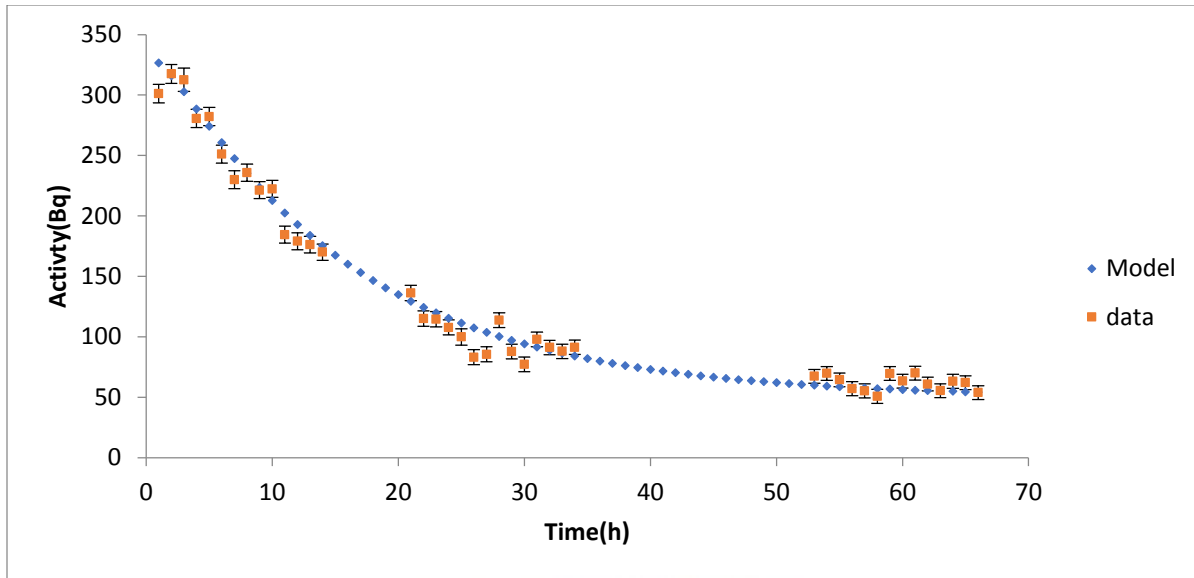
### 5.3.5 The percentage of Rn-220 pumped from the $\text{Th}(\text{NO}_3)_4 \cdot 6\text{H}_2\text{O}$

One of the parameters of the proposed Rn-220 standard source, is that its emanation has to be high to give enough and stable concentration of Rn-220 gas. The emanation power of the Rn-220 source is the ratio of Rn-220 gas released by the pumping compared to the total of the number of Rn-220 produced by the decay in the source (IAEA 2013). One of the main aims of our study is to find the emanation power of our proposed Rn-220 source.

For the estimated efficiencies of full energy peaks of interest, it is possible to monitor the activity of the source and estimate the percentage activity pumped out. The main interest is in the Tl-208 peak at 2614 keV and it is observed that there is a clear reduction in its intensity with time, see Figure 5.10. This reduction is due to pumping Rn-220 out by bubbling and thus reducing the chance of the Rn-220 to decay in the solution. Therefore, the gamma lines of the Rn-220 daughters do not get fed by Rn-220 and their intensity will reduce in time more or less in line with the Pb-212 half-life, but not to zero because of a fraction of the Rn-220 decay in the solution due to its relatively short half-life.

Once we need to monitor the activity of the source in order to estimate the fraction of the Rn-220 removed, it is important to know the initial activity of the source. Therefore, a theoretical activity of the Rn-220 source was calculated based on 0.22 g (same method used in section 5.2.3) of the  $\text{Th}(\text{NO}_3)_4 \cdot 6\text{H}_2\text{O}$  in the small bottle. Then the theoretical activity was estimated to be  $354 \pm 5$  Bq. Since there is an uncertainty about the purity of the  $\text{Th}(\text{NO}_3)_4 \cdot 6\text{H}_2\text{O}$  source, the bulk of the solution was measured using the HPGe detector as described in section 4.3.1.1. The HPGe results implied that the activity of the solution in the small bottle was about 331 Bq. This activity is close enough to the theoretical value if we consider the possible impurity and the unknown history of the source.

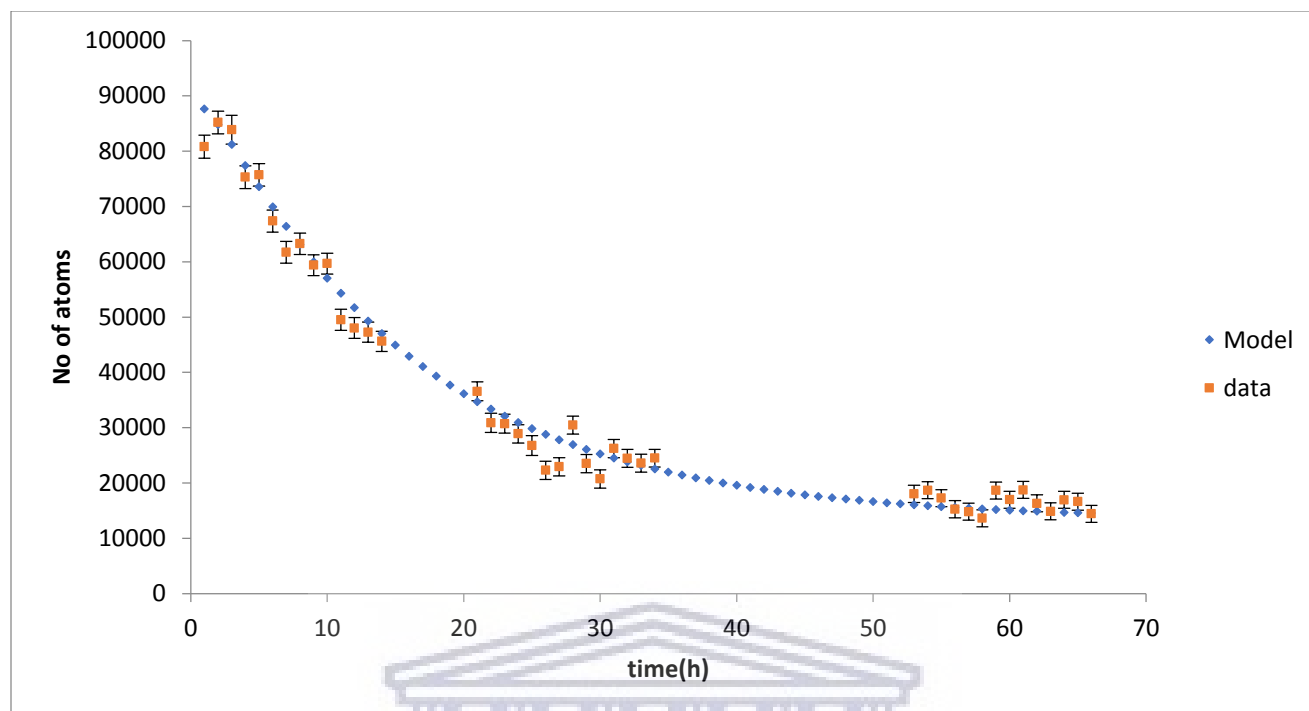
Figure 5.14 represents the variation of the activities with time during the bubbling process. The measurements were taken for 66 hours. It should be noted the activities were obtained using the measured counts of Tl-208 in the 2614 keV peak and its corresponding photopeak efficiency, and the associated branching ratio using equation 4.2.



**Figure 5.14:** The Tl-208 activity (diamond) as calculated with the Bateman equations (Eq. 2.25 with a fitted value of the Rn-220 source of  $S= 50$  Bq) and the measured, corrected activity (square) using the 2614 keV photopeak, as a function of the time.

From Figure 5.14 the value of the source,  $S$ , that fits the Bateman equation (Eq. 2.25) is about 50 Bq when the initial activity of the source is 331 Bq. This implies that the amount of Rn-220 that is pumped out of the solution is about 85% which is  $(1 - \frac{S}{331}) \times 100$  of the initial activity.

In order to have more quantitative data, the variation in the number of the Tl-208 atoms with time was obtained. Figure 5.15 shows the number of Tl-208 atoms which vary with time during the bubbling process.



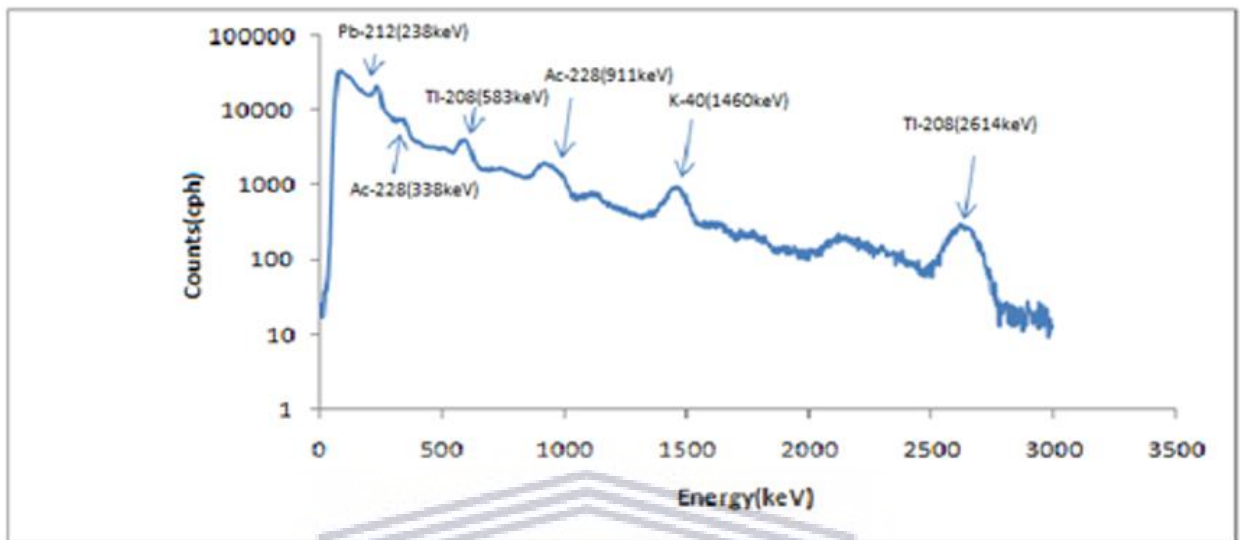
**Figure 5.15:** The measured Tl-208 (2614 keV) atoms number (square) and the calculated number of Tl-208 atoms using the Bateman equations (diamond) as a function of time.

Figure 5.15 shows the number of Tl-208 atoms decreasing with time due to the growing disequilibrium between Rn-220 and Tl-208. It should be noted that the number of atoms of Tl-208 does not decrease to zero because some fraction of Rn-220 atoms decay in the solution before it is pumped from the solution.

### 5.3.6 Bubbling using different flow rates

In order to test our model, a pump with different flow speed was used to check the reproducibility of the model. To achieve this goal, the Pb-212 had to regenerate in our solution in the small bottle. The waiting period had to be more than three days. After secular equilibrium was achieved and the Pb-212 regenerated, an experiment was conducted using a flow rate of 1 L/min and the measurements were conducted for 12 hours continuously. The setup used for conducting the 12 hour measurements was the same as the setup for the previous 66 hours measurements. Figures

5.16 and 5.17 are the spectra accumulated for the first hour of bubbling and the 12<sup>th</sup> hour of bubbling respectively. A combination of the two spectra is presented in Figure 5.18



**Figure 5.16:** Gamma ray spectrum for the first hour of bubbling using flow rate 1 L/min.

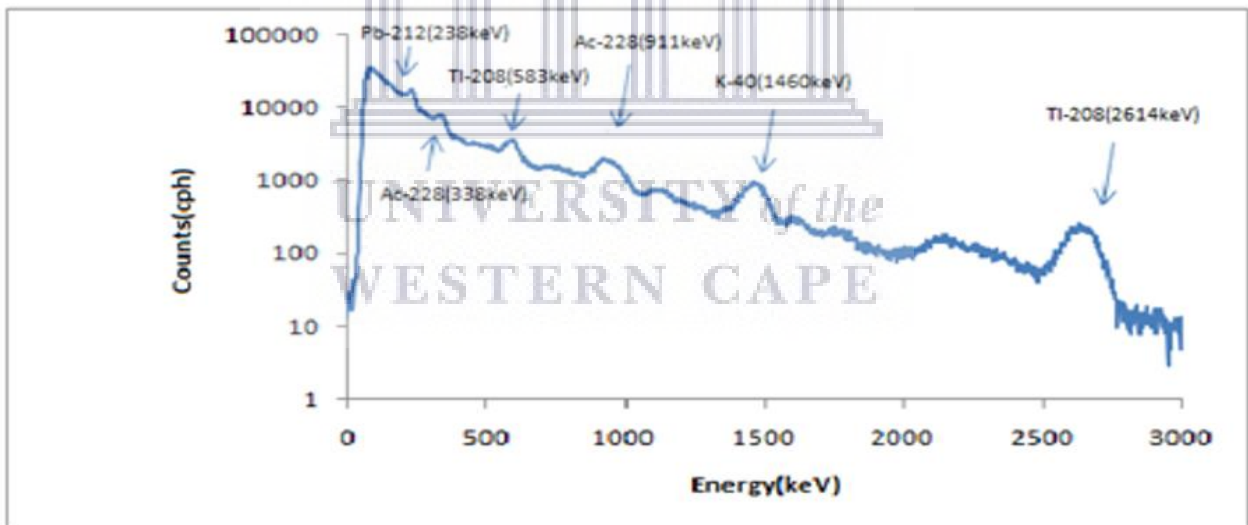


**Figure 5.17:** Gamma ray spectrum for the 12<sup>th</sup> hour of bubbling using a flow rate of 1 L/min.

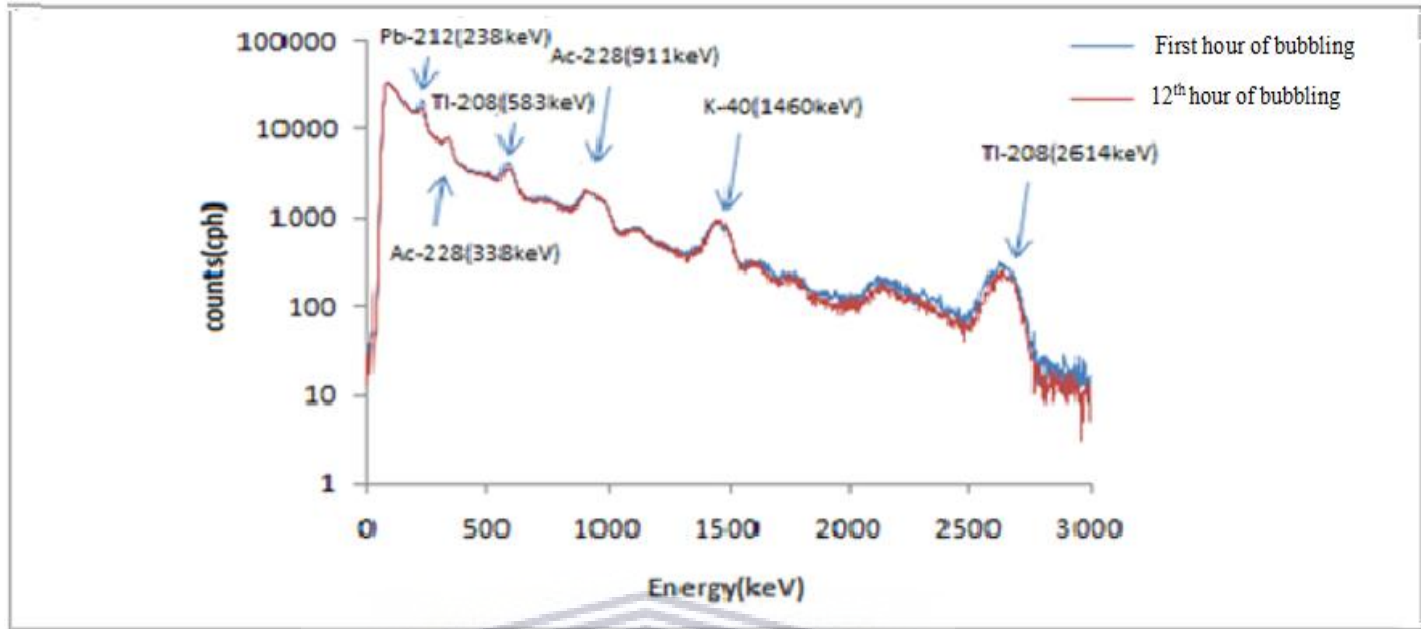


**Figure 5.18:** Combined gamma ray spectra for the first hour and 12th hour of bubbling.

To have more quantitative results, the change in the number of counts of Tl-208 (2614 keV) is converted to the activity (using equation 4.2) which is presented in Figure 5.19. Figure 5.19 shows for the 12 hours of bubbling using a flow rate of 1 L/min, the change in the Tl-208 (2614 keV) activity as a result of the amount of Rn-220 pumped off the solution.

UNIVERSITY of the  
WESTERN CAPE

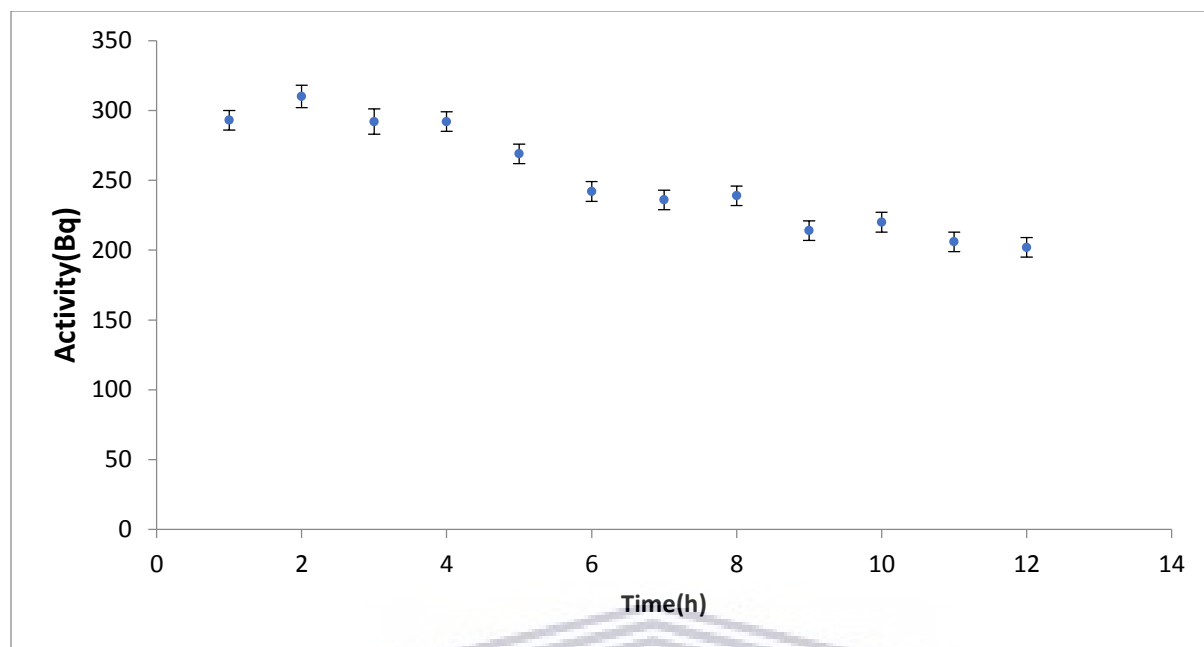


**Figure 5.19:** The corrected activity of Tl-208 (2614 keV) as a function of time using a flow rate of 1 L/min.

### 5.3.7 Bubbling setup using a lead castle as shielding

A further test in order to improve our statistics in the gamma measurements, was performed by putting the bubbling set-up inside a lead castle. This led to a large reduction in the room background. Moreover, to check the reproducibility the bubbler was modified and the air was humidified by passing it first through a bottle of water (see Figure 4.5) before bubbling to reduce evaporation.

#### 5.3.7.1 Background measurements

Before the Rn-220 measurements were conducted, the detector was placed in the lead castle placed horizontally and then background measurements were conducted without the Rn-220 source. The measurement was conducted for 7 hours and seven spectra were accumulated for periods of one hour each. The average spectrum for the first hour is illustrated in Figure (5.20).

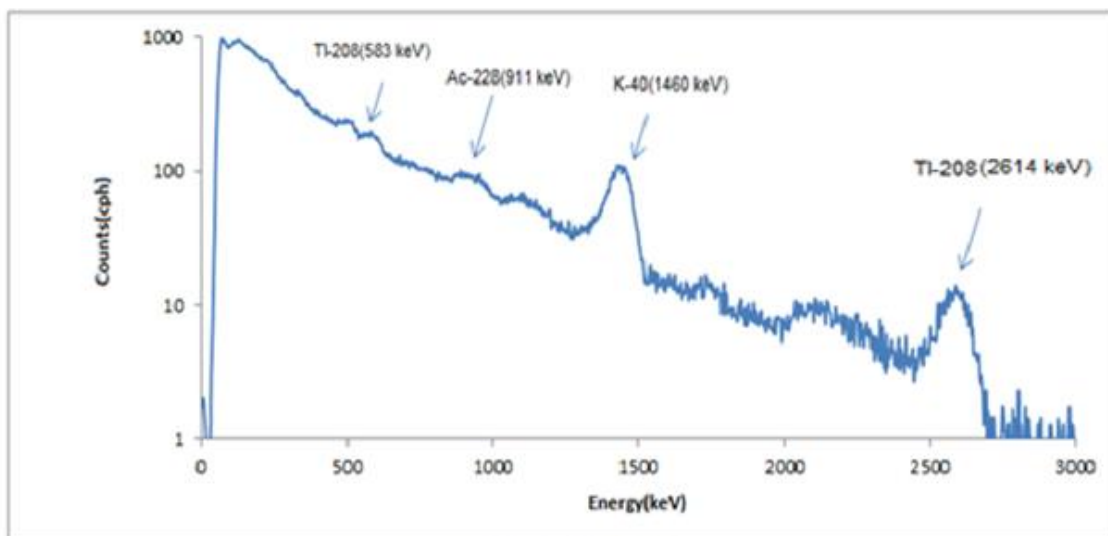


**Figure 5.20:** The gamma ray spectrum lines of the background when the detector was shielded by the lead castle. Comparison to Figure 5.5 shows a large reduction in background.

Several experiments were performed to test the set-up, all using the same solution. During one test, water bubbled into the exit pipe and a small fraction of the solution was lost. Experiments in this section were performed with this source where the initial activity is now less than 331 Bq. The initial activity was taken as 235 Bq based on the initial spectra.

The results obtained when the experiment was conducted using the setup shown in Figure 4.5 is shown in Figures 5.21 and 5.22. A total of 72 spectra were obtained, however only two spectra are presented here.

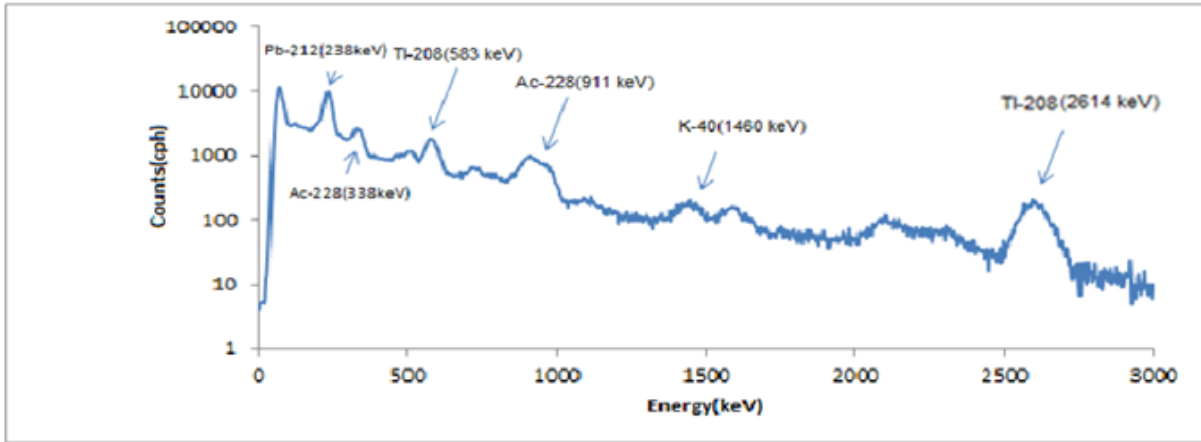


**Figure 5.21:** Gamma ray spectrum for the first hour of bubbling, with the detector shielded by the lead castle.

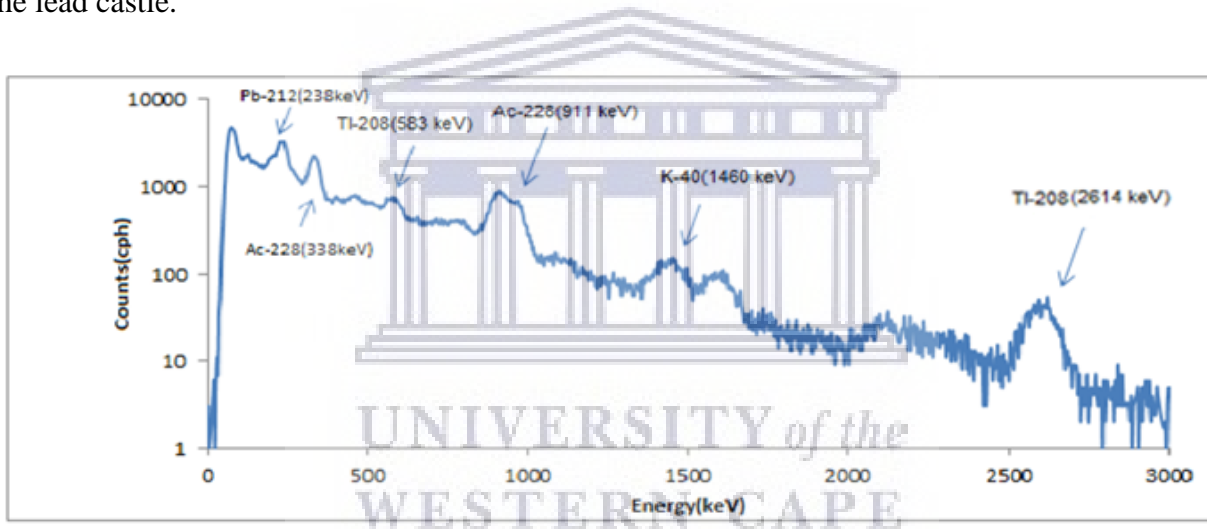


**Figure 5.22:** Gamma ray spectrum for the 72<sup>nd</sup> hour of bubbling when the detector is shielded by the lead castle.

Figure 5.21 and 5.22 are combined and presented in Figure 5.23 for easy comparison.



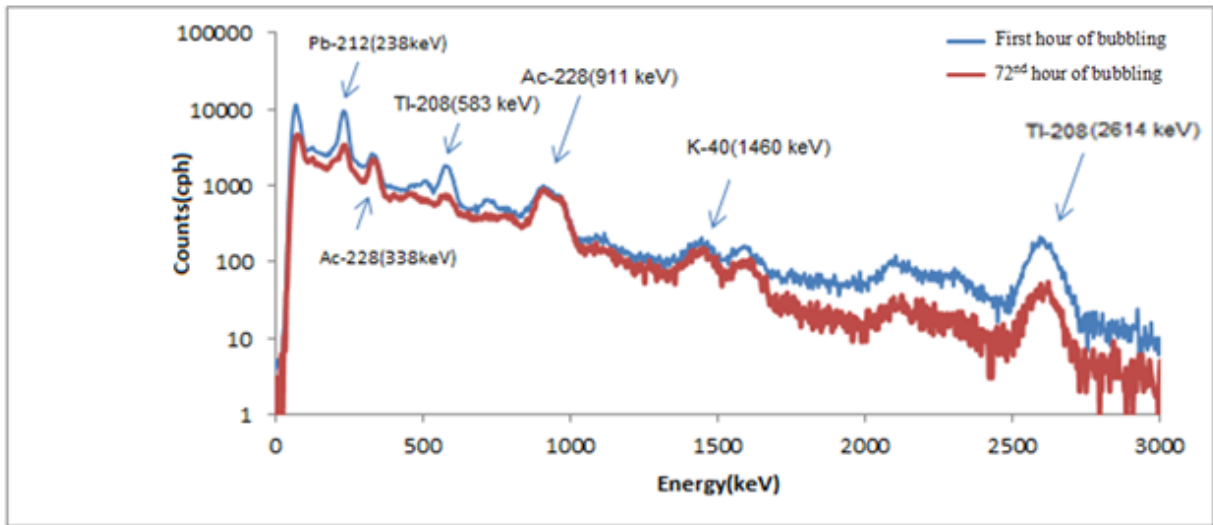


**Figure 5.23:** The gamma ray spectra of bubbling for the first hour and the 72<sup>nd</sup> hour.

Consequently, Figure 5.24 shows the calculated activity after extracting the number of counts of the Tl-208(2614 keV) peak using equation 4.2.

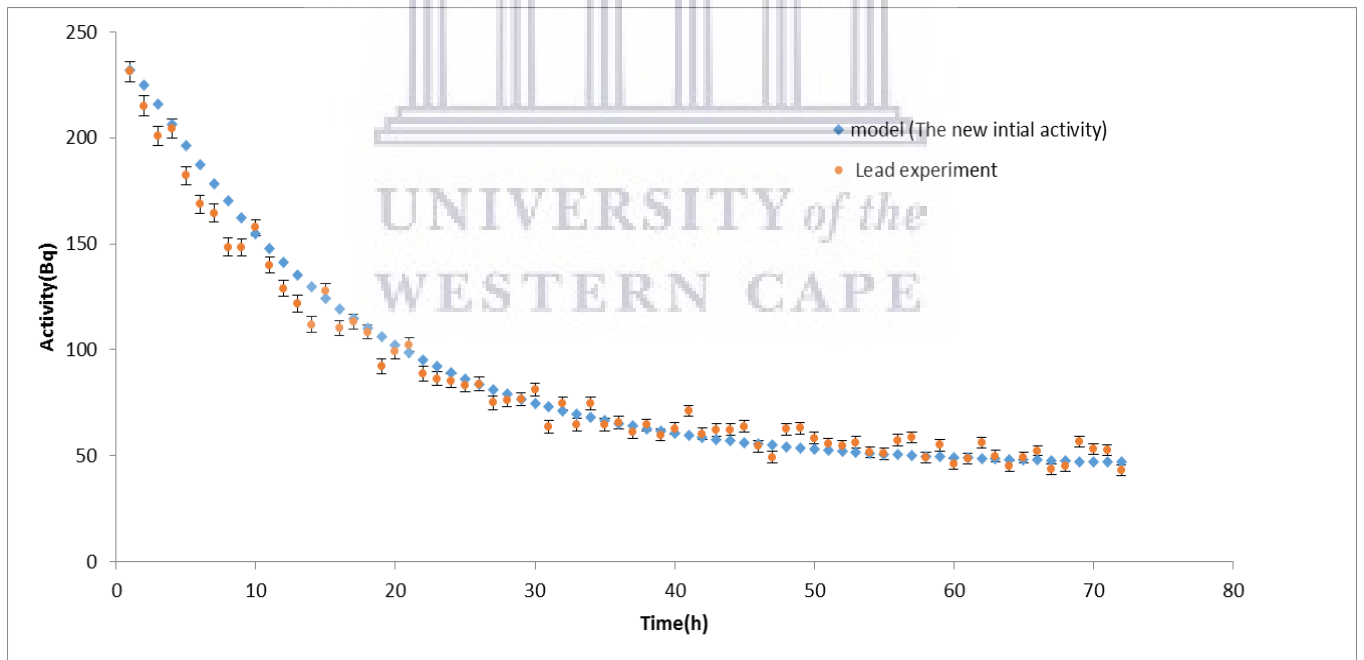


**Figure 5.24:** The measured activity (brown circle) using Tl-208 (2614 keV) as a function of time fitted to the new predict calculated activity (blue circle) using the Bateman equation with  $S = 45$  Bq.

From Figure 5.24 the value of the new S that fits the Bateman equations for the faster flow rate and different bubbler is found to be about 45 Bq when the initial activity of the source is reduced to 235 Bq. This implies that the amount of Rn-220 that pumped out of the solution is about 81% which is  $(1 - \frac{S}{331}) \times 100$  of the initial activity.

In order to have more quantitative data, the variation in the number of the Tl-208 atoms with time was obtained. Figure 5.25 shows the number of Tl-208 atoms which vary with time during the bubbling process.

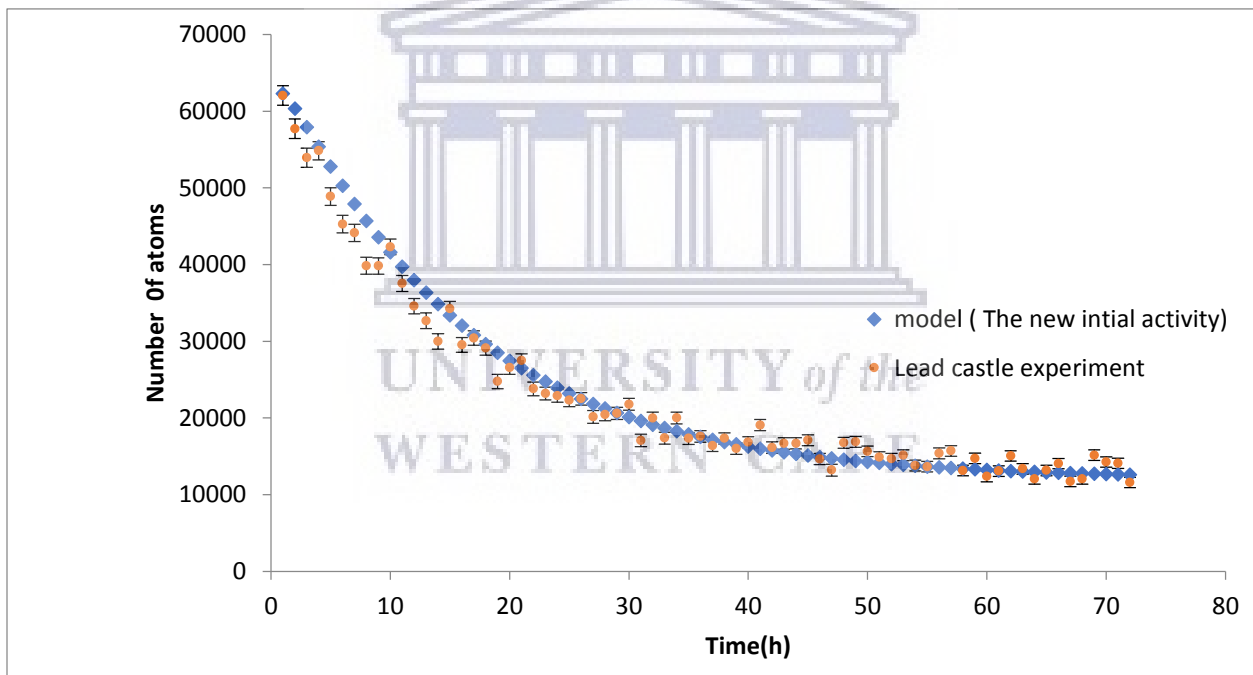


**Figure 5.25:** The measured number of Tl-208 (2614 keV) fitted to the calculated Bateman (using the new initial activity) equations (2.25) as a function of time.

In order to combine the result of the first measurements of the bubbling method used with flow rate of 0.6 L/min and the result of bubbling by using the lead castle with flow rate of 1 L/min, the modified bubbler and the humidified air are plotted in Figure 5.26. As seen from Figure 5.26 the uncertainty of lead castle measurements is smaller since the lead castle reduced the room background radiation.

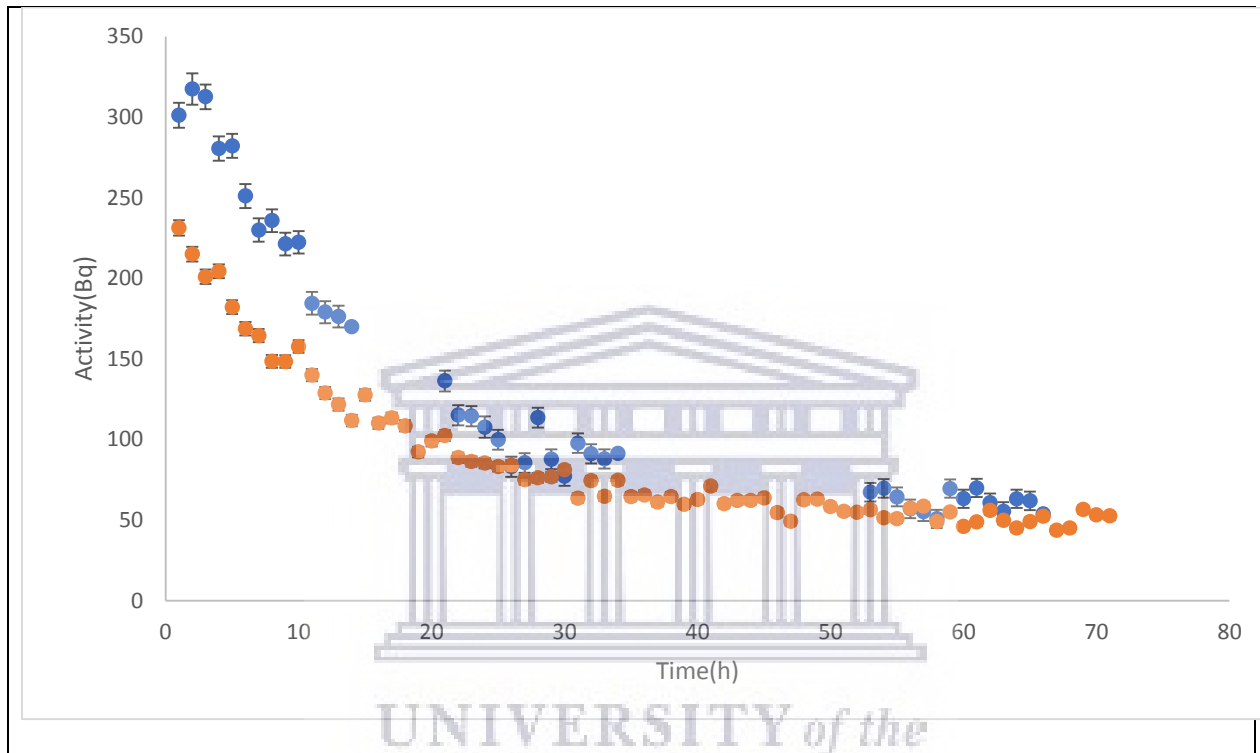


**Figure 5.26:** The blue circles show the Tl-208 (2614 keV) decreasing as a function of time without shielding (66 hrs measurements), with the flow rate 0.6 L/min. The brown circles show the Tl-208 (2614 keV) decreasing as a function of time with shielding and a flow rate of 1 L/min.

#### 5.4 RAD7 measurements

In this section the measurements made with the RAD7 in order to compare the RAD7 reading to the Rn-220 predicted value pumped out from the solution is presented.

In order to produce a steady Rn-220 gas stream, the developed liquid source was used (see section 4.2). As mentioned in section 4.3.5.2, the RAD7 detector was used to measure the activity concentration of the Rn-220 at different times. The data recorded by the RAD7 were transferred to the computer system using the *CAPTURE* software (DurrIDGE 2015). This software is able to correct the activity concentration for the relative humidity if needed. Figure 5.27 shows the measured activity concentration of Rn-220 in the exit stream after bubbling as a function of the time.

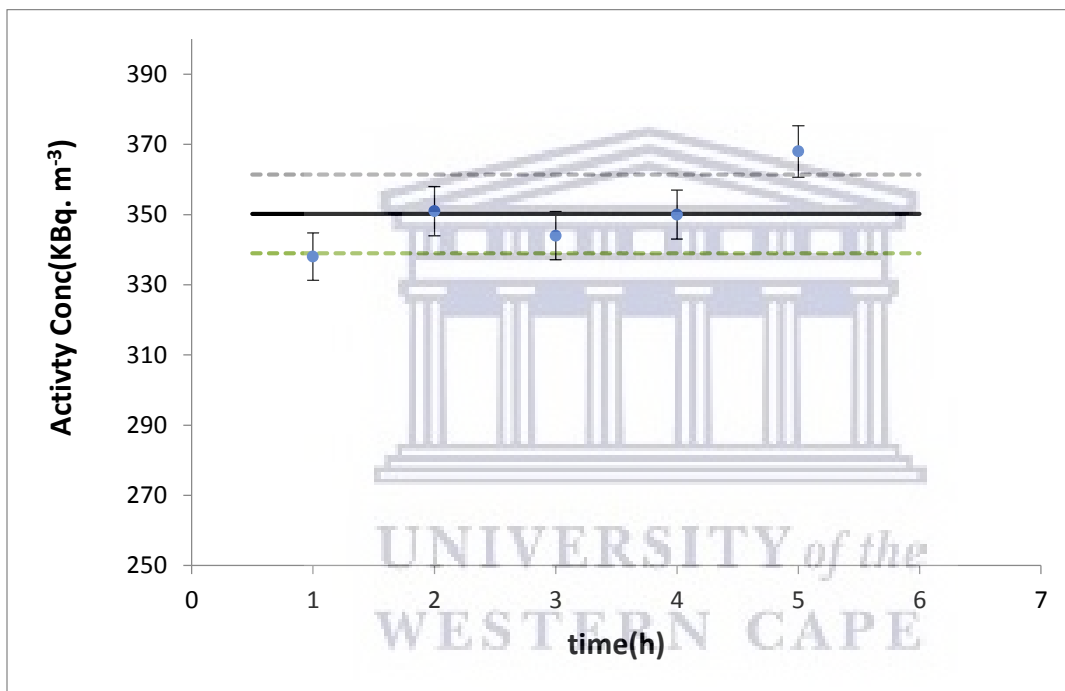


**Figure 5.27:** The Rn-220 activity concentration at the exit stream of the pipe as obtained with the RAD7 (circle). The solid line indicates the mean calculated value. The dashed line indicates the uncertainties.

The activity concentration in the exit stream is given by the activity pumped out per second divided by the volume of air coming out per second.

This activity concentration is

$$C = \frac{N \cdot x \cdot \lambda}{V} \quad (5.7)$$

Where

$C$  = The activity concentration of the Rn-220 in the exit stream of the pipe (Bq/m<sup>3</sup>)

$N$  = The number of the Rn-220 nuclei that are created every second in the solution in the small bottle from the decay of Ra-224 (nuclei/s)

$x$  = The fraction of the Rn-220 nuclei that is pumped out from the solution

$\lambda$  = The decay constant of Rn-220 (= 0.012 s<sup>-1</sup>)

$V$  = Volume of air that contains the pumped out thoron per second  
 = flow rate = 0.6 L/min = 0.6 x 10<sup>-3</sup>/60 m<sup>3</sup>/s.

The RAD7 measurements agreed well with the developed formula for calculating the activity concentration at the exit stream of the pipe.

The number of Rn-220 nuclei created in the small bottle every second by the decay of Ra-224 was obtained from the HPGe measurements. While the fraction of the Rn-220 which is pumped off from the solution was measured using the NaI(Tl) spectra and by looking at the reduction in intensity of the Tl-208 (2614 keV) photopeak. The reduction is proportional to the percentage of the Rn-220 pumped from the solution.

In this study, the percentage of the Rn-220 pumped out of the solution was measured to be 85% (see section 5.3.5) and the initial number of the Rn-220 atoms created per second was found to be 331 ± 5. The measurements were conducted using a flow rate of 0.6 L/min (=10<sup>-5</sup> m<sup>3</sup>/s). When applying these values, the activity concentration at the exit stream of the pipe is found to be about 350 kBq.m<sup>-3</sup>. The calculated activity concentration agreed well with the measured activity concentration as measured by the RAD7 as shown in Figure 5.27.

The uncertainty in  $C$  depends mainly on the uncertainties of the measured masses of the Th(NO<sub>3</sub>)<sub>4</sub>.6H<sub>2</sub>O, the flow rate and the fraction of Rn-220 pumped off the solution. The factors that

influence the uncertainty based on equation 5.7 are listed in table 5.3. The procedure of obtaining the uncertainties is presented in the Appendix E.

**Table 5.3:** Factors influencing the uncertainty based on equation 5.7.

| Quantity                                    | Value | Assigned standard uncertainty  | Relative amount (%) |
|---|-------|--|---------------------|
| The fraction of Th removed                  | 0.85  | 0.02 (based on a Chi-square change of 1 per degree of freedom in the fit shown in Fig 5)   | 1                   |
| $\lambda_{thoron}$                          |       | 0.00006  |                     |
| $N$ -Number of radioactive nuclei in water. | 331   | 5 based on the counting statistics in the HPGe. A systematic uncertainty for the HPGe and mass measurements of 10% is estimated. | 32                  |
| Flow rate                                   | 0.6   | 0.1  | 67                  |

The initial activity of the Rn-220 source was inferred to be 331 Bq in the small bottle. This value implies that there are 26 500 ( $=331/\lambda$ ) Rn-220 atoms in the small bottle before we started pumping. Then the strength of the source term was measured to be about 50 Bq which implies that only about 4000 Rn-220 nuclei were *not* pumped off the solution and are present in the bottle while pumping after a steady state is reached. A separate experiment was conducted to check the behaviour of the developed system and to see when the equilibrium state is reached. Therefore, a cycle was set up to measure at two minute intervals. The measurements were started before air

was pumped through the solution and then later the pumping was started. These measurements are presented in Figure 5.28

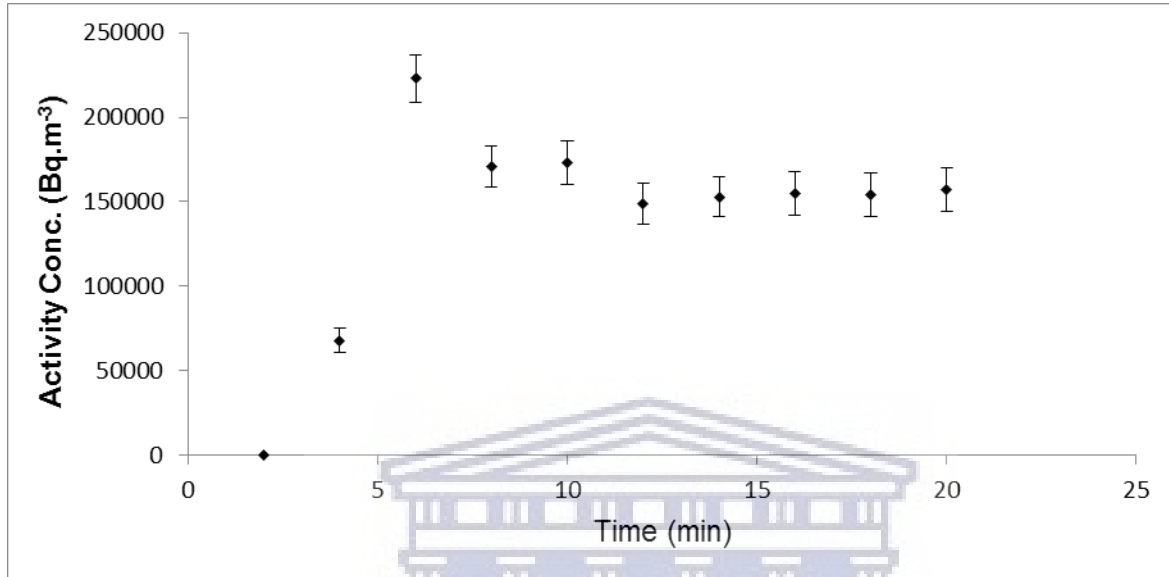


**Figure 5.28:** Activity concentration as measured by the RAD7 during the initial few minutes of pumping for a cycle of 2 minutes. The pump was started at around  $t = 2$  min. This figure shows that there was a clear spike in the initial measurements and then there was a steady state after about 6 minutes from the beginning.

#### 5.4.2 The Rn-220 activity concentration using a flow rate of 1 L/min

An experiment was conducted to check the effect of the flow rate on the activity concentration of the Rn-220. The results are presented on Figure 5.29. Note the value of 85% of Rn-220 pumped from the solution was used in equation of 5.7 to calculate the activity concentration. The calculated activity concentration of the Rn-220 in air agreed very well with the measured activity concentration.

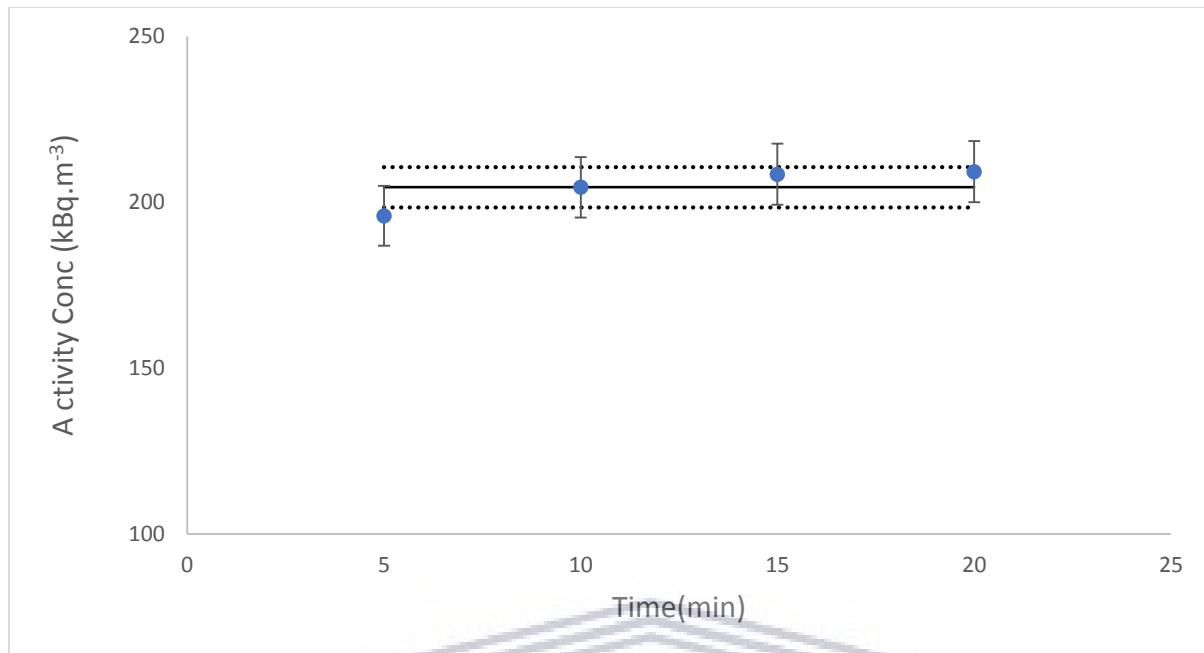


**Figure 5.29:** Rn-220 activity concentration using a flow rate 1 L/min. The circles indicate the measured activity concentration. The solid line indicates the calculated activity concentration. The dashed lines indicate the standard deviation.

### 5.4.3 Lead Castle measurements

In order to check the reproducibility of our model using different parameters as we mentioned in chapter 4, a separate experiment was conducted (see Figure 4.7b). The main difference here was that the bottle with the bubbler and the detector were put in a lead castle. This will reduce the room background considerably and would test if this gave less uncertainty in the gamma counts in the photopeak, especially after 40 hours when the net counts are small. The same Rn-220 source was used after the regeneration of Pb-212. However, there was a reduction in the activity of the solution as mentioned earlier. The bubbling was continuous over three days and the RAD7 measurements were conducted intermittently over the three days. Figure 5.30 shows the results of the new setup. The measurements show near stability in the Rn-220 activity concentration over three days. However the measured activity concentration did not fit as well with the calculated activity concentration using equation 5.7 as in the other experiments. The uncertainty in the flow rate and the change in the geometry of the bottle may explain this result.



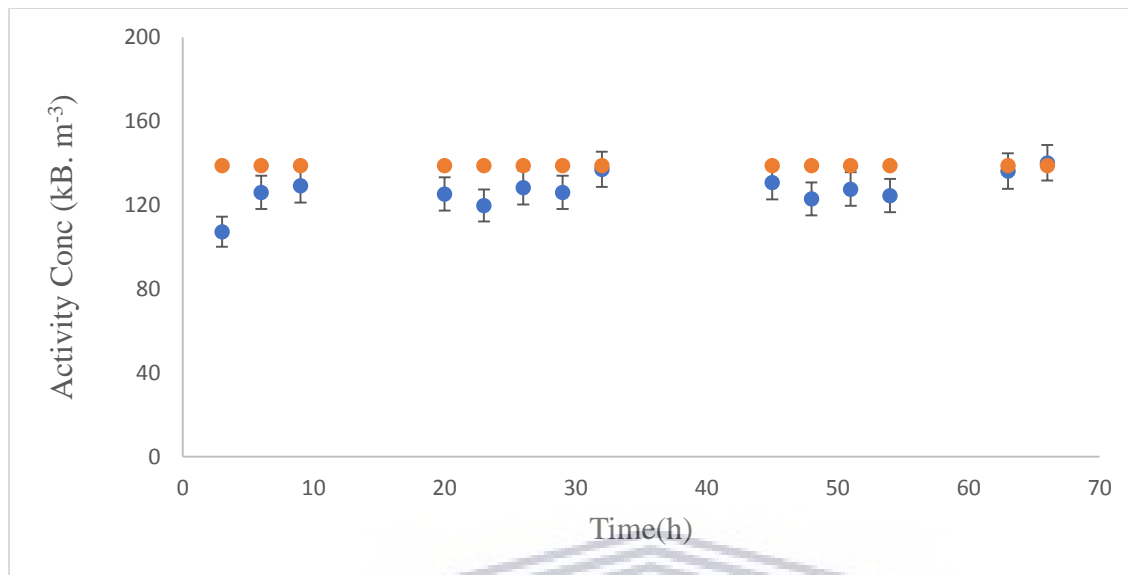


**Figure 5.30:** The Rn-220 activity concentration in the exit stream of the pipe as obtained with the RAD7 (blue circles). The brown circles indicate the calculated activity concentration. The modified bubbler, humidified air and flow rate of 1 L/min were used.

## 5.5 Summary

In this chapter the result of the characterization of the Rn-220 source ( $\text{Th}(\text{NO}_3)_4 \cdot 6\text{H}_2\text{O}$ ) using the HPGe detector was presented. The weighted average concentration was found to be  $11460 \pm 180$  Bq/L. This activity concentration of the solution in the Marinelli beaker implies the activity of the Rn-220 source in the small bottle was  $331 \pm 5$  Bq.

Thereafter the bubbling method results were presented including some spectra and plots. From Figure 5.14 the percentage of the Rn-220 pumped off the solution was found to be 85% and the strength of the source was about 50 Bq during pumping. When the lead castle was used about 80% of the Rn-220 was pumped off the solution and the strength of the source was found to be 42 Bq.

The activity concentration of Rn-220 was measured at the exit of the pipe stream and for the 66 hours measurement, it was found to be  $350 \pm 11$  kBq.m<sup>-3</sup> which agrees very well with the calculated activity concentration using equation (5.7). When the flow rate 1 L/min was used, the activity

concentration was  $204 \pm 6 \text{ kBq.m}^{-3}$  and also agreed well with the calculated activity concentration of Rn-220.

The activity concentration was also measured while a modified bubbler was used, the air was humidified and the flow rate was changed to 1 L/min in order to check the reproducibility of the developed method. The average activity concentration was measured to be  $127 \pm 8 \text{ kBq.m}^{-3}$  which did not agree as well with the calculated activity concentration.



# CHAPTER 6

## Discussions

### 6.1 Introduction

In this chapter, the HPGe, the NaI(Tl), and the RAD7 detector results will be discussed. In the first section the HPGe measurements (characterization of the Rn-220 source) will be presented and discussed. The second section will present a discussion on the results obtained by the NaI(Tl) detector using a novel bubbling method to produce a Rn-220 standard source, while the last section will present a discussion on the RAD7 detector results.

### 6.2 The HPGe measurements

In order to check and measure the activity of the Rn-220 source, a  $(\text{Th}(\text{NO}_3)_4 \cdot 6\text{H}_2\text{O})$  solution was divided into two parts; a small bottle (about 40 mL) and Marinelli beaker (bulk one). The solution in the small bottle was used for the bubbling method and the other, in the Marinelli beaker, was used for characterization. The bulk sample was measured using the HPGe detector and the activity concentration was obtained.

Since the activity of the  $(\text{Th}(\text{NO}_3)_4 \cdot 6\text{H}_2\text{O})$  crystal sample used in this study was uncertain since we are not sure of its purity, the measurement of the  $(\text{Th}(\text{NO}_3)_4 \cdot 6\text{H}_2\text{O})$  solution (in Marinelli beaker) by HPGe was necessary in order to find its activity. HPGe detectors have been used for a long time to characterize radioactive samples (soil, liquid, etc.). It is a reliable and trusted method, once it is calibrated for both energy and efficiency.

The activity concentration of the  $\text{Th}(\text{NO}_3)_4 \cdot 6\text{H}_2\text{O}$  solution was extracted from the Ac-228 and Tl-208 lines based on the assumption that secular equilibrium has been reached.

It has been seen from Figure 5.4 that the activity concentration of Ac-228 (338 keV, 794 keV, 911 keV and 968 keV) and Tl-208 (583 keV, 860 keV and 2614 keV) were nearly equal. Therefore, the ratio of the average activity concentration of Ac-228 to Tl-208 is equal within the uncertainty, which indicates that the  $\text{Th}(\text{NO}_3)_4 \cdot 6\text{H}_2\text{O}$  solution is in secular equilibrium. The theoretical absolute

activity concentration of the  $\text{Th}(\text{NO}_3)_4 \cdot 6\text{H}_2\text{O}$  solution and the measured activity concentration (see section 5.2.3) are relatively close but not equal which indicates that the  $\text{Th}(\text{NO}_3)_4 \cdot 6\text{H}_2\text{O}$  solution might not be pure.

### **6.3 NaI(Tl) measurements.**

#### **6.3.1 Why the bubbling method?**

During the course of this research, Rn-220 from a solid source was initially measured in order to investigate the RAD7 detector measurements. Unfortunately, no appreciable Rn-220 was measured from several solid source. For this reason, the idea of using a liquid Rn-220 source was implemented (see Figure 4.4).

The main idea of our Rn-220 source was to remove the Rn-220 gas from the Th-232 series (see Figure 1.1) in a controlled and repeatable manner. In an ideal world, the Th-232 series is in secular equilibrium since the head nuclide of the series has a long half-life and the daughters have shorter half-lives. When the Rn-220 was removed from the series, the disequilibrium between the nuclei before and after the Rn-220 occurred. Consequently, the gamma intensities of Pb-212 and Tl-208 would be reduced but the gamma intensity of Ac-228 would not be affected. The NaI(Tl) detector was used, which has disadvantages such as poor resolution. Due to this, this study focused on the reduction of the Tl-208 nuclide decays, especially at the 2614 keV line, because it has lower continuum background and the photopeak sits on a linear background and therefore it is easy to subtract the background. Moreover, the 2614 keV is not mixed with any peak, hence it is easy to detect with a NaI(Tl) detector. The 583 keV and 860 keV peaks have a higher net count rate which would lead to lower uncertainty, but due to the non-linearity of background it is harder to subtract the background consistently. The 583 keV and 860 keV peaks also suffer from interference with the 510 keV and 968 keV lines, respectively.

In the bubbling method to develop the Rn-220 standard source, we started with an initial activity in the small bottle of  $331 \pm 5$  Bq for the Rn-220 source as calculated from the HPGe measurement for the large liquid sample of which the water in the bottle is a sub-sample. This is not in agreement with  $351 \pm 5$  Bq, the theoretical activity as calculated from the measured mass of Thorium Nitrate.

This indicates that the  $\text{Th}(\text{NO}_3)_4 \cdot 6\text{H}_2\text{O}$  is probably not 100% pure, which is why we preferred to use the value based on the HPGe value (331 Bq).

It can be seen from Figure 5.10, that the net counts in the Tl-208 (2614 keV) photopeak decreases with time due to the Rn-220 pumped from the solution. After a certain period of pumping of the Rn-220, equilibrium is reached and there was no further decrease which indicates that the Tl-208 peak decreased with time but not to zero.

Figure 5.14 shows that the measured values and the calculated values using the Bateman equations agreed well. The reduction of the Tl-208 indicates the percentage of the Rn-220 pumped off. Figure 5.14 also shows that about 85% of the Rn-220 was pumped from the solution. The results in this study have been compared with other studies using solid sources. The study by Wang *et al.*, 2017 reported the emanation coefficient of Rn-220 between only 0.5% and 1.3% whereas Csordas *et al.*, 2015 got up to 7.69%. Other studies include, Kanse *et al.*, 2013; Jobbagy *et al.*, 2010; and Röttger *et al.*, 2010. In these studies, the Rn-220 emanation coefficient was 7.9%, up to 1.44% and up to 41%, respectively. The findings of this study (85%) indicates that the bubbling method extracts a much larger fraction of the produced Rn-220, is more practical and the stability of the activity concentration of the produced Rn-220 can be easily and effectively used to investigate Rn-220 detectors. Table 6.1 shows a summary of the percentage of Rn-220 produced from sources developed by various researchers.

In Figure 5.14 the strength of the effective source due to the Rn-220 that is not removed by pumping was found to be about 50 Bq. The strength of the source can be defined as the amount of Rn-220 that was not pumped off (which decays in the solution).

**Table 6.1:** Percentage of Rn-220 reported by various researchers

| Author                      | Source   | Rn-220 produced (%) |
|-----------------------------|--|---------------------|
| Rottger <i>et al.</i> 2010  | Th-228 (electrodeposition)                                 | 41                  |
| Jobbagy <i>et al.</i> 2010  | Thorium nitrate(porous clay)                               | 0.16 - 1.44         |
| Tang <i>et al.</i> 2012     | Th <sup>4+</sup> (ion-exchanged resin)                     | 38                  |
| Kanse <i>et al.</i> 2013    | Thorium oxide and Ammonium di urinate<br>(powder sandwich) | 1.2,7.9 , 7.4       |
| Buompane <i>et al.</i> 2013 | Thorium Oxide, Lantern mantle                              | N/A                 |
| Csordas <i>et al.</i> 2015  | Thorium nitrate(mix with ceramics)                         | 0.34 - 7.7          |
| Wang <i>et al.</i> 2017     | Incandescent gas mantles                                   | 1.33, 0.77, 0.57    |
| Current study               | Thorium nitrate (dissolved in water)                       | 85, 81              |

It can be seen in Figure 5.10 that the net count rate after bubbling for 60 hours is about 1300 counts per hour, with an uncertainty of 3% which is more than good enough for the purpose of providing a reliable Rn-220 source with an accuracy of a few percent. In Figure 5.11 the net counts of the Ac-228 (911 keV) photopeak is nearly constant in time. This is an indication that the peak was not affected by the bubbling as mentioned in section 5.3.2. This gives us full confidence that the reduction of the Tl-208 (2614 keV) is due to the Rn-220 pumped from the solution. The photopeak of Ac-228 (338 keV) can also be a good indicator of the reliability of the method proposed in this study, but unfortunately it has a nonlinear background. This makes it difficult to subtract the continuum background accurately.

### 6.3.2 Stability of the Rn-220 source

The stability of the source was tested by checking the Rn-220 source for various measurements at different times. The measurements were repeated after five months using the same setup, but the flow rate was changed to 1 L/min. The initial flow rate was 0.6 L/min. The measurements revealed good results compared to the first measurements that were conducted five months earlier. Figure

5.19 showed that the Rn-220 source is stable and can produce Rn-220 gas after the Pb-212 has regenerated. It should be noted that the activity of Tl-208 (2614 keV) of the first hour of bubbling for both measurements (the first measurements and after five months) were very close. These measurements showed experimentally that only 12 hours of bubbling was enough to fix the strength of the source.

### 6.3.3 Reproducibility of the Rn-220 source

The lead castle measurements (see Figure 4.5) were used to test the model for different parameters such as the flow rate which was changed to 1 L/min, and the air was passed through water before bubbling through the solution. The background was also reduced by introducing the shielding, and the bubbler was modified. According to Figure 5.24, our novel method showed very good reproducibility. However, the initial activity of the solution is less than the first measurements carried out for 66 hours due to loss of some of the solution. The theoretical (the developed model using Bateman model based on the new initial activity) and experimental measurements were in agreement.

In Figure 5.26, the bubbling measurements with and without the lead castle were combined together in one plot. It can be seen from the plot that the initial activity of the lead castle bubbling is less than the initial activity of first bubbling measurements (66hrs). This result showed that the reduction of the activity does not contribute significantly to the percentage of the Rn-220 pumped from the solution. Moreover, results have proved that the change of the flow rates and the modification of the bubbler do not significantly change the percentage of Rn-220 pumped from the source. In addition, it should be noted that the equilibrium part of the curve is flatter than the first measurements carried out.

From the literature, it can be seen that if one wants to install or copy a chamber similar to the one in Germany (by PTB) or JAPAN (NIRS), it will be costly and one will need many resources. Compared to that, the novel bubbling method introduced in this work produces a stable Rn-220 air stream and is cheap, practical and accurate.

The Rn-220 solid sources that have been used earlier to produce a yield of Rn-220 depend on the environmental conditions such as temperature, humidity, and the pressure (Kanse *et al.* 2013). The

emanation power of these solid sources therefore might change according to the mentioned environmental conditions. Among the advantages of the bubbling method employed in this study are that it is mostly independent of environmental parameters which makes the method easy to use.

The use of an HPGe detector and a system of pumping the exhaled Rn-220, must be very efficient in order to remove the Rn-220 from the source. This method has been used by Buompane *et al.*, (2013). This system needs a very expensive resource namely an HPGe while in this study, the NaI(Tl) detector was used to measure the Tl-208 (2614keV) photopeak rather than use the Pb-212 (300 keV) peak in measuring the Rn-220 source activity, to avoid the poor resolution of the detector.

According to Kanse *et al.* (2013) their powder sandwich technique is based on minimizing the losses of the Rn-220 before it emanates from the source. They managed to reduce the losses by making the powder sandwich very thin, almost less than the Rn-220 diffusion length. The technique also depends on the mass emanation rate which makes it complicated. Moreover, it depends on the surface area, grain size and the distribution of the Ra-224 inside the source. By contrast our method produced a steady Rn-220 gas stream with a well characterized source and used a simple system with the strength characterized by simultaneously measuring the gamma rays from the decay of the thoron and the daughters left in the solution.

#### **6.4 Checking the effect of the height variation of the Rn-220 source**

Some of the water evaporated from our source before using the humidifier, causing a change in the height of the solution in the bottle.

In order to test the effect of the Rn-220 source for different heights in the bottle, 5 grams of Th (NO<sub>3</sub>)<sub>4</sub>.6H<sub>2</sub>O was dissolved in a small amount of distilled water. The heights of the source in the small bottle was then changed by adding water and a measurement was taken at different heights as seen in Figure 6.1



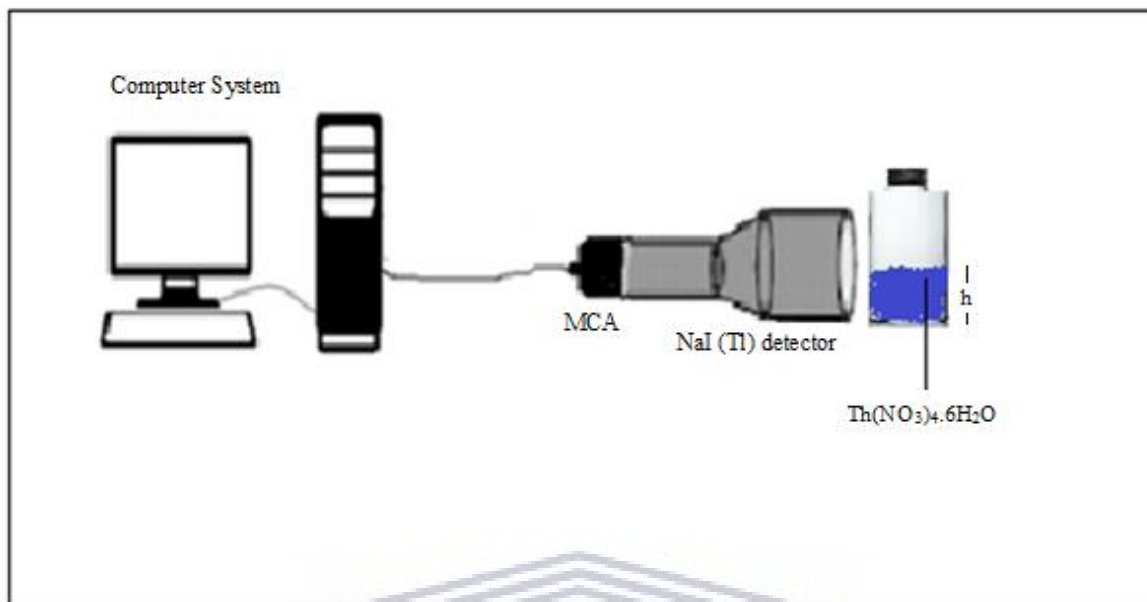


**Figure 6.1:** Experimental set up for measuring the gamma rays released from different heights of Th(NO<sub>3</sub>)<sub>4</sub>.6H<sub>2</sub>O in the sample bottle.

Using the setup in Figure 6.1, the gamma rays released from Th(NO<sub>3</sub>)<sub>4</sub>.6H<sub>2</sub>O was measured for different heights (the height was changed by adding distilled water to the solution). The spectra at different heights were generated and are presented in Figures 6.2, 6.3, 6.4, 6.5 and 6.6. It should be noted that each spectrum was measured for one hour.

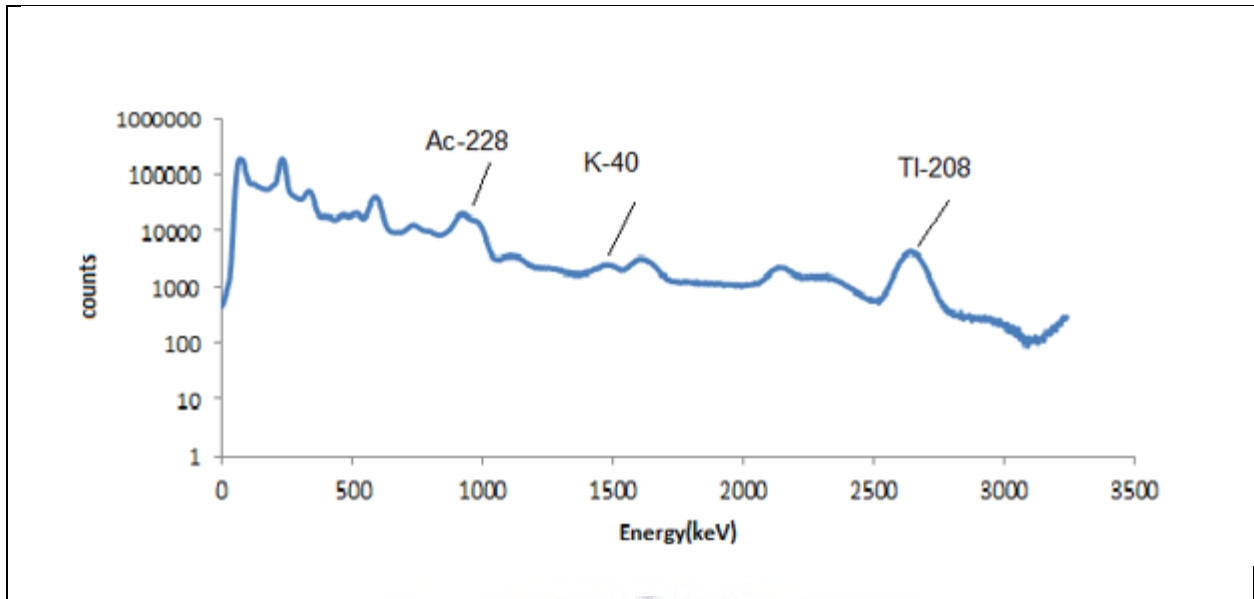


**Figure 6.2:** Gamma-ray spectrum for 15 mm height of  $\text{Th}(\text{NO}_3)_4 \cdot 6\text{H}_2\text{O}$

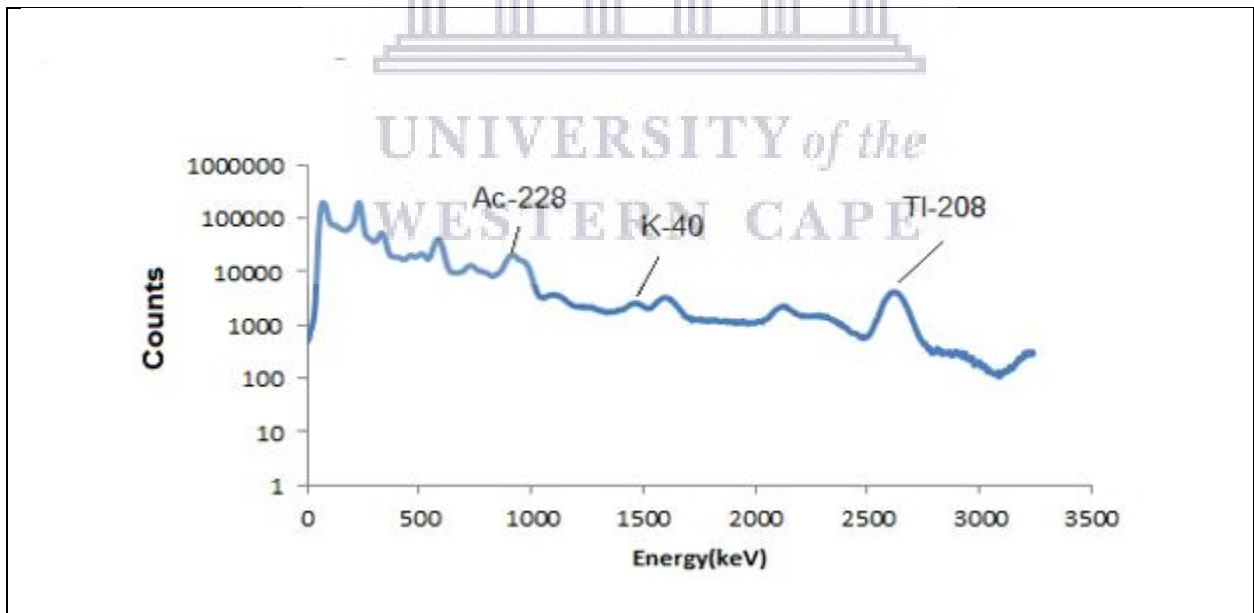


**Figure 6.3:** Gamma-ray spectrum for the 35 mm height of  $\text{Th}(\text{NO}_3)_4 \cdot 6\text{H}_2\text{O}$

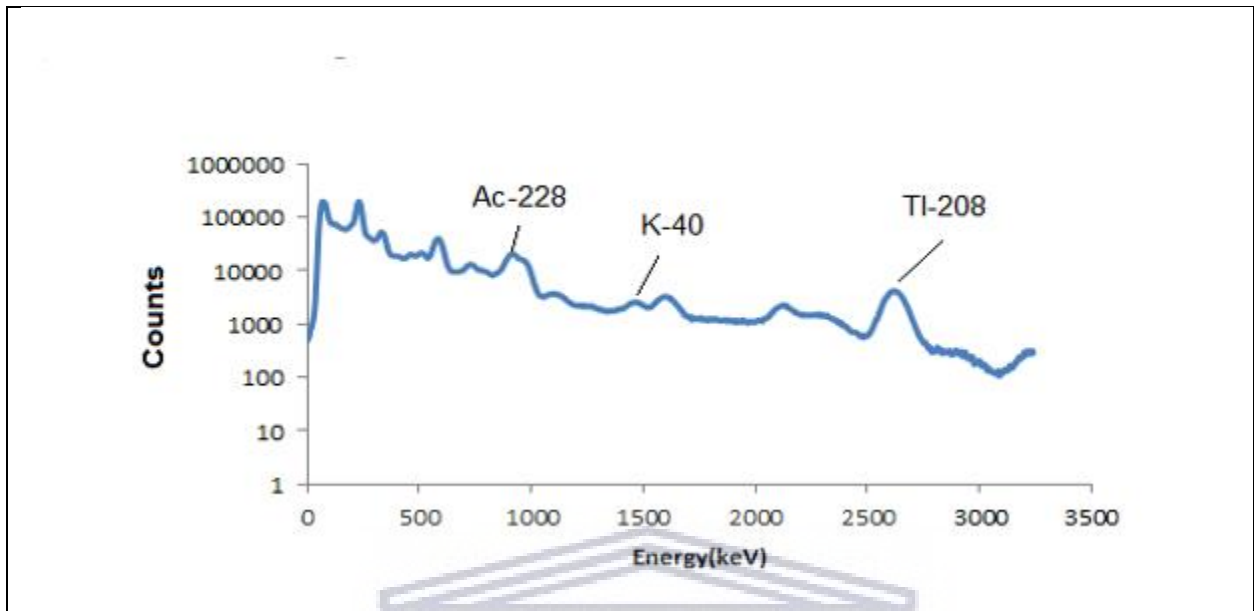


**Figure 6.4:** Gamma-ray spectrum for 45 mm height of  $\text{Th}(\text{NO}_3)_4 \cdot 6\text{H}_2\text{O}$

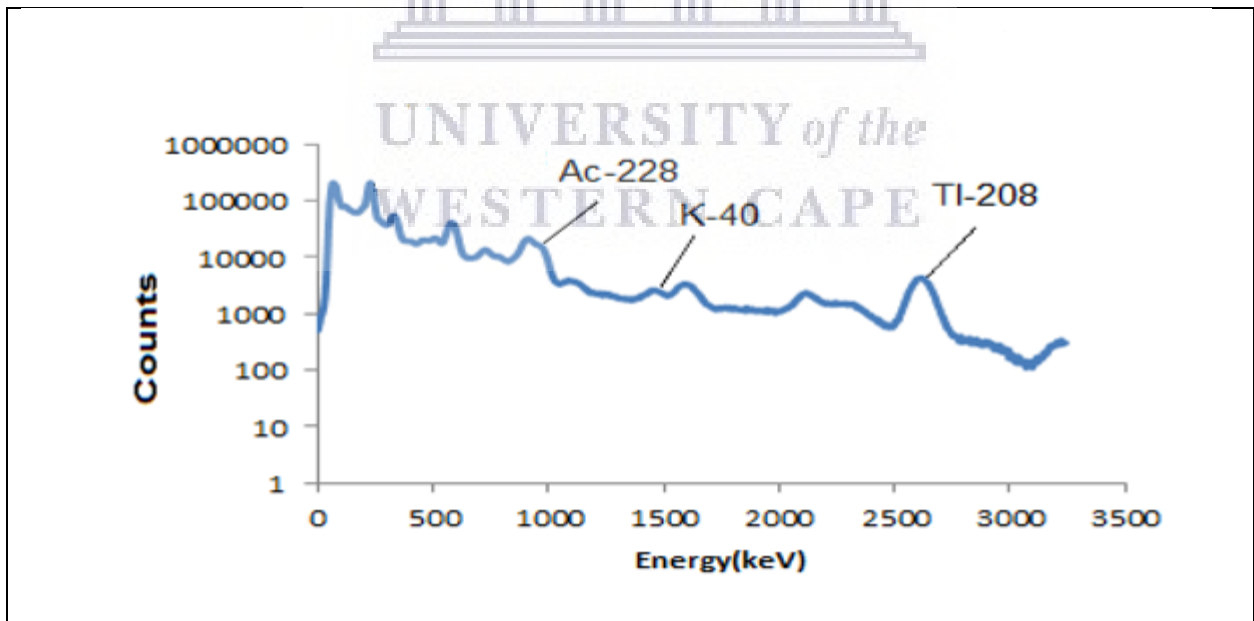


**Figure 6.5:** Gamma-ray spectrum for 60 mm height of  $\text{Th}(\text{NO}_3)_4 \cdot 6\text{H}_2\text{O}$

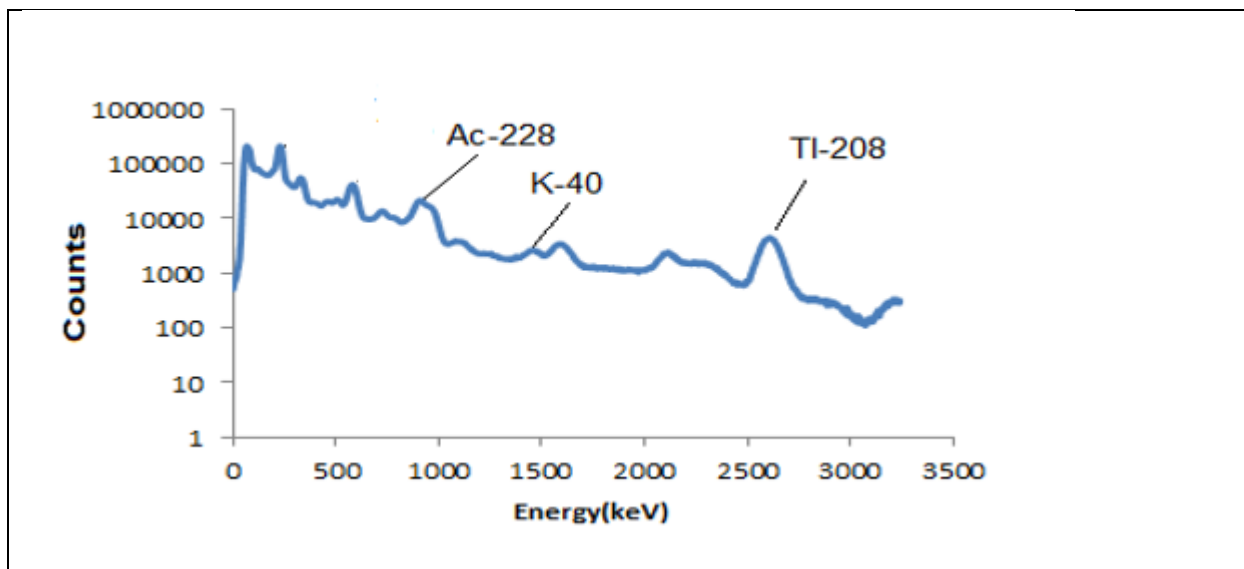


**Figure 6.6:** Gamma-ray spectrum for 75 mm height of  $\text{Th}(\text{NO}_3)_4 \cdot 6\text{H}_2\text{O}$

Since the interest is in detection efficiency of the Tl-208 (2614 keV) peak, the count rate of each level was measured and is displayed in Table 6.2.

**Table 6.2:** The height of the Rn-220 source in the small bottle and the corresponding counts and their associated uncertainties. The counts were corrected for the background radiation.

| Height (mm) | Counts per hour  |
|-------------|------------------|
| 15          | $180509 \pm 440$ |
| 35          | $180608 \pm 441$ |
| 45          | $179523 \pm 434$ |
| 60          | $183670 \pm 444$ |
| 75          | $183797 \pm 445$ |

From the table 6.2, it was clear that the geometry of the  $\text{Th}(\text{NO}_3)_4 \cdot 6\text{H}_2\text{O}$  inside the small bottle caused only small percentage changes to the values of the counts and their uncertainties as seen from the plot of counts versus heights (see Figure 6.7).

To further check this, the assumption was made that the amount of  $\text{Th}(\text{NO}_3)_4 \cdot 6\text{H}_2\text{O}$  is pure, and the absolute activity of the 5 grams was obtained. Then, the efficiency for the relevant height was calculated (see table 6. 3).

**Table 6.3:** The variation of the efficiency for different heights for the Tl-208 (2614 keV) peak.

| Height (mm) | Counts per second | Efficiency |
|-------------|-------------------|------------|
| 15          | 50.1414           | 0.0176     |
| 35          | 50.1689           | 0.0177     |
| 45          | 49.8675           | 0.0175     |
| 60          | 51.0194           | 0.0180     |
| 75          | 51.0547           | 0.0180     |

From Table 6.3, the efficiencies at the heights of 60 mm and 75 mm are similar while at the heights of 15 mm, 35 mm and 45 mm, varied by only a small fraction. This is an indication that in the bubbling experiment, the changing in height of the Rn-220 source due to evaporation, does not alter the results significantly.

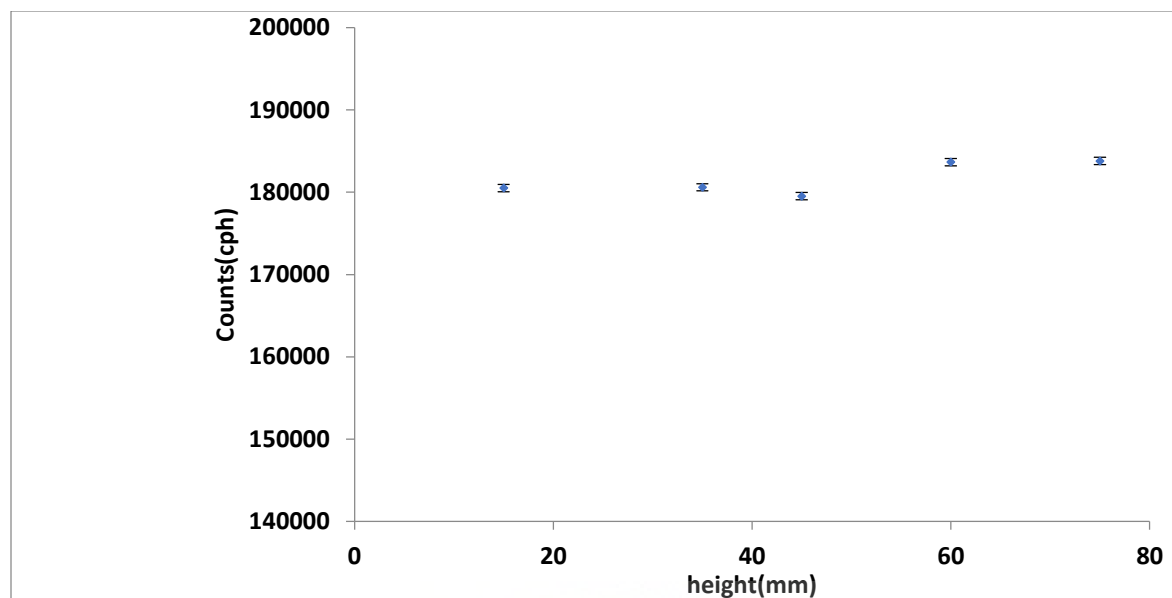


**Figure 6.7:** The variation of the counts of Tl-208 (2614 keV) with height.

A further advantage of our bubbling method to produce a Rn-220 source, is that the method can be applied without measuring the efficiency of the Na(Tl) detector, since we can use ratios of the gamma intensities of the peaks (Lindsay *et al.*, 2019). In this study the simulation of the efficiencies was carried out in order to check the consistency.

### 6.5 RAD7 measurements

As mentioned in the RAD7 manual (Durrige 2015), when the standard setup is used for measuring Rn-220, the measured activity concentration will be corrected based on the sample decay and flow rates. The correction factor recommended in the manual is 2 (Durrige, 2015). For our first measurements (66 hours), the standard setup was used and no corrections were needed since the RAD7 automatically corrects the activity concentration based on its saved parameters.

In the 12 hours measurements and the lead castle measurements, our method was checked for repeatability and reproducibility. The RAD7 measurements were conducted to measure the activity concentration at the exit stream of the pipe. The RAD7 setup was changed compared to the standard protocol, especially the different flow rate as discussed in chapter four. Therefore, the

activity concentration measured in the RAD7 would not be correct. To fix this we corrected the RAD7 measurements based on the new value of the flow rate which was 1 L/min. The formula below was used (for the two flow rates) to correct the activity concentration of the RAD7 based on the new setup.

$$\left(1 + \frac{\lambda \times V}{L}\right) \quad (6.1)$$

where:

$\lambda$  is the Rn-220 decay constant,

$V$  is the volume of RAD7 internal cell and,

$L$  is the flow rate.

As seen from the results in Figure 5.29, when the flow rate was increased, the activity concentration of the Rn-220 in the exit air decreased due to the increase in the volume of air that contained nearly the same amount of the pumped Rn-220. The pump speed did not change the percentage pumped out by much.

## 6.6 The disadvantages of our method

After bubbling for more than 50 hours, the number of counts in the 2614 keV (Tl-208) peak of our Rn-220 source would be less, close to the room background, hence the uncertainty in the counts increases. This can be fixed by increasing the mass of the  $\text{Th}(\text{NO}_3)_4 \cdot 6\text{H}_2\text{O}$  but unfortunately the RAD7 which was used to measure Rn-220 is limited to a maximum concentration of 400 kBq/m<sup>3</sup>. Due to this limitation the increase of the mass of the  $\text{Th}(\text{NO}_3)_4 \cdot 6\text{H}_2\text{O}$  was not possible. This can work if we investigate other Rn-220 monitors with a wide measurement range. Alternatively, we can reduce the room background by a lead castle as was studied in chapter 5.3.7. However, this will make the setup of the simple method of making a Rn-220 standard source developed in this study more complicated.

In our bubbling method, air with high humidity is constantly pumped to the RAD7. This required the regular change of the desiccant to keep the detector dry. This can be fixed by employing the DRYSTIK system developed by DurrIDGE to the setup.

The intermittent measurement conducted every hour or three hours using the RAD7 disturbs the setup of the experiment. Therefore a fixed setup using a T- tube with a valve would be useful.

In order to measure the emanation power of the source, one needs to pump for more than 30 hours as can be seen in the Figure (5.14).

The bubbling method to develop a standard Rn-220 source is only for investigating the Rn-220 detectors measurements in the laboratory. It is unlikely that it can be applied in field measurements.





# CHAPTER 7

## Summary, Conclusion and Future work

### 7.1 Introduction

As presented in chapter one, Rn-220 detectors need to be calibrated in order to measure Rn-220 accurately. Therefore, a Rn-220 standard source is required in order to produce Rn-220 gas which can be used for calibration. In this study a Rn-220 standard source was developed based on  $\text{Th}(\text{NO}_3)_4$  dissolved in distilled water followed by a method which we call the “bubbling method” for measuring Rn-220. In this Chapter a brief summary and conclusion of the thesis will be presented, followed by plans for future work.

### 7.2 Summary and Conclusion

The main aim of this study was to develop a simple, cheap and reliable Rn-220 standard source, which can be used to investigate and check Rn-220 detectors. The work done to achieve this main aim as stated in Section 1.2 is as follows:

Our source consists of dissolving  $\text{Th}(\text{NO}_3)_4 \cdot 6\text{H}_2\text{O}$  in water. A steady predictable concentration of thoron is present in the air that is bubbled through this solution. The short half-life of Rn-220 implies that some of the Rn-220 decays in the solution in the bottle before it is pumped out. This percentage needs to be known accurately. This was done in this work by measuring the gamma rays from the decay products of Rn-220 in the solution. This required a model since the half-lives of the Rn-220 daughters cause only a slow reduction in the gamma counts, driven mainly by the decay of Pb-212 with a half-life of 10.6 hours. The theoretical model was developed using the Bateman equations based on the decay chain of Rn-220. The model was derived starting with the Pb-212 considering the short half of Po-216. The model aimed to calculate the number of counts in the Tl-208 (2614 keV) photopeak. From the model it was possible to monitor the reduction in the intensity of the Tl-208(2614 keV) peak over time and measure the strength of the source term

(amount of Rn-220 that decayed in the solution) as well, as described in Chapter 2 section 2.3. The developed model was used to fit the experimental data and deduce the percentage of Rn-220 pumped out.

Since the Rn-220 source was prepared using a known amount of  $\text{Th}(\text{NO}_3)_4 \cdot 6\text{H}_2\text{O}$ , it was possible to determine the activity concentration of the solution. Some of the solution was transferred into a Marinelli beaker and characterized using the HPGe detector at iThemba LABS. The prominent energy lines were used for calculating the activity concentration with the associated number of counts of gamma peaks in Ac-228 and Tl-208 (see Figure 5.4). The activity concentration of the solution was measured to be  $11460 \pm 180$  Bq/L which is close to the calculated value of  $12280 \pm 140$  Bq/L but does not agree with it. Considering the possible impurity of the  $\text{Th}(\text{NO}_3)_4 \cdot 6\text{H}_2\text{O}$ , the measured value was preferred. The value of the activity concentration measured in the Marinelli beaker implied that the solution in the small bottle has an activity of  $331 \pm 5$  Bq.

In order to use the NaI(Tl) detector for measuring the gamma rays released from the solution while bubbling, the detector was calibrated for energies up to 3 MeV since the gamma ray line of 2614 keV associated with Tl-208 was to be investigated. Moreover, to obtain the activity of the 2614 keV gamma peak, a simulation was done for the NaI(Tl) detection efficiency using the MCNPx program. The geometry of the NaI (Tl) detector and the small bottle partially filled with KCl solution were simulated as shown in Figure 5.13. A separate experiment was done using the KCl solution in a small bottle and the NaI(Tl) detector and the absolute efficiency of 1460 keV was obtained and used in scaling the simulated efficiencies. Moreover, an experiment conducted to check on the efficiency of the Tl-208(2614 keV) line when different heights of the  $\text{Th}(\text{NO}_3)_4 \cdot 6\text{H}_2\text{O}$  solution was performed. Only a small change was observed in the efficiency- see Chapter 6 section 6.2 for the efficiency as a function of the height.

In order to measure the strength of the effective source that keeps feeding the radon daughters (amount of the Rn-220 that decays in the solution) it was bubbled for more than 40 hours. The Tl-208 (2614 keV) decreases with time due to the amount of Rn-220 pumped off the solution. Note that some fraction of Rn-220 decayed in the solution and is not pumped off, which feeds the Tl-208(2614 keV) line. The result is that the counts in the peak do not tend to zero, but to a finite value. The developed method using the Bateman equations based on the calculated activity of Tl-

208 (2614 keV) was fitted to the measured activity of Tl-208(2614 keV) and the strength of the source was found to be about 50 Bq (see Figure 5.14). Since our initial activity in the small bottle was about 331 Bq and the strength of the effective source term was estimated to be 50 Bq, the amount of Rn-220 that was pumped from the solution is equivalent to  $85\% = (1 - \frac{50}{331}) \times 100$ .

The reliability of our developed Rn-220 source was checked by conducting an experiment after 5 months. The experiment was conducted for 12 hours and the flow rate was changed from 0.6 L/min to 1 L/min (see Figure 5.19). The developed Rn-220 source proved that it can be used and produce a stable stream of Rn-220 gas. After using the developed source for a calibration measurement, it can only be re-used after Pb-212 regenerates for measuring the strength of the source.

Further experiments were performed to test the developed source for reproducibility. Therefore, a separate experiment (using a new initial activity) was conducted where the setup changed by incorporating a lead castle to reduce background, changing the flow rate to 1 L/min, developing a new bubbler and the air was humidified to reduce evaporation. The measurements were conducted for 72 hours (see Figure 5.24). The strength of the source (S) was found to be about 45 Bq and which implied that 81 % of Rn-220 was pumped off the solution.

The Rn-220 gas produced from the Rn-220 source that was developed using the  $\text{Th}(\text{NO}_3)_4 \cdot 6\text{H}_2\text{O}$ , was detected and measured using the RAD7 detector (see Figure 4.6). The measurements were done at various times during the two day experiment. The RAD7 measurements remain near constant and the activity concentration was found to be  $350 \pm 11 \text{ kBq}\cdot\text{m}^{-3}$  which agreed well with the calculated value (see Figure 5.27). After 5 months the RAD7 measurements were conducted for a 12 hours bubbling measurements when the flow rate was 1 L/min. The activity concentration was found to be  $204 \pm 6 \text{ kBq}\cdot\text{m}^{-3}$  and agreed well with the calculated activity concentration (see Figure 5.29). Rn-220 gas activity concentrations that was produced was also measured when the bubbling procedure was used for 72 hours when the lead castle was used, humidified air and the flow rate was set to 1 L/min. The activity was found to be  $127 \pm 8 \text{ kBq}\cdot\text{m}^{-3}$ . The value obtained for the activity did not correspond as well in this case to the calculated activity concentration value. The uncertainty in the flow rate and the change in the geometry of the bottle are suspected as reasons.

This work presents the findings of this study for the Rn-220 standard source which was developed using resources which are inexpensive. The Rn-220 standard source is simple to use and can give a high concentration of Rn-220 with good repeatability when compared with other solid sources. The appreciable percentage of Rn-220 that is produced from our source can be used to investigate measurements of Rn-220 detectors.

The Rn-220 source developed as explained in this present work can be a significant addition to the environmental nuclear laboratories, since it can be used to conduct calibration for Rn-220 detectors.

### **7.3 Future work**

The method we used to develop Rn-220 standard source is new and it can be improved further as follows:

- An investigation using a different gamma ray detectors such as Lanthanum Bromide ( $\text{La Br}_3$ ) could be used to study the new developed standard source, allowing other Tl-208 peaks to be used.
- The RAD 7 was used to investigate the Rn-220 gas generated from the new developed Rn-220 source for this present work. Different Rn-220 detectors could be used to obtain results in order to compare with the present work.

## References

- Agarwal, T. K. *et al.* (2014). CFD based simulation of thoron ( $^{220}\text{Rn}$ ) concentration in a delay chamber for mitigation application. *Environmental Radioactivity*. Elsevier Ltd, 136, pp. 16–21.
- Akiba, S. *et al.* (2010). Thoron: its metrology, health effects and implications for radon epidemiology: a summary of roundtable discussions. *Radiation Protection Dosimetry*, 141, pp. 477–481.
- Amanat, B. *et al.* (2014). Calibration and optimization of a low cost diffusion chamber for passive separated measurements of radon and thoron in soil by Lexan PC SSNTD. 12(1), pp. 61-67
- Benz, R. *et al.* (1987). *Gmelin Handbook of Inorganic Chemistry*. 8<sup>th</sup> edition Springer- Verlag Berlin Heidelberg.
- BEIR Report VI (1999) National Research Council. *Health effects of exposure to radon: BEIR VI* (Vol. 6). National Academies Press.
- Bell, S. (2001). Measurement Good Practice Guide. No (11) issue 2. National Physical Laboratory.
- Briesmeister, J. F. (2000). MCNP6 – A General Monte Carlo N-Particle Transport Code. Los Alamos National Laboratory, (March), p. 790.
- Buompane, R. *et al.* (2013). Realization and characterization of a  $^{220}\text{Rn}$  source for calibration purposes. *Applied Radiation and Isotopes*. Elsevier, 81, pp. 221–225.
- Chege, M. W. *et al.* (2015). Estimation of annual effective dose due to radon and thoron concentrations in mud dwellings of Mrima Hill, Kenya. *Radiation Protection Dosimetry*, 167(1–3), pp. 139–142.
- Chen, J. and Moir, D. (2012). A study on the thoron sensitivity of radon detectors available to Canadians. *Journal of Radiological Protection*. 32(4), pp. 419–425.
- Croft, S. and Hutchinson, I. G. (1999). The measurement of U, Th and K concentrations in building materials. *Applied Radiation and Isotopes*. 51(5), pp. 483–492.
- Csige, I., Szabó, Z. and Szabó, C. (2013). Experimental Technique To Measure Thoron Generation Rate of Building Material Samples Using Rad7 Detector. 59, pp. 201–204.
- Csordás, A. *et al.* (2015). Preparation and characterisation of ceramic-based thoron sources for thoron calibration chamber. *Radiation Protection Dosimetry*. 167(1–3), pp. 151–154.

- Debertin, K. and Helmer, R. G. (2001). Gamma and X-ray spectrometry with semiconductor detectors. North Holland: Elsevier Science B.V.
- De Villiers, D. (2011). Characterization of Heavy Mineral Sands and Soils by Radiometry and its use in Mineral Beneficiation and Agriculture. PhD, thesis, University of Stellenbosch, South Africa.
- Dinh Chau, N. *et al.* (2011). Natural radioactivity in groundwater - a review. *Isotopes in Environmental and Health Studies*, 47(4), pp. 415–437.
- Doi, M. and Kobayashi, S. (1994). Characterization of Japanese wooden houses with enhanced radon and thoron concentrations. *Health Physics*. 66(3), pp. 274–282.
- Durrige (2015). Rad7 Radon Detector manual. pp. 1–89.
- Eappen, K. P., Sapra, B. K. and Mayya, Y. S. (2007). A novel methodology for online measurement of thoron using Lucas scintillation cell. *Nuclear Instruments and Methods in Physics Research, Section A: Accelerators, Spectrometers, Detectors and Associated Equipment*.572(2), pp. 922–925.
- Gaware, J. J. *et al.* (2011). Development of Online Radon and Thoron Monitoring Systems for Occupational and General Environments. (318), pp. 45–51.
- Gilmore, G. R. (2008). Practical gamma-ray spectrometry, 2nd Edition. John Wiley & Sons, Ltd.
- Guo, Q. *et al.* (1995). Measurements of thoron concentration by passive cup method and its application to dose assessment. *Journal of Nuclear Science and Technology*, 32(8), pp. 794–803.
- Guo, Q., Sun, J. and Zhuo, W. (2000). Potential of high thoron exposure in china. *Journal of Nuclear Science and Technology*, 37(8), pp. 716–719.
- IAEA, (2013). National and Regional Surveys of Radon Concentration in Dwellings. International Atomic Energy Agency, Vienna.
- Irlinger, J. (2015). Development of an electronic monitor for the determination of individual radon and thoron exposure. Available at: [http://edoc.ub.uni-muenchen.de/18342/%5Cnhttp://edoc.ub.uni-muenchen.de/18342/1/Irlinger\\_Josef.pdf](http://edoc.ub.uni-muenchen.de/18342/%5Cnhttp://edoc.ub.uni-muenchen.de/18342/1/Irlinger_Josef.pdf).
- Ismail, A. H. and Jaafar, M. S. (2011). Design and construct optimum dosimeter to detect airborne radon and thoron gas: Experimental study. *Nuclear Instruments and Methods in Physics Research, Section B: Beam Interactions with Materials and Atoms*. Elsevier B.V., 269(4), pp. 437–439.
- Janik, M. *et al.* (2014). Invited Article: Radon and thoron intercomparison experiments for

- integrated monitors at NIRS, Japan. *Review of Scientific Instruments*. 85, 022001.
- Janik, M. (2017). Intercomparisons Exercises of Radon and Thoron Monitors Provided by Four Laboratories: A Review. *Japanese Journal of Health Physics*, 52(2), pp. 114–121.
- Jobbágy, V. and Bety-Denissa, B. (2010). Solid thoron source preparation in a porous mineral matrix. *Radiation Protection Dosimetry* 141(4), pp. 440–443.
- Kanse, S. D. *et al.* (2013). Powder sandwich technique: A novel method for determining the thoron emanation potential of powders bearing high  $^{224}\text{Ra}$  content. *Radiation Measurements*. Elsevier Ltd, 48(1), pp. 82–87.
- Kavasi, N. *et al.* (2012). Thoron experimental room at the national institute of radiological sciences (NIRS), Japan. *Radiation Protection Dosimetry*. 152(1–3), pp. 150–153.
- Knoll, G. E. (2010). *Radiation Detection and Measurement*. Fourth Edition. John Wiley & Sons, Ltd.
- Kohn, H. I. (2006). *Health Effects of Exposure to Low Levels of Ionizing Radiation (BEIR V)*. Radiation Research.
- Kotrappa, P. and Steck, D. (2010). Electret ion chamber-based passive radon-thoron discriminative monitors. *Radiation Protection Dosimetry*, 141(4), pp. 386–389.
- Kumar, A. *et al.* (2015). Estimation of radionuclides content and radon–thoron exhalation from commonly used building materials in India. *Environmental Earth Sciences*. Springer Berlin Heidelberg, 74(2), pp. 1539–1546.
- Kumar, P. A. *et al.* (2014). Development of a PIN diode - based on  $\alpha$ -line measurement system for radon ( $^{222}\text{Rn}$ ) and thoron ( $^{220}\text{Rn}$ ) in the environment. 37(2), pp. 80-88.
- Lilley, J. S. (2001). *Nuclear Physics- Principles and Applications*. John Wiley & Sons, Ltd
- Lindsay, R. *et al.* (2019). Thoron standard source. *Applied Radiation and Isotopes*. Elsevier Ltd, 147(February), pp. 99–104.
- Magill, J. and Galy, J. (2005). *Radioactivity Radionuclides Radiation*. Springer-Verlag Berlin Heidelberg
- Magnoni, M. *et al.* (2018). Thoron exhalation rate in stony materials: A simplified approach. *Construction and Building Materials*. Elsevier Ltd, 173, pp. 520–524.
- Maleka, P. P., Maučec, M., & De Meijer, R. J. (2011). Deficiency in Monte Carlo simulations of coupled neutron- $\gamma$ -ray fields. *Nuclear Instruments and Methods in Physics Research*

*Section A: Accelerators, Spectrometers, Detectors and Associated Equipment, 640(1), 151-159.*

- Phon, L. K. *et al.* (2015). Estimation of effective dose rates caused by radon and thoron for inhabitants living in rare earth field in northwestern Vietnam (Lai Chau province). *Journal of Radioanalytical and Nuclear Chemistry.* 306(1), pp. 309–316.
- Pornnumpa, C. *et al.* (2018). Development of Radon and Thoron Exposure Systems at Hirosaki University. *Radiation Environment and Medicine.* 7(1), pp. 13–20.
- Qiu, S. (2006). Calibration of a  $^{220}\text{Rn}$  flow-through source. *Radiation and Environmental Biophysics.* 45(3), pp. 215–220.
- Ramachandran, T. V.; Athish, L. A. (2014). Environmental Thoron ( $^{220}\text{Rn}$ ): a review. *Research Journal of chemical and Environmental Sciences.* 2(April), pp. 5–31.
- Ramachandran, T. V. (2010). Environmental thoron ( $^{220}\text{Rn}$ ): A review. *Iranian Journal of Radiation Research.* 8(3), pp. 129–147.
- Ramola, R. C. *et al.* (2016). Dose estimation derived from the exposure to radon, thoron and their progeny in the indoor environment. *Scientific Reports.* Nature Publishing Group, 6, pp. 1–16.
- Röttger, A. *et al.* (2010). A primary standard for activity concentration of  $^{220}\text{Rn}$  (thoron) in air. *Applied Radiation and Isotopes.* 68(7–8), pp. 1292–1296.
- Röttger, A., Honig, A. and Linzmaier, D. (2014). Calibration of commercial radon and thoron monitors at stable activity concentrations. *Applied Radiation and Isotopes.* Elsevier, 87, pp. 44–47.
- Sabot, B. *et al.* (2015). Development of a primary thoron activity standard for the calibration of thoron measurement instruments. *Radiation Protection Dosimetry.* 167(1–3), pp. 70–74.
- Sathyabama, N. *et al.* (2014). A study of disequilibrium between  $^{220}\text{Rn}$  and  $^{216}\text{Po}$  for  $^{220}\text{Rn}$  measurements using a flow-through Lucas scintillation cell. *Radiation Protection Dosimetry.* 158(2), pp. 187–194.
- Schery, S. D. (1990). Thoron in the Environment. *Journal of the Air and Waste Management Association.* 40(4), pp. 493–497.
- Shang, B. *et al.* (2008). Radon survey in dwellings of Gansu, China: The influence of thoron and an attempt for correction. *Radiation and Environmental Biophysics.* 47(3), pp. 367–373.
- Sorimachi, A. *et al.* (2012). Performance test of passive radon-thoron discriminative detectors on environmental parameters. *Radiation Measurements.* Elsevier Ltd, 47(6), pp. 438–442.



- Sorimachi, A. *et al.* (2016). An intercomparison done at NIRS, Japan on continuous monitors for measuring  $^{220}\text{Rn}$  concentration. *Applied Radiation and Isotopes*. Elsevier, 107, pp. 145–151.
- Sorimachi, A., Sahoo, S. K. and Tokonami, S. (2009). Generation and control of thoron emanated from lantern mantles. *Review of Scientific Instruments*, 80, 015104.
- Srinivasan, P. *et al.* (2010). Development of a system for online measurement of  $^{220}\text{Rn}$  (Thoron) by gamma ray spectrometry method. International Atomic Energy Agency (IAEA).
- Steinhäusler, F. (1996). Environmental  $^{220}\text{Rn}$ : A review. *Environment International*, Suppl. 1, pp. S1111-S1123.
- Sugino, M., Tokonami, S., Zhuo, W., (2005). Radon and thoron concentrations in offices and dwellings of the Gunma prefecture. *Jpn. J. Radioanal. Nucl. Chem.* 266, pp.205-209.
- Sumesh, C. *et al.* (2011). Thoron interference test of different continuous passive radon monitors. *Radiation Protection and Environment*, 34(4), p. 257-261.
- Sumesh, C. G. *et al.* (2012). Estimation of thoron concentration using scintillation cell. *Radiation Protection Dosimetry*. 150(4), pp. 536–540.
- Sumesh, C. G. *et al.* (2013). Impact of flow rate on sensitivity of semiconductor type thoron monitor. *Radiation Measurements*. Elsevier Ltd, 59, pp. 241–244.
- Szabó, Z. *et al.* (2014). Radon and thoron levels, their spatial and seasonal variations in adobe dwellings - a case study at the great Hungarian plain. *Isotopes in Environmental and Health Studies*. 50(2), pp. 211–225.
- Talha Abdalla, S. A. (2009). Measurements and Applications of Radon in South African Aquifer and River Waters. PhD, thesis, University of the Western Cape, South Africa.
- Talha, S.A., Lindsay, R., Newman, R.T., de Meijer, R.J., Maleka, P.P., Hlatshwayo, I.N., Mlilo, N.A. and Mohanty, A.K., (2008).  $\gamma$ -Ray spectrometry of radon in water and the role of radon to representatively sample aquifers. *Applied radiation and isotopes*, 66(11), pp.1623-1626.
- Tan, Y. *et al.* (2014). Research on the lower detection efficiency of the RAD7 for  $^{220}\text{Rn}$  than for  $^{222}\text{Rn}$ . *Journal of Instrumentation*, 9, T06001.
- Tan, Y. and Xiao, D. (2013). The method for recalibration of thoron concentration reading of RAD7 and obtaining the thoron exhalation rate from soil surface. *Nuclear Technology and Radiation Protection*, 28(1), pp. 92–96.

Tang, F. *et al.* (2012). Preparation and emanation properties of an ion-exchanged solid thoron source. *Radiation Protection Dosimetry*, 152(1–3), pp. 66–70.

UNSCEAR (2000) ANNEX B: Exposures from natural radiation sources, UNSCEAR 2000 Report to the General Assembly, with Scientific Annexes.  
<http://www.unscear.org/docs/reports/annexb.pdf>.

Vaupotič, J. *et al.* (2013). Diurnal variations of radon and thoron activity concentrations and effective doses in dwellings in Niška Banja, Serbia. *Radiation Protection Dosimetry*, 157(3), pp. 375–382.

Wang, Y., Zhang, L. and Guo, Q. (2017). The experimental study on the emanation power of a flow-through thoron source made from incandescent gas mantles. *Journal of Radiological Protection*. IOP Publishing, 37(4), pp. 918–926.

Waters, L. S. *et al.* (2007) ‘The MCNPX Monte Carlo radiation transport code’, AIP Conference Proceedings, 896(1), pp. 81–90.

[www.nucleide.org](http://www.nucleide.org)

Yamada, Y. *et al.* (2005). Rn-Tn discriminative measurements and their dose estimates in Chinese loess plateau. *International Congress Series High Levels of Natural Radiation and Radon Areas Radiation Dose and Health Effects*, 1276, pp. 76–80.

Zhang, L. *et al.* (2010). Measurement of thoron gas in the environment using a Lucas scintillation cell. *Journal of Radiological Protection*, 30(3), pp. 597–605.

Zhao, C. *et al.* (2010). Characteristic and performance of a simple thoron chamber. *Radiation Protection Dosimetry*, 141(4), pp. 444–447.

Zhuo, W. *et al.* (2002). A simple passive monitor for integrating measurements of indoor thoron concentrations. *Review of Scientific Instruments*, 73(8), pp. 2877–2881.

# Appendices

## Appendix A

### KCl solution measurement analysis

Experimental measurements were conducted using a KCl solution to obtain the absolute efficiency of K-40 in order to correct the simulated detection efficiencies. To do so, the measured number of counts in the K-40 (1460 keV) photopeak was used to obtain the detection efficiency of K-40 (1460 keV). The procedure to obtain the absolute efficiencies is as follows:

The activity concentration of KCl powder was obtained first.

K-40 is a naturally occurring radioactive isotope of the common element potassium. The half-life of K-40 is  $1.248 \times 10^9$  year ( $3.94 \times 10^{16}$  s).

K-40 has an atomic percent abundance of 0.0124%. The branching ratio of the K-40 decay is 10.72% producing gamma-rays of energy 1460 keV

The activity can be calculated by the formula

$$A = N \lambda$$

Where A is the activity, N is the number of K-40 nuclei in the KCl sample and  $\lambda$  is the decay constant of K-40

$$\lambda = \ln 2 / t_{1/2}$$

Where  $t_{1/2}$  is the half-life of K-40

The number of K-40 nuclei in the KCl powder can be obtained by

$$N = (m/M) \times N_A$$

Where: -

$m$  = is the mass of K-40 in the K-nat (1 kg of K-nat contains 0.124 g of K-40 from the atomic percentage abundance of 0.0124%)

$M$  = Molar mass of K -40 (gram/mole)

$N_A$  = Avogadro's number  $6.02 \times 10^{23}$  atom/mole

Substituting the values of  $\lambda$  and  $N$  in the equations above, the activity of K-40 was found to be  $3.18 \times 10^4$  Bq /kg.

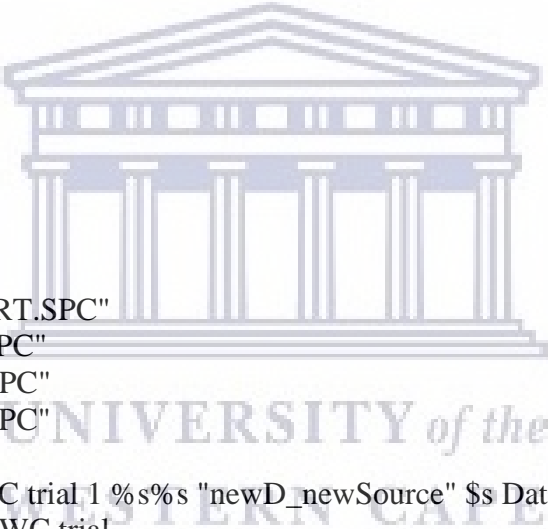
1 kg KCl contains  $39.098 / (39.098 + 35.453) = 0.524$  kg K-nat

1 kg KCl contains  $3.18 \times 10^4 \times 0.524 = 16663$  Bq/kg

Once we obtained the absolute activity of the K-40, it is possible to calculate the absolute efficiency for the photopeak of K-40 (1460 keV). From the experiment that measured the KCl solution, the net count rate of K-40 (1460 keV) was measured and was found to be about 0.5 cps. By using the measured value of net counts of 1460 keV and the calculated absolute activity of K-40 and re-arranging equation 5.1 the absolute efficiency was found to be 2.9%.

## Appendix B

Script program for stabilizing the fine gain every 6 minutes and to save the measured spectra from the Rn-220 source every hour.



```
Show Window 1
Wait 1
Window Frame 1 1 1 98 98
Window Frame 1 1 60 98 30

Set HV 1 $HV
Set Spectrum Name 1 "START.SPC"
Save Spectrum 1 "START.SPC"
Load Spectrum 2 "START.SPC"
Load Spectrum 3 "START.SPC"
Get Date sDate
Generate SPC Name Sp UWC trial 1 %s%s "newD_newSource" $s Date
Set Spectrum Name 1 $Sp UWC trial

Clear Spectrum 1
Set fine gain 1 1.525

For K=1 to 14
Increment Spectrum Name 1
Clear Spectrum 2
# Loop over 6 min intervals for every hour.
For J=1 to 10
Clear spectrum 3
Add Spectrum 1 3
Eval $time+360 time
Pre Set Live time 1 $time
Start Acquisition 1 &
```

```
Clear Spectrum 2
Add Spectrum 1 2
Subtract Spectrum 3 2
#Find the position of the 1460 peak and change fine gain to keep peak in same place
Integrate 2 Centroid FWHM Net Gros Back $e left $e right
```

```
Eval ($old result*1460)/$Centroid RESULT
Set fine gain 1 $RESULT
Eval $Result old result
Appendfile 0 "start9.txt" $RESULT $Centroid
Show Message 1 0 1 $Result
next J
Save Spectrum 1 ""
Clear Spectrum 1
Clear Spectrum 2
Eval 0 time
Next K
```

```
VARIABLES
s Date %s
Sp UWC trial %s
ci %d
I %d
J %d
J2 %d
K %d
Centroid %f
FWHM %f
Net %f
Gros %f
Back %f
e left %d 1320
e right %d 1526
factor %f
f gain %f
RESULT %f
HV %d 840
Old result %f 1.525
time %d 0
```



## Appendix C

### Visual Basic program

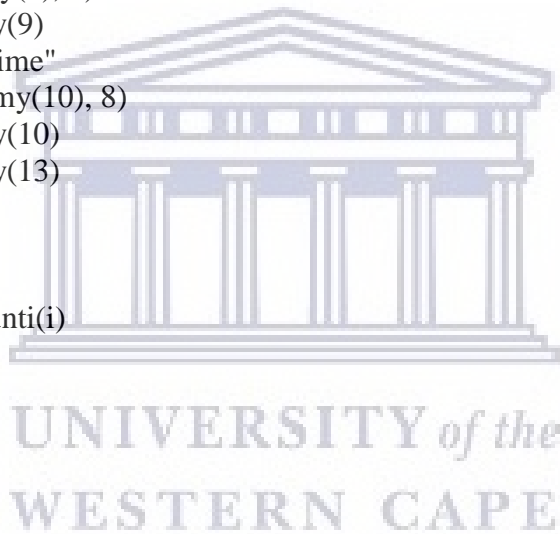
The program is used to import the number of counts in SPC files to an Excel spreadsheet and to put the data into columns.

```
Public Sub directory ()
' Programme to read all .SPC files in a directory and write the spectra in a column
Dim Filenames (5000), filenm As String
Dim counti(1024), ctemp, nr_of_files, ifile, Nr_name, file_len As Integer
Dim sdummy(50) As String

'This must give the directory
Application.Default File Path
ChDir ("C:\newsolution")
' Filenames (1) = Dir("C:*.SPC")
Filenames (1) = Dir("C:*.")
Cells(1, "A") = Filenames(1)
'change to number of files
nr_of_files = 200
j = 1
For i = 1 To nr_of_files
Filenames(i) = Dir
If (Filenames(i) = "*.xlsm") Then GoTo nottodo
If (Filenames(i) = "") Then GoTo DONE
j = j + 1
Cells(j, "A") = Filenames(i)
nottodo:
```

Next i  
DONE:

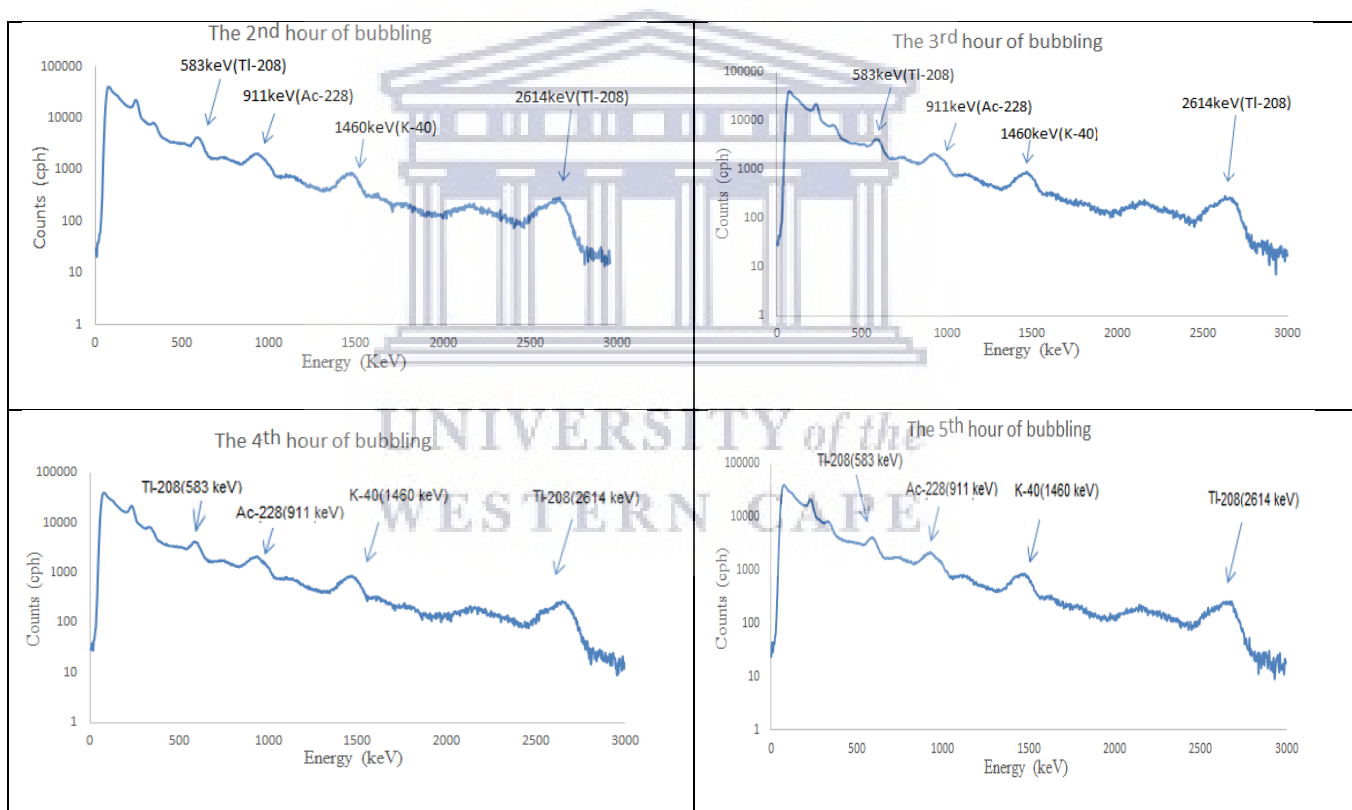
```
nr_of_files = j
' loop over the files
For ifile = 2 To nr_of_files
filenm = Cells(ifile, "A")
Open filenm For Input As 5
'Read heading
For i = 1 To 25
Input #5, sdummy(i)
Next i
'Select parts of the heading to write to Excel
Cells(1, ifile + 1) = filenm
Cells(2, ifile + 1) = "Real Time"
sdummy(9) = Right(sdummy(9), 8)
Cells(3, ifile + 1) = sdummy(9)
Cells(4, ifile + 1) = "Live Time"
sdummy(10) = Right(sdummy(10), 8)
Cells(5, ifile + 1) = sdummy(10)
Cells(6, ifile + 1) = sdummy(13)
For i = 1 To 1024
'now read spectrum
Input #5, counti(i)
Cells(i + 13, ifile + 1) = counti(i)
Next i
Close 5
Next ifile
End Sub
```

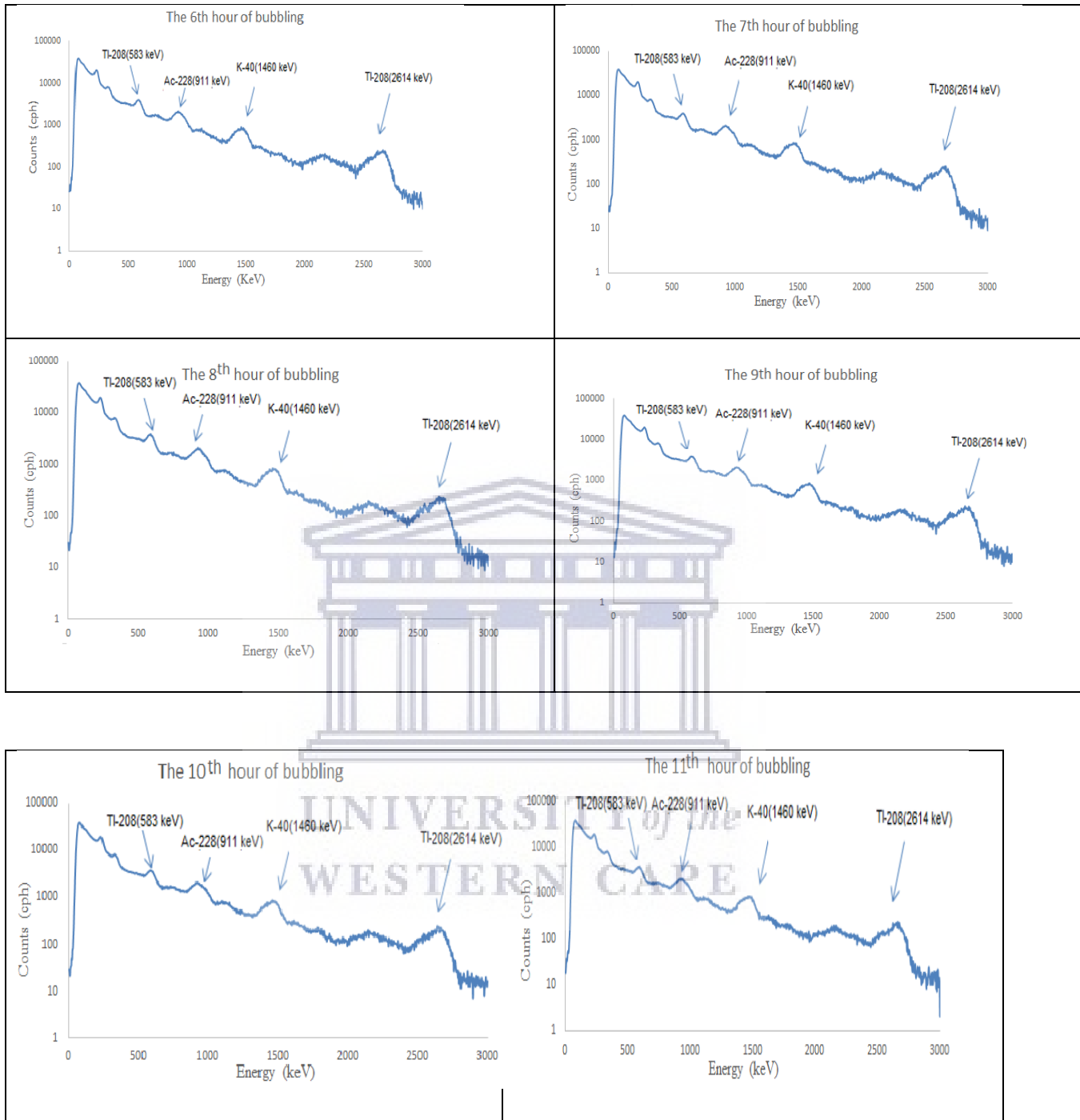


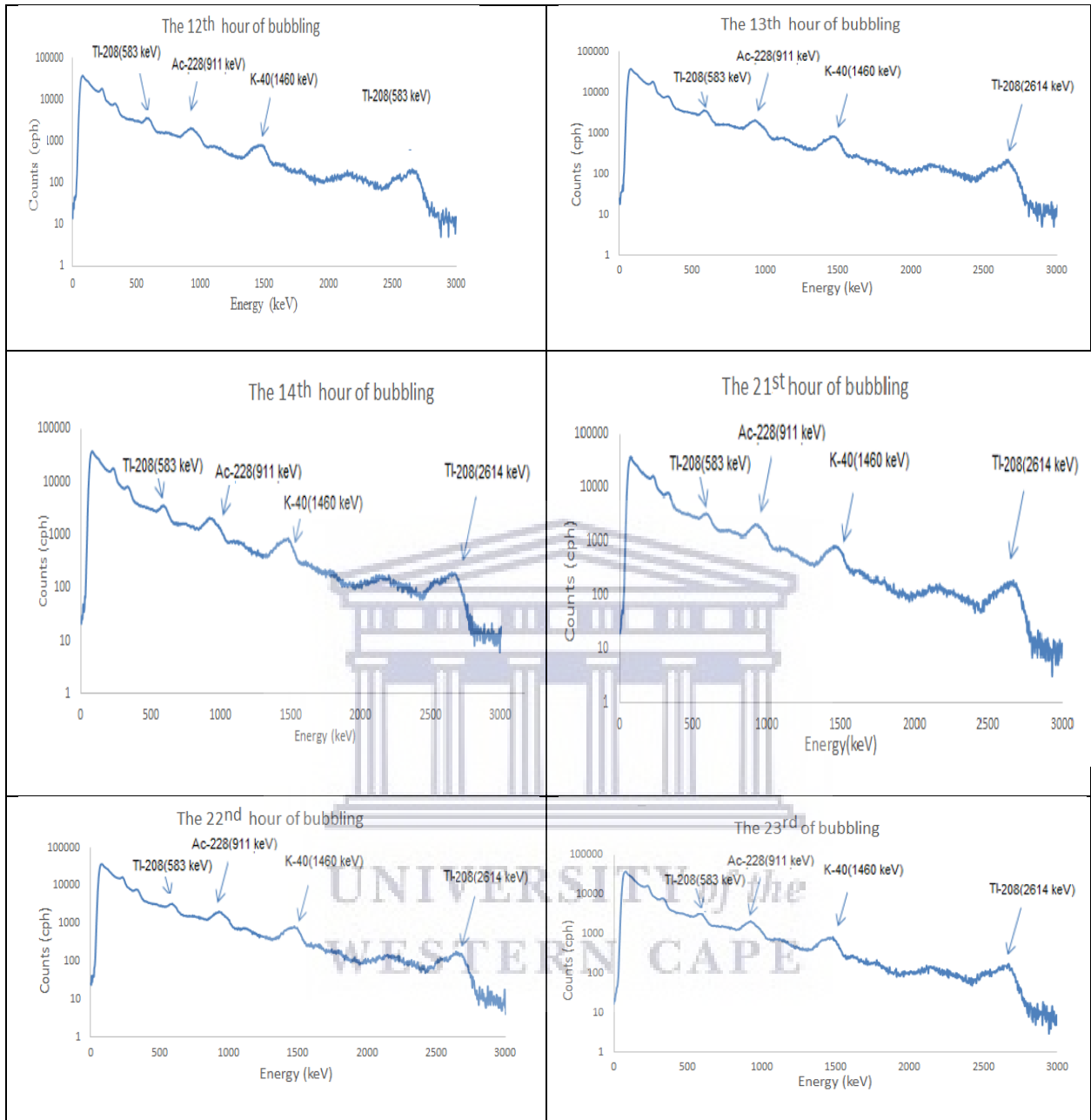


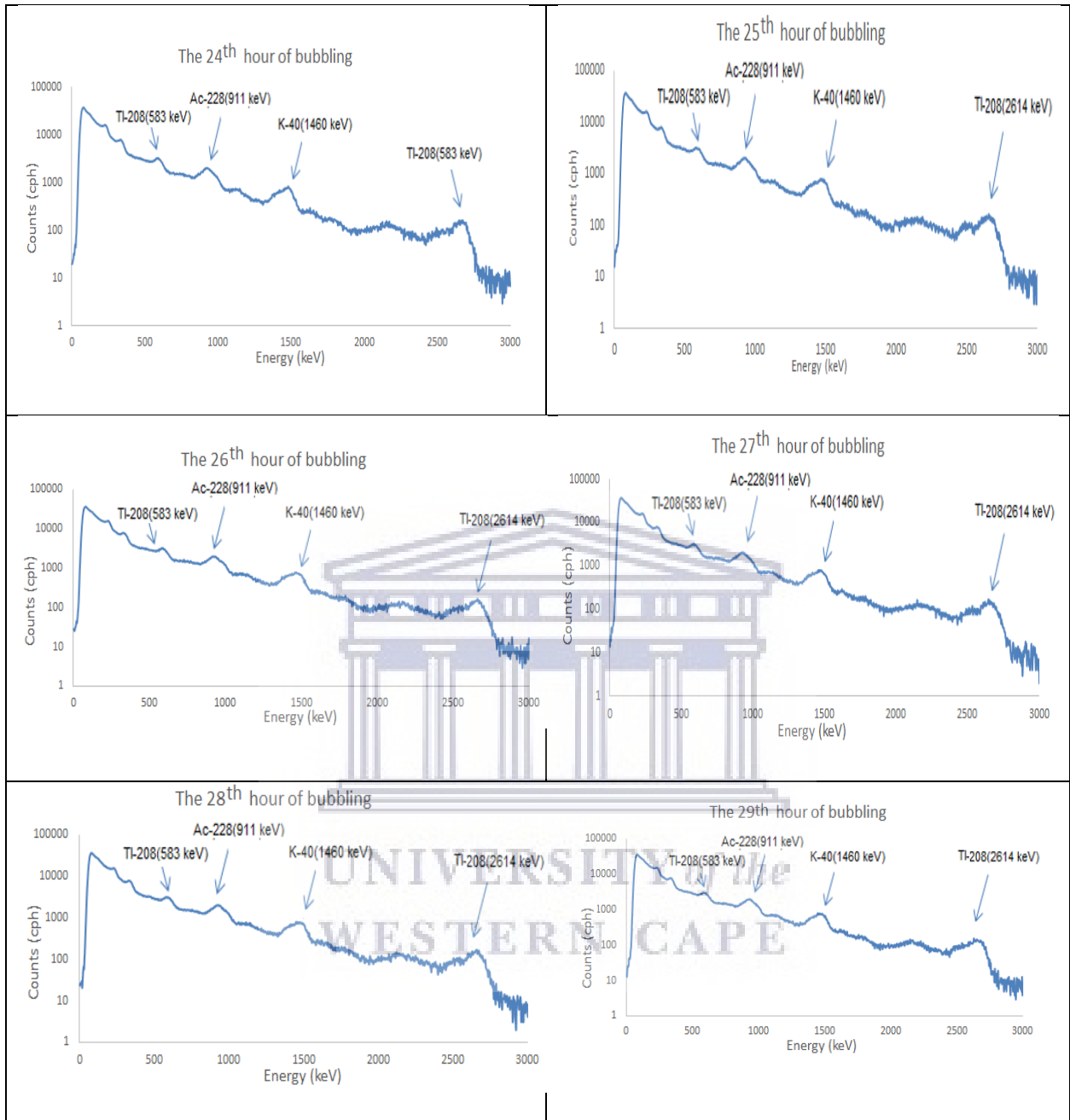
## Appendix D

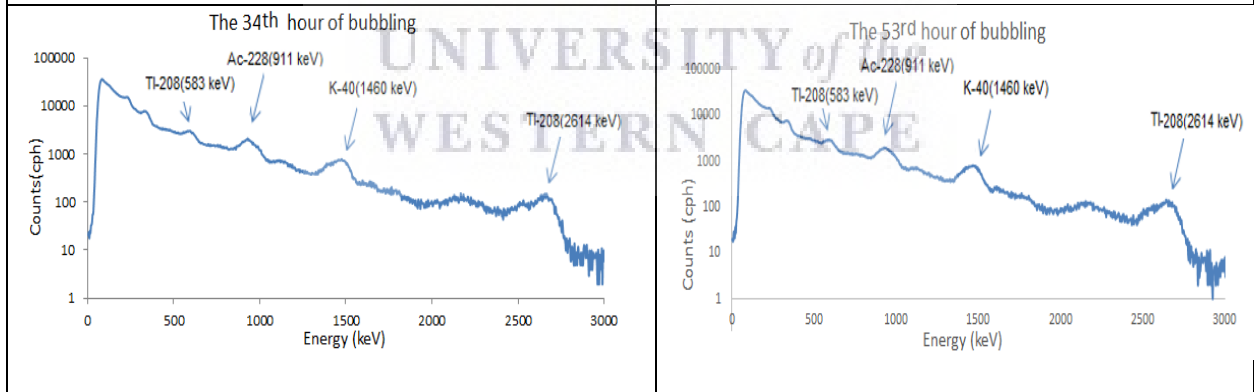
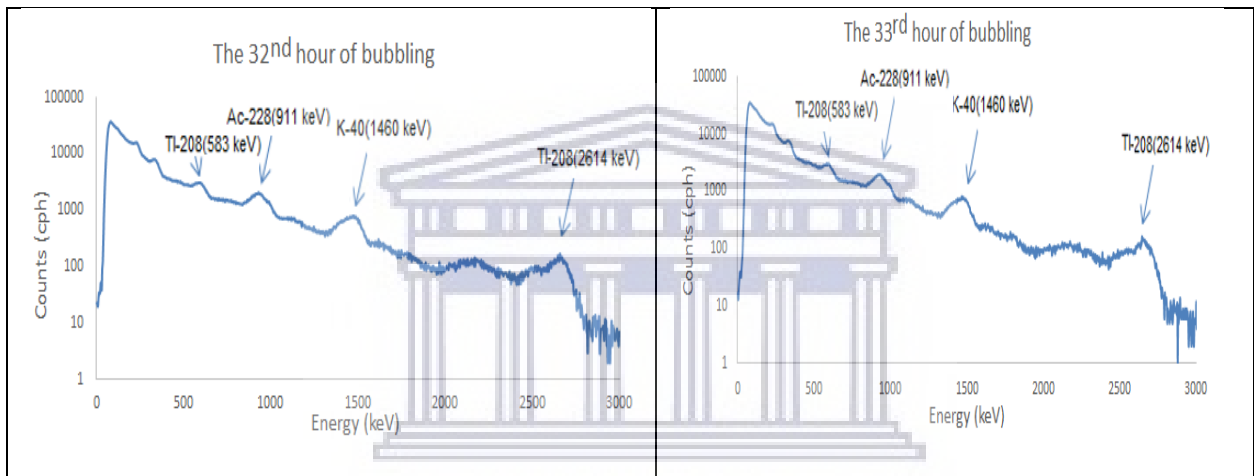
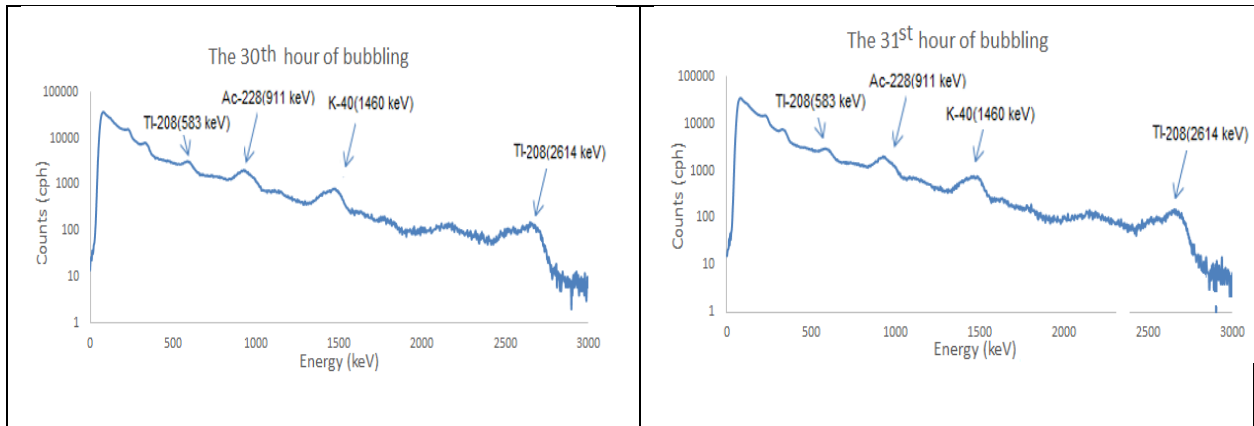
Gamma ray spectra measured from the  $\text{Th}(\text{NO}_3)_4 \cdot 6\text{H}_2\text{O}$  while bubbling.

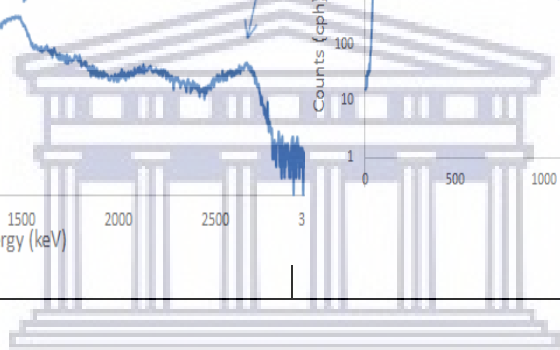
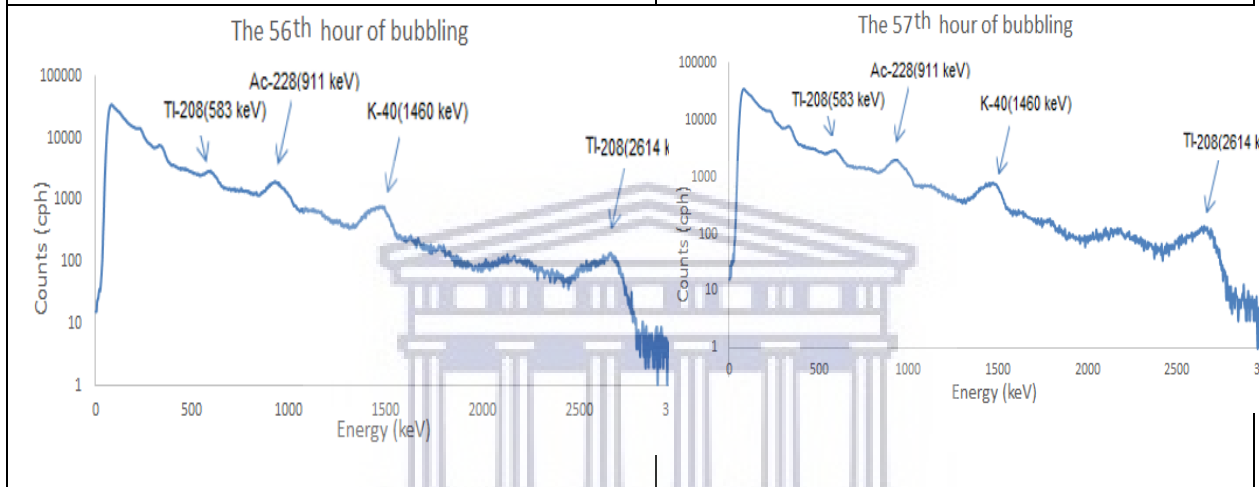
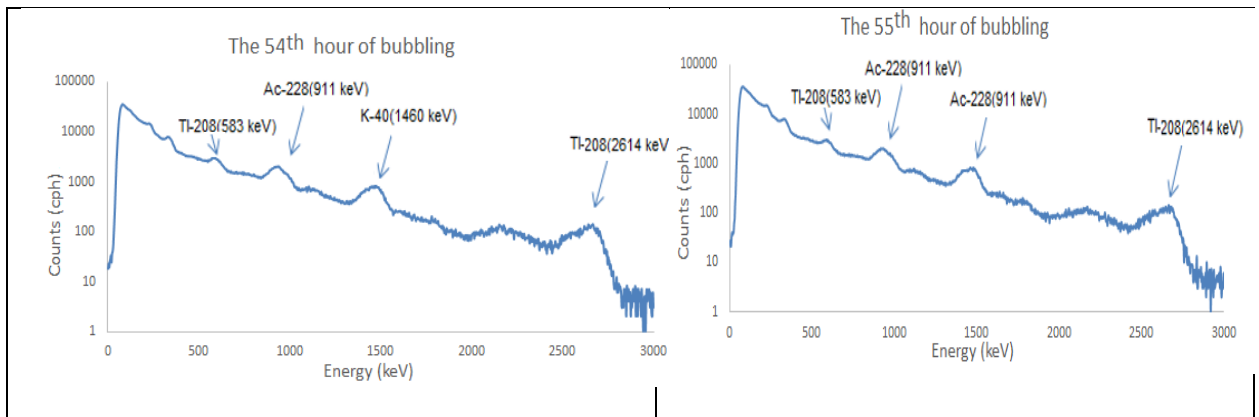




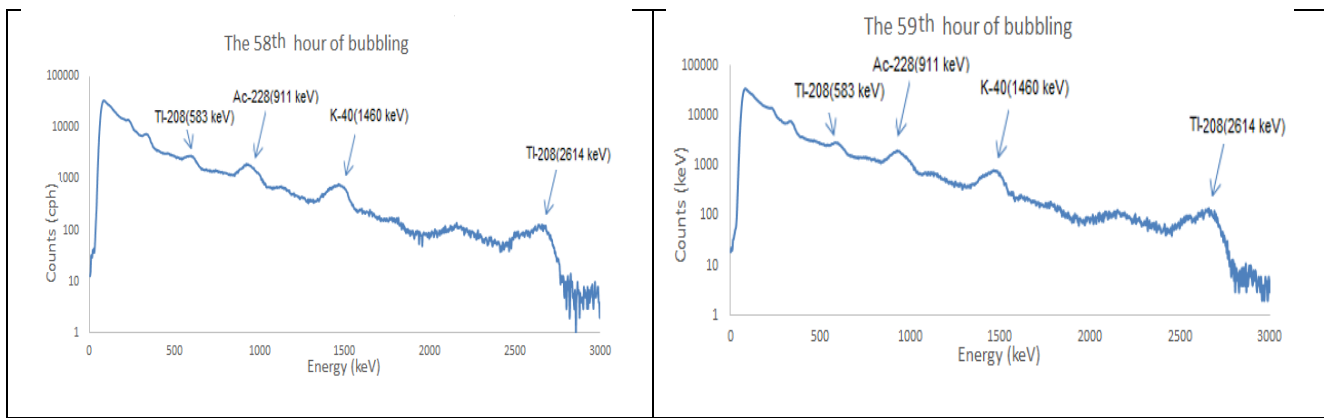


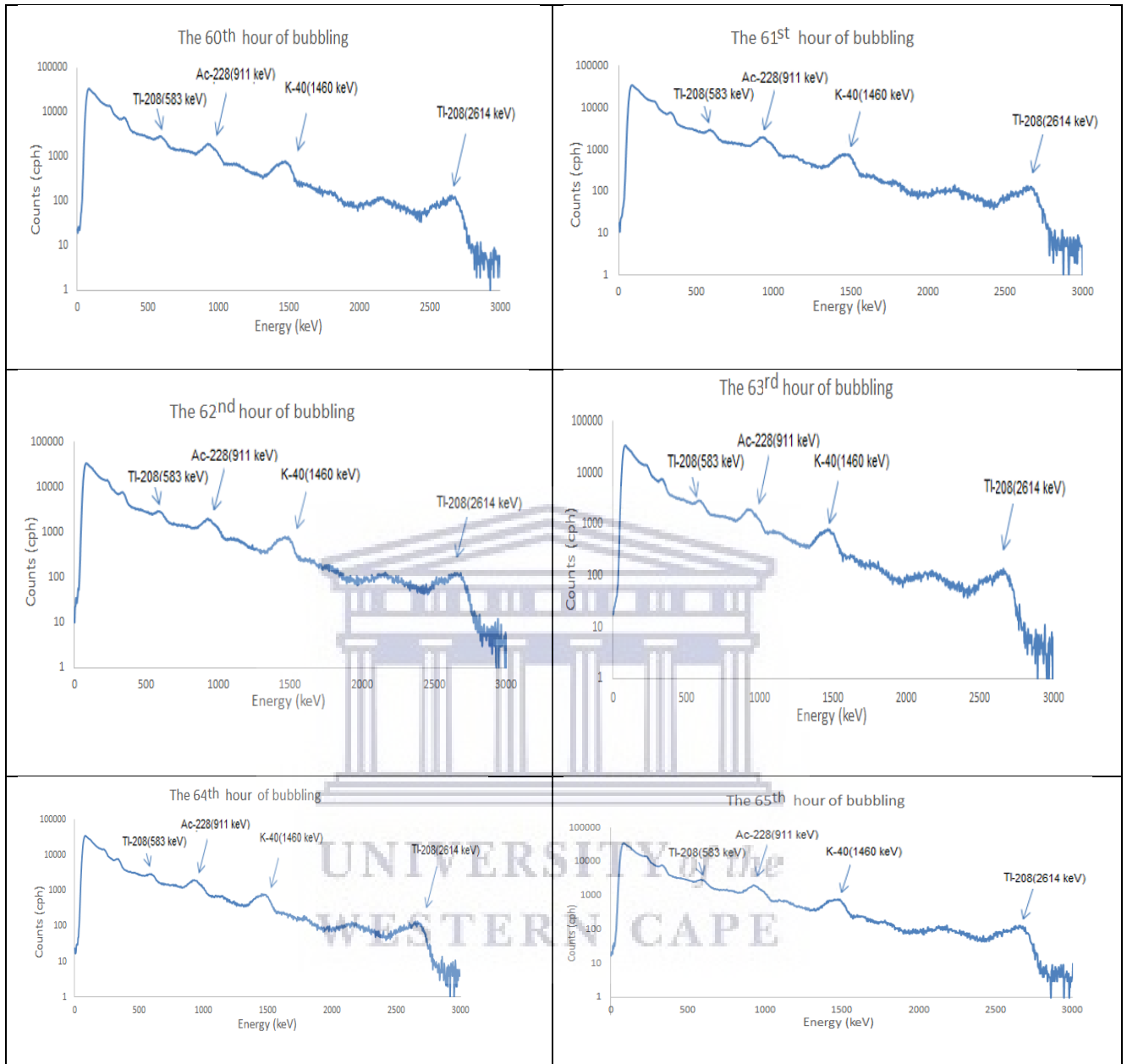






UNIVERSITY of the  
WESTERN CAPE





## Appendix E

### The uncertainty calculations

E1. The uncertainty for the activity ( $U(A)$ ) shown in Figure 5.14 was calculated using the following equation

$$U(A) = A \times \sqrt{\left(a \frac{u(N)}{N}\right)^2 + \left(b \frac{u(\varepsilon)}{\varepsilon}\right)^2 + \left(c \frac{u(B)}{B}\right)^2 + \left(d \frac{u(t)}{t}\right)^2} \quad \text{Bell (2001)}$$

Where

a, b, c and d are weighting constants equal to 1 for this formula, A is the activity, N is the counts in Tl-208(2614 keV),  $\varepsilon$  efficiency, B branching ratio, t time.  $u(N)$  the uncertainty in the counts,  $u(\varepsilon)$  the uncertainty in the efficiency,  $u(B)$  the uncertainty in the branching ratio and  $u(t)$  the uncertainty in the time.

In Figure 5.14 the activity of the Tl-208 (2614 keV) was measured for 66 hours. Each uncertainty for the activity was calculated using the above equation.

The uncertainty for the activity shown in Figure 5.24 was calculated using the same procedure.

E2. The uncertainty of the activity concentration ( $U(C)$ ) of Rn-220 at the exit stream of the pipe was calculated based on equation 5.7 as follows

$$U(C) = C \times \sqrt{\left(a \frac{uN}{N}\right)^2 + \left(b \frac{ux}{x}\right)^2 + \left(c \frac{u\lambda}{\lambda}\right)^2 + \left(d \frac{uv}{v}\right)^2}$$

Where a, b, c and d are constants equal to 1, C is the calculated activity concentration, N The number of the Rn-220 nuclei that are created every second in the solution in the small bottle from the decay of Ra-224 (nuclei/s), x is the fraction of the Rn-220 nuclei that is pumped out from the



solution (0.85),  $\lambda$  is the decay constant of Rn-220 ( $s^{-1}$ ) and  $v$  is the Volume of air that the pumped out thoron goes into per second = flow rate ( $0.6 \text{ (L/min} \times 10^{-3}/60 \text{ m}^3/\text{s}$ ).

( $uN$ ) the uncertainty in the number of the Rn-220 nuclei that are created every second in the solution in the small bottle from the decay, ( $u_x$ ) the uncertainty in the fraction of the Rn-220 nuclei that is pumped out from the solution, ( $u\lambda$ ) the uncertainty in the decay constant of Rn-220 and ( $uv$ ) the uncertainty in volume of air that the pumped out thoron. The value obtained using the expression above was 0.28 therefore the value of the activity concentration was found to be  $350 \pm 100 \text{ kBq/m}^3$

E3. The measured activity concentration of Rn-220 using RAD7 in Figure 5.27 contain statistical uncertainty. Figure 5.28 and Figure 5.29 contain statistical uncertainties as well. (Durridge, 2015)

